

UNIVERSIDAD POLITÉCNICA DE MADRID

**ESCUELA TÉCNICA SUPERIOR
DE INGENIEROS DE TELECOMUNICACIÓN**



**MÁSTER UNIVERSITARIO EN INGENIERÍA
BIOMÉDICA**

TRABAJO FIN DE MÁSTER

**DESIGN AND IMPROVEMENT OF A THORACIC
MANNEQUIN THAT SIMULATES THE
RESPIRATORY MOVEMENT FOR DOSYMETRIC
ANALYSIS IN RADIOTHERAPY**

Laura Regueira López de Garayo

2021

UNIVERSIDAD POLITÉCNICA DE MADRID

ESCUELA TÉCNICA SUPERIOR
DE INGENIEROS DE TELECOMUNICACIÓN



MÁSTER UNIVERSITARIO EN INGENIERÍA
BIOMÉDICA

TRABAJO FIN DE MÁSTER

DESIGN AND IMPROVEMENT OF A THORACIC
MANNEQUIN THAT SIMULATES THE
RESPIRATORY MOVEMENT FOR DOSYMETRIC
ANALYSIS IN RADIOTHERAPY

Autora

Laura Regueira López de Garayo

Tutores

Álvaro Gutiérrez Martín

Nuria Gómez González

2021

Abstract

Lung cancer is the most deadly cancer worldwide. It doubles the number of deaths caused by the next most lethal type of cancer. The most commonly used treatment is surgery. However, when the tumor is located in a difficult place to access or when it means a risk to the patient, radiotherapy is the best option.

In this type of cancer, the location of the tumor during the radiotherapy session is not exact since it moves due to the patient's breathing. To ensure that the tumor is irradiated, the radiotherapy beam is larger than in other cancers. Thus, more healthy cells are affected, producing greater side effects.

In this field, different studies have developed thoracic phantoms to simulate human breathing and to study the trajectory of lung tumors. However, many of the designed phantoms are too simple. Some of them only simulate internal deformation, others external deformation, and others do not consider more facts such as hysteresis or correlations of movements.

In this MSc Thesis, the design and implementation of a lung phantom that simulates internal and external deformation in a realistic way is proposed. Firstly, the materials needed to build the solution were analyzed. In that way, a Prestan CPR-AED mannequin was used as outer shell. Then, a latex structure was created to confine the material used to simulate the soft tissue and lungs. It was filled with small bags of water mimicking soft tissue and two polyurethane foams were inserted as lungs. On the other hand, a mechanical structure was designed to simulate the anterior-posterior and superior-inferior movement of the thorax. The structure was built based on 3D printed PLA pieces which were moved by two motors through a pulley system. Moreover, to simulate the anterior-posterior movement, two PVC sheets that were bent were included in the structure.

For each movement, third-degree polynomial curves were defined based on the pattern of inspiration and expiration during a normal breathing. In addition, four different respiratory frequency rates were defined to better approximate the movement according to the respiratory pattern of each patient.

Keywords: Lung phantom, respiratory movement, respiratory frequency rates, programmable.

Acknowledgments

First of all, I would like to thank my two tutors, Álvaro Gutiérrez and Nuria Gómez, for their ideas, their corrections and their almost immediate response whenever I needed it. I would like to highlight the close treatment by both of them, which has made the work more enjoyable.

Thanks to the radiophysics department of the Puerta de Hierro hospital for their help in the measurements of the materials when necessary, especially Ángela for her pleasant treatment.

I would also like to Miguel Gómez for his work in the 3D printing, for helping me to print all the pieces on time and for being available for anything I needed in the robotics laboratory.

Last but not least, I would like to thank my family for their encouragement and support throughout the project, who have even proposed ideas when I needed it, and have followed the whole evolution of this MSc Thesis, rejoicing with the promising results and providing solutions when difficulties have arisen.

Contents

Abstract	v
Acknowledgments	vii
General Index	ix
List of Figures	xi
List of Tables	xiii
List of Acronyms	xv
1 Introduction and Objectives	1
1.1 Introduction	1
1.2 State of the art	2
1.3 Objectives	6
1.4 Document structure	6
2 Clinical Background	9
2.1 Respiratory System	9
2.2 Cancer	16
2.2.1 Lung Cancer	17
2.3 Radiotherapy	19
3 Material and Methods	21
3.1 Materials	21
3.1.1 Soft tissue	22
3.1.2 Lungs	26
3.1.3 Bones and muscles	27
3.1.4 Markers	30
3.2 Phantom configuration	30
3.2.1 Mechanical structure	30
3.2.2 Assembly of the phantom	32
3.3 Movement implementation	34
3.3.1 Electronic components	34
3.3.2 Respiration curve description	38
3.3.3 Arduino Implementation	44

4	Results	65
4.1	Results and Modifications	65
4.2	Result conclusions	73
5	Conclusions	75
5.1	Conclusions	75
5.2	Future Lines	76
	References	77
A	Ethical, economic, social and environmental aspects	83
A.1	Introduction	83
A.2	Description of relevant impacts	83
A.3	Detailed analysis of some of the main impacts	84
A.4	Conclusions	84
B	Economic budget	87
C	Drawings of the 3D pieces	91

List of Figures

1.1	Number of deaths worldwide in 2020 depending on the type of cancer [1].	1
1.2	Cheung et al. lung phantom [20].	4
1.3	Ranjbar et al. lung phantom [21].	5
2.1	Respiratory system anatomy: Airways [23].	9
2.2	Respiratory system anatomy: Lungs [24].	10
2.3	Lung volume and capacities [25].	11
2.4	Respiratory system anatomy: Thorax [29].	12
2.5	Expiration compliance curves for chronic obstructive pulmonary disease (COPD), normal, and Fibrosis/Pneumothorax [32].	13
2.6	Lung and chest wall compliance diagram [33].	14
2.7	Normal breathing pattern [37].	15
3.1	SI and AP movements scheme.	21
3.2	Slime [54].	23
3.3	Homemade slime tests.	23
3.4	Slime CT scan.	24
3.5	Agar broken due to the finger pressure.	24
3.6	Camelback bag [56].	25
3.7	Cold/heat bag [57].	25
3.8	Camelback CT scan.	25
3.9	Cold/heat bag CT scan.	25
3.10	Structure for latex mold.	26
3.11	Polyurethane foam in CT scan.	27
3.12	Lungs in polyurethane foam	27
3.13	CPR mannequin as outer shell [60].	28
3.14	PLA in CT scan	28
3.15	PVC plastic for desk chairs.	29
3.16	Plastic sheets.	29
3.17	3D pieces designs.	31
3.18	Configuration scheme.	32
3.19	Resulted phantom configuration.	33
3.20	Final configuration.	33
3.21	DC motor with encoder and gearbox [61].	34
3.22	DC motor components [62].	34
3.23	Oscilloscope capture [61].	35

3.24	Arduino Due board [63].	36
3.25	X-NUCLEO-IHM04A1 expansion board.	37
3.26	Connection scheme.	37
3.27	Distance respiration function.	39
3.28	4.5 seconds frequency rate plot.	40
3.29	2.25 seconds frequency rate SI motor plot.	42
3.30	3.5 seconds frequency rate SI motor plot.	42
3.31	4.5 seconds frequency rate SI motor plot.	42
3.32	5 seconds frequency rate SI motor plot.	42
3.33	2.25 seconds frequency rate AP motor plot.	44
3.34	3.5 seconds frequency rate AP motor plot.	44
3.35	4.5 seconds frequency rate AP motor plot.	44
3.36	5 seconds frequency rate AP motor plot.	44
3.37	PID controller scheme [65].	45
3.38	Proportional action results [64].	46
3.39	Integral action results [64].	47
3.40	Derivative action results [66].	48
3.41	SI diagrams after first modification.	50
3.42	AP diagrams after first modification.	51
3.43	SI diagrams after second modification.	53
3.44	AP diagrams after second modification.	54
3.45	SI diagrams after last modification.	55
3.46	AP diagrams after last modification.	56
3.47	SI motor, 3.5 seconds frequency rate tuning.	58
3.48	SI motor, 4.5 seconds frequency rate tuning.	59
3.49	SI motor, 5 seconds frequency rate tuning.	60
3.50	SI motor, 2.25 seconds frequency rate tuning.	61
3.51	AP motor, 2.25 seconds frequency rate tuning.	62
3.52	AP motor, 3.5 seconds frequency rate tuning.	63
3.53	AP motor, 4.5 seconds frequency rate tuning.	63
3.54	AP motor, 5 seconds frequency rate tuning.	64
4.1	Cut lungs.	65
4.2	34:1 motor in SI movement results.	66
4.3	9.68:1 motor in AP movement results.	67
4.4	Polypropylene sheets.	67
4.5	New equation diagrams.	70
4.6	34:1 motor in AP movement results.	71
4.7	34:1 motor in AP movement results with polypropylene sheets.	72
4.8	Bent plastic sheets.	72
4.9	9.68:1 motor in SI movement results.	73

List of Tables

2.1	Respiratory rate by age [35].	14
3.1	Densities in Hounsfield units [53].	22
3.2	Encoder wires code.	35
3.3	Pin connections.	38
3.4	Selected points to describe SI movement of 4.5 seconds period.	39
3.5	Selected points as displacement for SI movement and 4.5 seconds period.	40
3.6	Motor values for SI movement.	41
3.7	Motor values for AP movement.	43
3.8	Summary of controller values.	64
4.1	Desired position (in centimeters) in each movement and frequency rate.	68
B.1	Discarded material costs.	87
B.2	Useful materials costs.	88
B.3	Total materials costs.	88
B.4	Total technical costs.	88
B.5	Total human resources costs.	89
B.6	Total budget.	89

List of Acronyms

INE: Instituto Nacional de Estadística.

AP: Anterior-posterior.

SI: Superior-inferior.

DC: Direct current.

PLA: Polylactic acid.

CPR: Cardiopulmonary resuscitation.

PVC: Vinyl polychloride.

GECP: Grupo Español de Cáncer de Pulmón.

CT: Computed tomography.

MR: Magnetic resonance.

PWM: Pulse-width modulation.

HU: Hounsfield units.

Chapter 1

Introduction and Objectives

1.1. Introduction

In 2020, lung cancer was the cancer which caused the most deaths worldwide, 1.8 million of deaths (Figure 1.1) [1]. In Spain, regarding the data measured from January to May by the Instituto Nacional de Estadística (INE), this kind of cancer was also the deadliest one, causing 9143 deaths, which correspond to almost 20% of all cancer deaths. Moreover, it doubles the number of deaths of the next most deadly tumor in these months of 2020 [2].

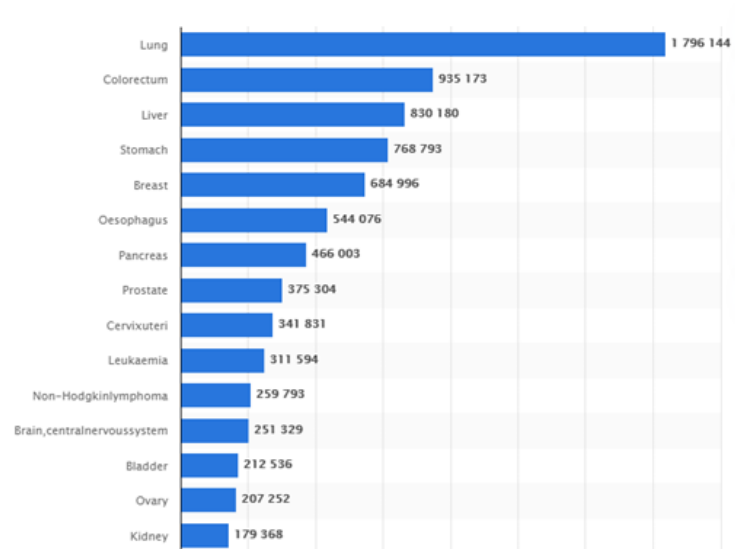


Figure 1.1: Number of deaths worldwide in 2020 depending on the type of cancer [1].

Moreover, the GECP (Grupo Español de Cáncer de Pulmón) has highlighted from the INE report that, without the impact of Covid, lung cancer would be the fourth leading cause of death globally in both sexes and the first among men, above cardiovascular diseases. In total, around 23,000 people die each year in Spain from this disease [2]. Therefore, these data show the real mortality problem in lung cancer and the need for an action program to improve it.

Nowadays, some efforts have been focused on smoking prevention since it is the main trigger of the disease. In this regard, from the 1990s to this day, the percentage of smokers has fallen significantly. However, since 2010 the decreasing slope has been much slower, which could mean that the current smoking prevention is not working as it should [3]. Thus, it becomes relevant to invest effort in lung cancer treatments.

The most used treatments for lung cancer are surgery, radiotherapy, and chemotherapy. Surgery is the most common, but sometimes it is not recommended since it could involve some risks for the patient, or the tumor could be in a difficult place in the lungs to be removed. Therefore, in these cases it is preferable to treat the cancer with radiotherapy.

Usually, in radiotherapy treatments it is necessary to perform a previous simulation to determine parameters which depend on the type, location and extension of the lung, and the patient's anatomy. In this simulation, CT scanners are used to visualize the tumor and the surrounding tissues in each patient, and the appropriate dose is calculated [4]. In addition, in case of lung cancer, the treatment planning must consider that the tumor will be moving in each patient's breathing. This movement cannot be easily measured. Therefore, during radiotherapy treatment, a considerably larger beam than would be necessary to reach the tumor is projected. The aim of this is to hit the tumor wherever it moves during respiration, but it causes many healthy lung cells to be damaged with corresponding consequences and side effects [5].

In this way, some lung phantoms appeared with the aim of studying the tumor trajectories. The phantoms with this purpose are structures made of material with similar densities to human body and programmed to move as a human thorax while breathing. That allows to study the path of a tumor in lungs depending on where it is located. Therefore, it can be used to describe a track for the radiotherapy beam, affecting as less as possible to the healthy cell around the tumor.

1.2. State of the art

Thorax phantoms are mainly used to study pulmonary edema, lung cancer and breast cancer. Depending on those cases different features are implemented in the phantom. For example, in case of pulmonary edema studies, the main goal is to evaluate the elastic properties of the lung and the use of ultrasound instead of CT scan to visualize the edema in a less expensive and more effective way [6][7].

On the other hand, in case of breast cancers, different studies have been done with phantoms. Most of these research have been developed to evaluate the use of microwaves for the detection the tumors, since it is considered a promising technique [8][9].

Then, the implementation of a thorax phantom in lung cancer has been carried out, on the one hand, as studies to evaluate new imaging detection methods [10]. On the other hand, to simulate human respiration and to visualize the trajectory of the tumor depending on its location in lungs [11][12][13].

In this way, the main problem found in research about the implementation of lung phantoms has been their simplicity. The designs have not simulated properly

the complex of human respiration, such as the external and internal deformation, the variable hysteresis, and the variable correlation between different parts of the thoracic anatomy. Studies carried out in this field over the years will be explained in the following paragraphs.

First of all, in 2006 Nioutsikou et al. [11] contributed by developing a deformable phantom composed of two accordion-type flexible bottles which simulated lungs mounted inside a container. A solid cylindrical “tumor” with several clefts to hold dosimetric films was placed into one of the bottles and the tumor was linked to a 3D position and it was moved according to a programmed 3D trajectory.

After that, Kashani et al. in 2007 [12] implemented a phantom made of simple materials which made it easy to build. In addition, it was combined with standard components for imaging and motion studies. The phantom was used for experiment both diagnostic imaging and dosimetry. It was made by inserting foam infused with iodine inside a rigid commercial thoracic phantom (RS-330; Radiology Support Devices; Long Beach, CA). The deformable interior was compressed and decompressed to simulate the SI motion of respiration.

Moreover, Remmert et al. [13] in 2007 used porcine heart–lung explants to build a rigid and deformable lung phantom with periodic motion to evaluate a 4D-MR imaging method. In this case, a vacuum pump was connected to the container to expand the lung. In addition, a water-filled silicon balloon which could be inflated and deflated by another pump was inserted into the container simulating the diaphragm.

In 2008, Serban et al. [14] developed a phantom which consisted of a Lucite cylinder stuffed with water containing a latex balloon filled with moistened natural sponges. The balloon was attached to a piston which simulated the human diaphragm. Moreover, nylon wires and Lucite beads were glued in the sponges emulating vascular and bronchial bifurcations. This phantom was programmed simulating irregular breathing patterns with varying periods and amplitudes; and a tissue equivalent tumor was embedded in the sponge. The piston moved in three different stages of compression, and the trajectory of the tumor was evaluated. In this case, the phantom was externally rigid and internally deformable, and it was later modified to emulate the respiratory motion while the delivered dose was measured at different positions in a tumor in real time [15].

Another deformable phantom was developed by Chang et al. in 2010 [16]. In this case, the phantom was an acrylic cylinder filled with water and a latex balloon located in the inner space of the cylinder. A silicon membrane was attached to the inferior end of the phantom to simulate a real diaphragm and to reduce workload of the motor. The main purpose of this configuration was to reduce the metal use to prevent infrared sensing.

Then, in 2012 Niu et al. [17] implemented a deformable phantom using gel dosimeters. In this case, gold seeds that have been used for image-guided prostate cancer radiotherapy were implanted in the gel for motion tracking and an actuator was used to apply sinusoidal compressions to the gel.

At the same time, Steidl et al. in 2012 [18] developed a phantom which consisted of an artificial thorax with ribs to introduce density changes. The contraction was controlled by a stepping motor. A robotic driven detector head positioned inside

the thorax simulated the lung tumor. The phantom's breathing and the 6D tumor motion (3D translation, 3D rotation) was programmed independently and adjusted online. This flexibility allowed to study the dosimetric effects of correlation gaps between internal and external motions, irregular breathing, or baseline drifts.

All the phantoms described above were based on a rigid exterior shell and a deformable interior. In contrast, Court et al. [19] in 2010 implemented a deformable-deformable phantom with a flexible resin model tumor based on a CT image of a real patient's tumor. This model was inserted into a dynamic breathing phantom (Radiology Support Devices, Inc., Long Beach, CA). Both the pump that inflates and deflates the lung phantom and the motor that drives the tumor were programmed according to the real patient's respiratory motion trajectory.

Therefore, in last years the main goal have been the implementation of a deformable-deformable lung phantom. In this sense, Cheung et al. [20] in 2015 used a commercially available lung phantom (RS-1500, RSD, Inc.) as a shell, and foams to implement their phantom. The shell had a chest cavity with a flexible anterior surface, with an embedded vertebra, ribcage, and sternum. They used a piece of natural latex foam block, and a motion platform was programmed to perform sinusoidal movement. This platform drove a rigid foam "diaphragm" that compressed/decompressed the phantom interior. They looked for the reproducibility and the external-internal correlation of external and internal marker trajectories extracted from kV x-ray fluoroscopy in order to validate the geometric accuracy of the VisionRT surface photogrammetry system; validate an image registration tool, NiftyReg; and quantify the geometric error due to irregular motion in four-dimensional computed tomography (4DCT). This prototype is shown in Figure 1.2:

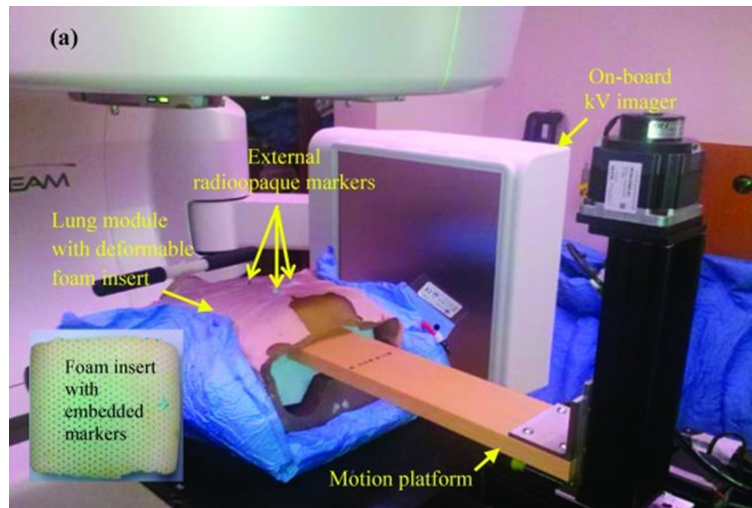


Figure 1.2: Cheung et al. lung phantom [20].

In a similar way, in 2019, Ranjbar et al. [21] used natural latex foam inserted inside an outer shell of a commercially available lung phantom (RSD, Long Beach, CA). Then, spherical glass marbles (as radiopaque markers) were placed in the foam

along the phantom midline. Two independently programmable linear actuators of high-precision were used to reproduce the anterior–posterior (AP) and primarily superior–inferior (SI) in order to enable the variable correlation between the displacement of interior volume and the exterior surface, independent changes in the amplitude of the AP and SI motions, and variable hysteresis. In this case, the ability of the phantom to produce the desired motion accurately and reproducibly was evaluated by programming the two actuators with mathematical and patient-recorded lung tumor motion traces and recording the trajectories of several markers using kV fluoroscopy. The structure of this phantom is indicated in Figure 1.3:

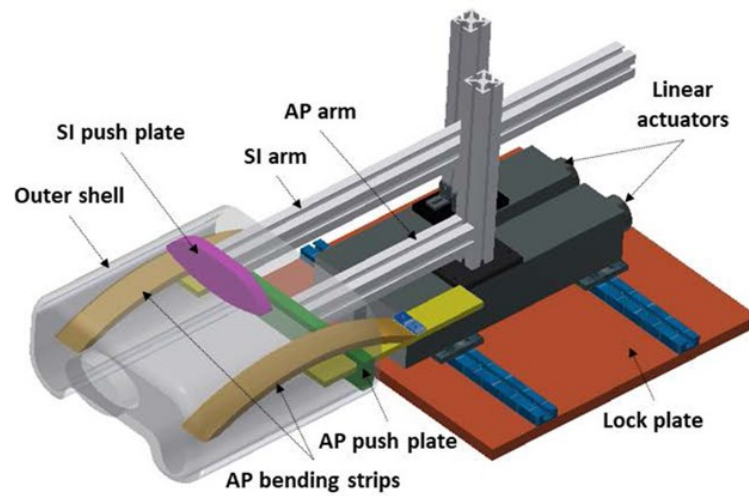


Figure 1.3: Ranjbar et al. lung phantom [21].

1.3. Objectives

This project has been performed with the help of the “Fundación para la Investigación Biomédica Puerta de Hierro”, located at the Hospital Universitario Puerta de Hierro. It started as an internship in which the main goal was to find the accurate material to build the phantom, and it continues in this study with the definitive construction of the phantom, the implementation of the mechanism and the programming of the motors to simulate the respiration.

Therefore, the main goal of the project has been the design and implement a thoracic phantom that adequately simulates human breathing. The design will take into consideration the failures previously made in the construction of phantoms. It seeks to capture as accurately as possible the internal and external deformation and the correlation of the movements of the thoracic anatomy.

In this case, it is necessary to define subobjectives which allow to achieve the main goal. These subobjectives are:

- To find materials with different densities to mimic the densities inside the human thorax and be able to reproduce the human breathing as accurate as possible. Those materials must be a low-density material to simulate lungs, a water-density material for soft tissues, and high-density material for bones and muscles.
- To insert in the phantom several markers to be able to observe their trajectories during respiration.
- To design and build a structure which allows to reproduce the human breathing by using two linear motor actuators.
- To program a reproducible movement considering different breathing patterns depending on each patient and simulating internal and external deformations.

1.4. Document structure

After this introduction, the document is followed by four different parts:

- Section 2: Clinical Background is a theoretical framework in which the aspect of the respiratory system that could be necessary to understand before simulating the human breathing are explained; as well as important aspects about cancer, lung cancer and radiotherapy.
- In Section 3: Materials and Methods, all the implementation of the phantom, including the material research, the built of the mechanical platform and the programming of the two actuators is explained.
- In Section 4: Results, the tests and obtained results are related and analyzed, and some adjustments are carried out.

- In Section 5: Conclusions, after the results of the construction of the lung phantom, conclusions are explained.

Chapter 2

Clinical Background

2.1. Respiratory System

The respiratory system is the set of organs and tissues responsible for the gas exchange and breathing. It includes different parts: the airways, the lungs, the muscles and bones, and others.

The airways, shown in Figure 2.1, are comprised by the mouth and nose, which pull air from the outside into the body; the sinuses, that regulate the temperature and humidity of the air; the pharynx, in charge of deliver the air from the mouth and nose to the trachea; and the trachea, which is the duct connecting throat and lungs [22].

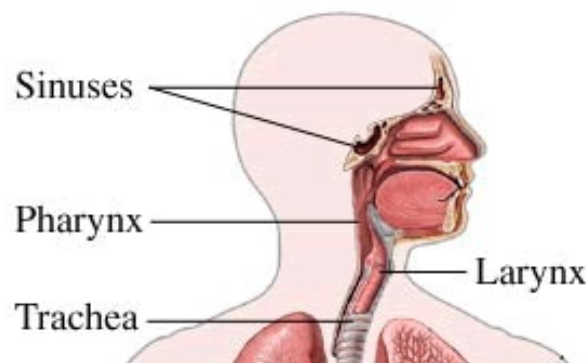


Figure 2.1: Respiratory system anatomy: Airways [23].

On the other hand, lungs are two organs with spongy texture whose main function is to develop the gas exchange from the environment into the bloodstream. In this way, oxygen is transported through the airways in the lungs into the capillary network and pass into the arterial system, ultimately reaching the tissues.

Lungs are next to the trachea. The trachea is divided into the bronchi, which branch into smaller and smaller airways. This is called the bronchial tree, and at the end of these bronchial trees are tiny air sacs, the alveoli, where the gas exchange takes place [24]. A schematic draw is shown in Figure 2.2.

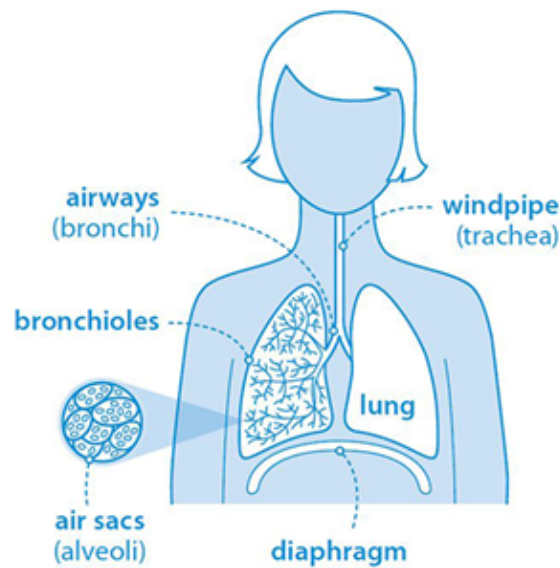


Figure 2.2: Respiratory system anatomy: Lungs [24].

Different volumes and capacities have been described in lungs [24]:

- Tidal volume (TV): Volume inspired and expired in each breath.
- Inspiratory reserve volume (IRV): Volume that can be breathed after a normal inspiration.
- Expiratory reserve volume (ERV): Volume that can be expired after a normal breath.
- Residual volume (RV): Volume remaining in lung after maximal expiration.
- Inspiratory capacity (IC): Volume that can be breathed after normal exhalation.
- Functional residual capacity (FRC): Volume remaining in the lungs after normal expiration.
- Vital capacity (VC): Maximum volume able to be expired after maximal inspiration.
- Total lung capacity (TLC): Volume of air in the lungs after maximal inspiration.
- Forced expiratory volume (FEV₁): Volume that can be expired in 1 second of maximum forced expiration.

They are shown in Figure 2.3:

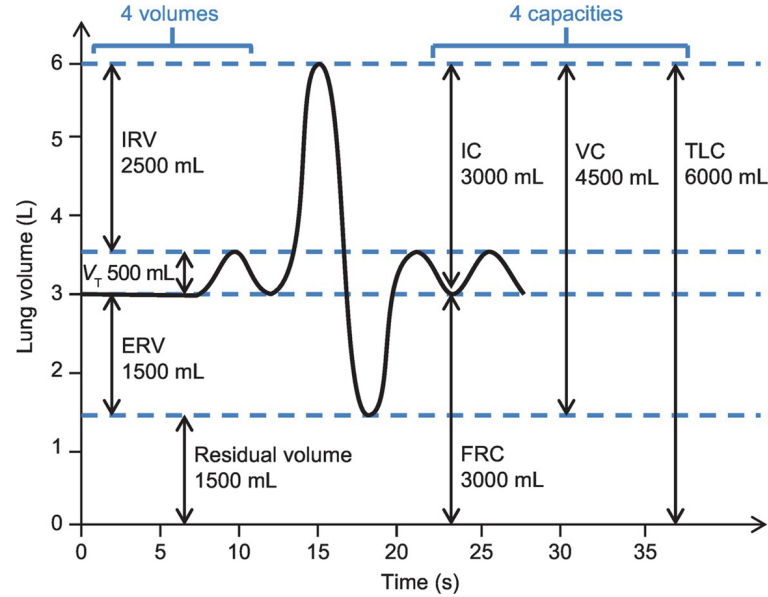


Figure 2.3: Lung volume and capacities [25].

After that, regarding the muscles and bones involved in respiration, it is remarkable the function of diaphragm and ribs.

The diaphragm is a dome-shaped muscle located just below the lungs and heart, and contracts and expands continuously with each inhalation and exhalation. These diaphragm movements allow air to enter the lungs by creating a vacuum effect.

Therefore, during inhalation it contracts and flattens, and, during exhalation, it relaxes, and the air is pushed out of lungs. At rest, the diaphragm moves about 1 cm, while during forced inspiration and expiration, the movement can be up to 10 cm.

The diaphragm is also involved in non-respiratory functions, for instance, it increases the abdominal pressure to help to eliminate vomit, urine, and feces. Moreover, it prevents acid reflux in esophagus by placing pressure in it [26].

On the other hand, ribs are the bony framework in thoracic cavity. There are twelve pairs of ribs, and most of them articulate posteriorly with two thoracic vertebrae by the costovertebral joint. According to their attachment to the sternum, it is possible to define three groups: true, false, and floating ribs. True ribs are the first seven ribs, and they are directly articulate with the sternum with their costal cartilages. The false ribs are the eighth, ninth and tenth ribs, which are indirectly articulate with the sternum since their costal cartilages are joined to the seventh costal cartilage. Last, floating ribs are the distal two ribs, that do not articulate with the sternum at all.

Therefore, this structure has a critical function. First, they protect organs in the thoracic cavity and mediastinum. Second, they move superiorly, inferiorly, anteriorly, and posteriorly allowing and facilitating breathing. Third, they are the structure where several muscles are originated and attached. Last, they are critical in erythropoiesis during development.

Regarding respiration, ribs play an important role since their flexibility during breathing allows to increase and decrease the size of the thoracic cavity. These movements are related to diaphragm, external intercostals and the intercartilaginous portion of the internal intercostals movement [27].

Therefore, external intercostal muscles are placed from the inferior border of rib above to the superior border of rib below; and internal intercostal muscles goes from the costal groove (lower part of inner surface of rib near the inferior border) of the rib above to the upper border of rib below. During breathing, these muscles contract and pull the rib cage upward, expanding the thorax and filling the lungs with air [28]. The different parts of the thorax are shown in Figure 2.4:

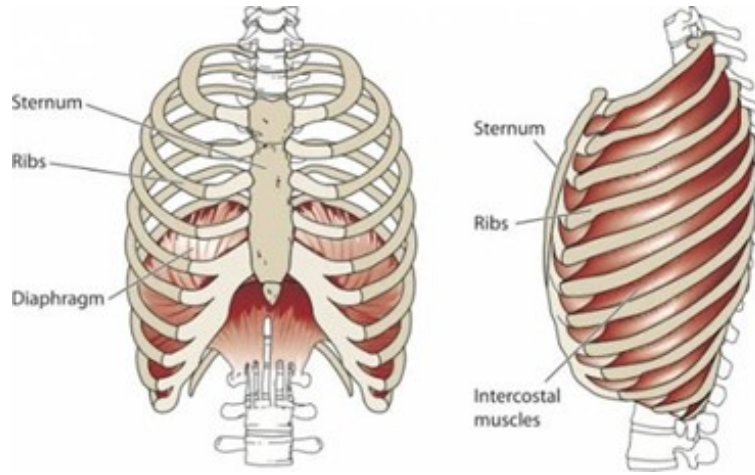


Figure 2.4: Respiratory system anatomy: Thorax [29].

Last, in respiratory system there are other components involved. These are the cilia, which move in a wave-like motion to filter dust and other irritants out of the airways; the epiglottis, placed on the entrance to the trachea and it closes during swallow to keep food and liquids out of the airways; and larynx, which allows to talk and produce sounds when air moves in and out.

After that, regarding the properties of the respiratory system, the four significant aspects in this field are lung compliance, chest wall compliance, respiratory rate, and airway resistance. These elements work in conjunction and create a negative pressure in lungs and pleural space, allowing the air, as was mentioned before, to be drawn into the lungs. In doing so, while lung volume decrease, pressure in lung is increased and air is forced out [30].

Generally, the compliance of a system is the changes in volume due to changes in pressure. In other words, compliance could be defined as the ease with which an elastic structure stretches. Regarding to pulmonary compliance, it is the total compliance of both lungs, measuring the extent to which the lungs will expand for each unit increase in the trans-pulmonary pressure. Therefore, it is defined as:

$$C = \frac{V}{(P_{alv} - P_{pl})} \quad (2.1)$$

Where, C is lung compliance, V is lung volume, P_{alv} is alveolar pressure, and P_{pl} is pleural pressure.

Transpulmonary pressure is the pressure gradient between the inside alveolar pressure and the outside pleural pressure. It mainly measures the force of lung elasticity at each point of respiration. On the other hand, alveolar pressure is the air pressure inside the alveoli. In healthy adults, the total compliance of both lungs is about 200 ml/cm H₂O.

When different measures of the lung volume are taken at specific pressure points and then plotted on a diagram, a pressure-volume curve representing both elastic and airway resistance properties of the lung is obtained. This compliance is truly important since it determines 65% of the work of breathing. If lungs have low compliance, they require more effort from breathing muscles to inflate the lungs. Therefore, in specific pathologies, the lung compliance curve is useful to diagnose them and to understand the progression of the conditions [31]. An example is shown in Figure 2.5:

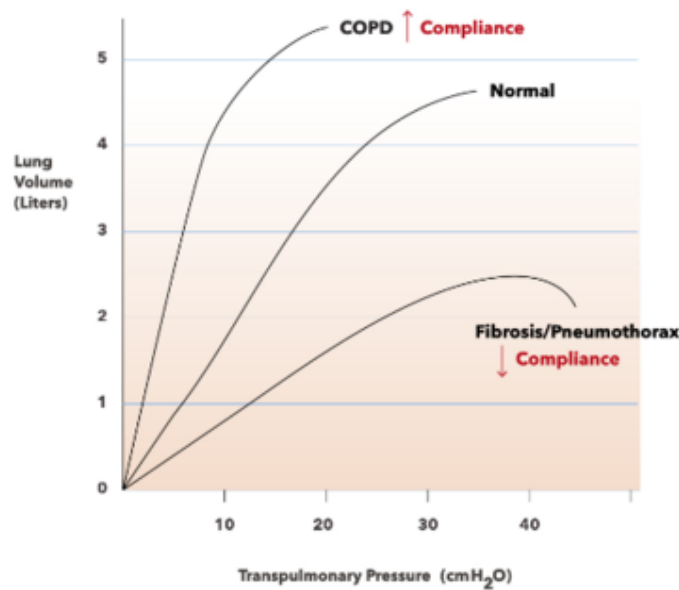


Figure 2.5: Expiration compliance curves for chronic obstructive pulmonary disease (COPD), normal, and Fibrosis/Pneumothorax [32].

Actually, Figure 2.5 not only represents lungs compliance, but it is the result of lung compliance and chest wall compliance, which counteracts the force of lung compliance, attempting to increase lung volume (contrary to lung compliance where the lungs attempt to decrease volume) [30]. Lung and chest lung compliance are shown in Figure 2.6:

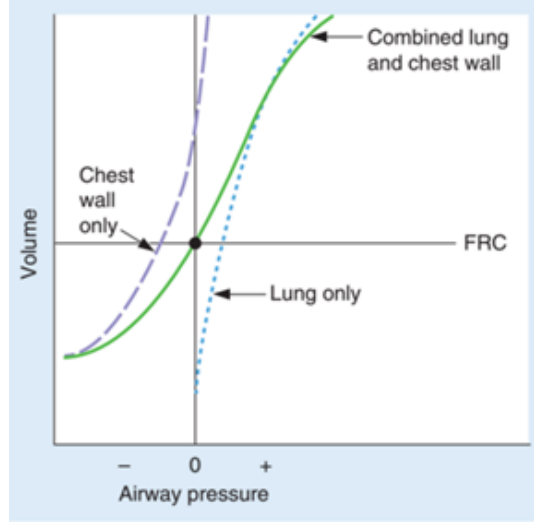


Figure 2.6: Lung and chest wall compliance diagram [33].

On the other hand, it is important to define the respiratory rate, an aspect which will be essential in the development of this project.

The respiratory rate (RR) is one of the human vital signs that need to be monitored in clinical and non-clinical applications for diagnosis and control purposes [34]. This rate describes the number of breaths per minute, understanding as breath the number of inhalations followed by an exhalation. It can vary depending on the age of the person, being in children higher than in adults, as it shown in Table 2.1:

Age	Normal Respiratory Rate
1 year	30 to 40
2 - 5 years	20 to 40
6 - 10 years	15 to 25
11 - 18 years	15 to 20
18 - 70 years	12 to 20
> 70 years	15 to 20 years

Tabla 2.1: Respiratory rate by age [35].

Another significant aspect in the respiratory system is the airway resistance. This can be described by Poiseuille's law [30], which states:

$$R = \frac{8nl}{\pi r^4} \quad (2.2)$$

Where R is the resistance, n the viscosity of air, l the length of the airway, and r the radius of the airway. It is essential to note the inverse fourth power relationship between the radius of the airway and the resistance, which means that small adjustments in airway radius will substantially alter their resistance.

Normal breathing

The four aspects described above have an important role in the respiratory mechanics. Therefore, aforementioned, our main goal is to reproduce the normal breathing, thus it will be necessary to understand which movements will take place [36].

In normal breathing at rest, there are small in breaths (inhalation) followed by the out breaths (exhalation) and then followed by an automatic pause (or period of no breathing) [36].

Diaphragm is the main muscle during inhalation, and intercostal muscles and some muscles in the chest and neck work as accessory muscles of breathing, which can become active to increase air flow in and out of the lungs. Exhalation is passive, thus there is no active muscle activity, and it is due to the natural elastic recoil of the lungs, complemented by the relaxation of all breathing muscles [36].

Therefore, at rest, the normal breathing takes 1 to 1.5 seconds for inhalation; 1.5 to 2 seconds for exhalation; and 1 to 2 for an automatic pause. Moreover, exhalation is slightly longer than inhalation [36].

Furthermore, during normal breathing around 500-600 ml of air are breathed (Tidal Volume mentioned before). This breathing is characterized for a slow and regular movement in which air goes only through nose, the diaphragm moves gently, and it is quiet. In Figure 2.7, this pattern is shown:

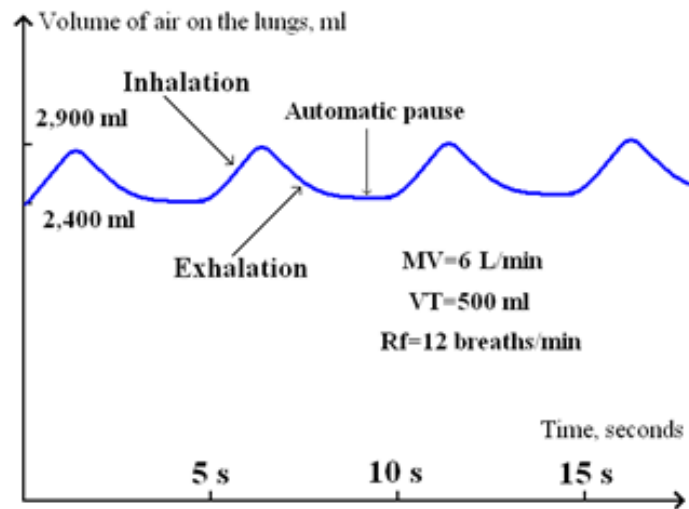


Figure 2.7: Normal breathing pattern [37].

On the other hand, it will be important to understand the thorax movements during breathing. In relaxing normal breathing, chest expansion on inspiration should be similar in each breath. The chest wall is symmetrical, and there is no paradoxical movement, in other words, the chest and abdomen move in the same direction on inspiration, and, thus, back in the same direction exhalation [38].

Regarding different studies, age, posture, and gender are analyzed in order to

determine if they could play an important role in respiratory frequency and the thoraco-abdominal movements [39]. With respect to the age, it has been demonstrated that it is not a particular factor that vary the breathing in adults. It could be considered a determining factor only for the frequency rate when differentiating between children and adults [40].

On the other hand, regarding the effect of posture in breathing, studies show that an increase in inclination of the trunk determines a reduction of rib cage displacement and an increase of abdominal contribution to tidal volume. In other words, the rib cage movements are smaller in supine position than seated, while abdominal movements are bigger in supine position than seated [41].

Moreover, other studies explain that in quiet breathing as men and women have a similar breathing movement. However, the rhythm in deep breathing is significantly different in men and women, with an inspiration/expiration ratio of 1:1.23 for men and 1:1.40 in women [40].

Therefore, considering the exceptions mentioned before, the movements of the upper level of the chest cage in anteroposterior and vertical directions, ranging from 16.7 to 28.6 mm in healthy individuals [42].

2.2. Cancer

Cancer is produced when the mechanism in body of removing and repairing cells does not work properly, and the abnormal and old cells are not eliminated. Those cells start to reproduce themselves out of control, displacing healthy cells and affecting the functionality of the organs or tissue where they are.

Nowadays it is possible to find a treatment for this disease, obtaining successful results, especially if the pathology is diagnosed in the early stages. In fact, more people than ever before lead full lives after cancer treatment [43].

There are two main categories of cancer: Hematologic cancers, which affect blood cells, including leukemia, lymphoma, and multiple myeloma; and solid tumor cancers which is found in any of the other body organs or tissues. The most common solid tumors are breast, prostate, lung, and colorectal cancers.

The different types of cancers are similar in some ways, but they can grow, spread, and respond to treatment faster or more slowly than others. Likewise, some cancers are likely treated with surgery, others with chemotherapy, and others with radiotherapy, although two or more treatments are usually used to obtain the best result.

On the other hand, it is important to know that not all lumps are cancer; they can be benign or malignant (cancer). In the case of malignant tumors, they can spread to other parts of the body while benign tumors do not [43].

Cancer is produced by multiple changes in the genes of the mutated cells. These changes are influenced by the lifestyle habits, genes inherited from parents, or for being exposed to cancer-causing agents in the environment. However, none of these

causes are totally decisive [43].

Besides that, there are different tests to diagnose and explore cancer, which are mainly: Blood and urine tests; imaging tests as X-rays, computed tomography (CT) scans, magnetic resonance imaging (MRI), radionuclide scanning and ultrasonography; and biopsy, a procedure in which a small sample of the tumor is taken and analyzed [44].

2.2.1. Lung Cancer

Lung cancer is characterized by the uncontrolled growth of abnormal cells in one or both lungs. Most lung cancers begin in the bronchial tubes that conduct air in and out of the lungs.

Regarding to the signs and symptoms of lung cancer, the most common symptoms are a persistent cough, shortness of breath and blood in the sputum (mucus coughed up from the lungs). Moreover, it can produce chest discomfort or pain, trouble breathing, wheezing, hoarseness, loss of appetite, fatigue, difficulty swallowing or weight loss [45].

The major risk factor for lung cancer is smoking. The earlier in life a person starts smoking, the more often a person smokes, and the more years a person smokes, the greater the risk of developing lung cancer. People between the ages of 55 and 79 years who have 30 pack years of tobacco exposure have the highest risk [46].

Furthermore, other risk factors include lung cancer survivors, history of pneumonia, a first degree relative that developed lung cancer before the age of 60, exposure to “secondhand” smoke, being exposed to radiation from previous radiation therapy to the breast or chest, diagnostic imaging tests like CT scans, atomic bomb radiation Radon exposure in the home or workplace, or exposure to asbestos, arsenic, soot, or tar in the workplace. Moreover, risk of cancer increases with age [45].

Regarding the diagnosis and test of lung cancer, when it is suspected, the type, the presence of biomarkers, and its spread or stage should be defined in order to determine the best treatment. Therefore, to define the presence of lung cancer and its type, a biopsy is performed. In this kind of cancer there are different ways to develop a biopsy. First, a bronchoscopy, in which a bronchoscope is inserted through the nose or mouth to the trachea and bronchi. Through this bronchoscope, it is possible to examine the inside of the trachea, bronchi and lung and collect cells or small tissue samples. Second, the fine needle aspiration, in which a needle is inserted through the chest into the cancer to remove a tissue sample for examination under the microscope. Third, the thoracentesis, which consists of using a needle to remove a sample of the fluid that surrounds the lungs to check for the presence of cancer cells. Fourth, the thoracotomy, which is a major operation, since involves opening the chest. Last, sputum cytology, a procedure that examines the coughed-up mucus from the lungs or breathing tubes [45].

In addition to diagnosing the type of lung cancer, it is important to determine the stage or the extent of the spread of the cancer, since it is a key factor in determining

the best treatment. The non-small cell lung cancer and the small cell lung cancer follow different classifications. First, the stages of non-small cell lung cancer are [47]:

- Stage 0 is an early stage only found in the top lining of the lungs and it has not spread outside them.
- Stage I divided into two sub-stages, 1A and 1B, depending on the size of the tumor and whether it has spread to the lining of the lung. In this stage, the cancer has not spread to the lymph nodes or other parts of the body.
- Stage II is divided into stage IIA and IIB, with each stage then broken into additional sections, based on the size of the tumor, where it is found, and whether the cancer has spread to the lymph nodes. These tumors may be larger than in stage I and have begun to spread to nearby lymph nodes or other structures near the lung. However, the cancer has not spread to distant organs.
- Stage III is classified as stage IIIA, IIIB or IIIC, depending on the size and location of the tumor and how far it has spread. The tumor may be hard or impossible to remove through surgery depending on where it has spread.
- Stage IV is the most advanced form of lung cancer. In this stage, the cancer has metastasized, or spread, from the lungs into other areas of the body. For most patients, there are several treatment options available for patients with advanced-stage disease.

On the other hand, small cell lung cancer is described using two stages: limited and extensive. Limited stage lung cancer is determined only in one lung or in the nearby tissue. Extensive stage lung cancer has spread to tissue outside of the originally affected lung as the opposite lung or another organ [47].

Therefore, the most used test for diagnosing and determining these stages are [45]:

- Computed Tomography (CT) Scan: A CT scan is a technique for imaging body tissues and organs, in which X-ray transmissions are converted to detailed images, using a computer to synthesize X-ray data. A CT scan is performed with a large machine positioned outside the body that rotate to capture the images.
- Magnetic Resonance Imaging (MRI): MRI uses a magnetic field which allows to distinguish between healthy and diseased tissue. Therefore, it gives better pictures of tumors located near bone than CT, does not use radiation as CT does, and provides pictures from various angles that ease to construct a three-dimensional image of the tumor.
- Mediastinoscopy: A mediastinoscopy indicate whether the cancer has spread to the lymph nodes in the chest. During this technique, a mediastinoscope is inserted through a small incision in the neck. This allows to examine the center of the chest (mediastinum) and nearby lymph nodes, as well as remove a tissue sample.

- Positron emission tomography (PET): This method has been used to improve the detection of cancer in lymph nodes. In this procedure, a substance containing a type of sugar attached to a radioactive isotope (a molecule that spontaneously emits radiation) is injected. The cancer cells take the sugar and the attached isotope, which emits positively charged, low energy radiation (positrons). The positrons react with electrons in the cancer cells producing gamma rays, which are detected by the PET machine, and the information is transported into a picture.
- Bone Scan: A bone scan is used to determine whether cancer has spread to the bones. First, a small amount of radioactive substance is injected into a vein. This substance travels through the bloodstream and collects in areas of abnormal bone growth. A scanner measures the radioactivity levels in these areas and records them on x-ray film.

After that, regarding to the treatments in lung cancer, it will depend on the type of lung cancer and how far it has spread. Therefore, in small cell lung cancer, patients are usually treated with radiation therapy (radiotherapy) and chemotherapy; while in non-small cell lung cancer, the treatment can be by surgery, chemotherapy, radiation therapy, targeted therapy, or a combination of these treatments [48].

2.3. Radiotherapy

According to our goal described in Section 1 of this document, with regard to the treatments mentioned before, we will focus our attention on the radiation therapy or radiotherapy.

This treatment is based on the use of high energy rays or radioactive substances, to damage tumoral cells and to halt their growth and division. This is produced by the direct damage of DNA or other important cellular molecules, as well as of an indirect cellular damage which occurs after the productions of free radicals. Therefore, the radiation can produce physical, chemical, biological or biochemical effects on the irradiated tissues, as emission, transfer and absorption of energy; a direct alteration of atoms and molecules or indirect damage through the productions of free radical; the breaking of bonds, polymerization or depolymerization phenomenon; molecular alterations; damage to DNA, RNA, cytoplasm or enzymes; or morpho-functional and metabolic lesions, or damage to the genetic material [49].

Thus, the main issue using radiation therapy is that normal cells, especially those which divide frequently, may also be damaged and killed by the radiation. For this reason, the radiation beam should be focus on the tumor and the total dose should be fractioned, so the healthy tissues are not damaged [49].

Regarding to the basics of radiotherapy, the most common modality used in radiation oncology is external beam radiation therapy; in which radiation can be by photons, protons, or electrons beam. The photons travel through the body, and

scatter little bits of radiation along their path. Then, when they reach the tumor, they do not stop and go into normal tissue past it. On the other hand, proton beams do not scatter radiation on their path through the body and they stop once they reach the tumor, the problem with this kind of radiation is its high cost and size of the machine. Last, electron beams cannot travel very far through body tissues. Therefore, their use is limited to tumors on the skin or near the surface of the body [50].

In case of lung cancer, it is possible to find radiation-delivery limitations. This is due to the presence of organ motion, which causes a blurring of the static dose distribution over the path of the motion. This displacement results in a deviation between the intended and delivered dose distributions. Therefore, in the radiotherapy of this type of cancer, more healthy cells are affected by the radiation, causing more damage [51].

Chapter 3

Material and Methods

As was explained in Section 1, the idea of this MSc Thesis is to develop a phantom which mimic human breathing. It is possible to divide this work into three points. Firstly, it is necessary to find materials with similar densities to the thorax densities, since the inside of the mannequin should be similar to real human to reproduce the breathing movements. Secondly, it is important to build a structure which moves the phantom by using two actuators, the first one to reproduce the anterior-posterior (AP) movements, and the second one to perform the superior-inferior (SI) movements. The scheme shown in Figure 3.1 illustrates these movements. Lastly, it is necessary to program the actuators to simulate the breathing, considering independent AP and SI movements and different respiration frequency rates.

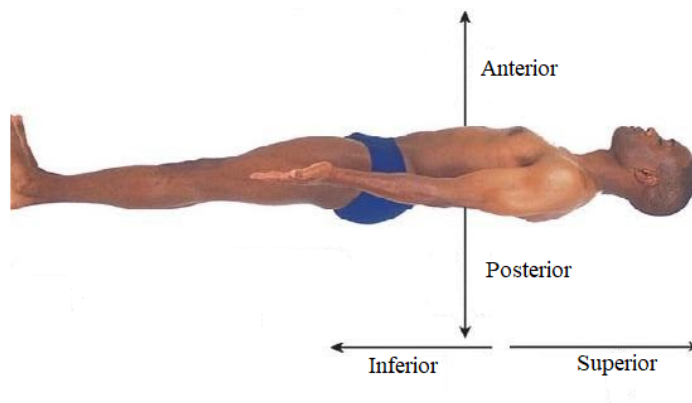


Figure 3.1: SI and AP movements scheme.

3.1. Materials

Regarding the needed materials, it has been necessary to perform a deep search in order to find mainly three different materials with water density, lower density and higher density. The water-density material has been used to simulate the soft tissue

surrounding the lungs, the low-density material has reproduced the lungs, and the high-density material has been chosen to mimic bones and muscles.

Moreover, it is important to consider the mechanical platforms which will simulate the movement, since they will be also integrated in the phantom. In this sense, another searched have been performed to find a plastic sheet that could produce the SI movements, similar to Ranjbar et al.'s phantom [21].

When a material has seemed promising, it has been measured in the hospital's CT scanner. The scanner allows to measure the different levels of radiodensity of materials, giving a result in Hounsfield units. The Hounsfield unit is calculated by a linear transformation of the baseline linear attenuation coefficient of the X-ray beam [52]. The normal densities found in human body are shown in Table 3.1.

Materials	Hounsfield unit
Air	-1000
Fat	-100 to -50
Water	0
Muscle	10 to 40
Blood	30 to 80
Bone	700 to 3000

Tabla 3.1: Densities in Hounsfield units [53].

The subsections below present the search performed to find the most suitable materials, considering in every case the importance of not including any metallic material in the phantom since it could produce disturbances on the CT scanner.

3.1.1. Soft tissue

The search for water-density material to simulate soft tissues has been the most challenging. In this case, slime was the first material evaluated to reproduce the tissues, shown in Figure 3.2. It is a material made of guar gum, viscous, soft, and non-toxic; usually sold as a toy for children. It is cheap and, apparently, it has a similar density to water. As an advantage, it is manageable, thus it would be possible to control its shape better than other more liquid materials.



Figure 3.2: Slime [54].

In order to study the material, a little amount was bought, and its mass and volume was measured at home, obtaining a similar density to water. Then, some tests of homemade slime made of toothpaste, detergent, white glue, hairspray, and cornstarch, among others, were carried out as shown in Figure 3.3. However, the results were not promising, thus commercially available slime was evaluated as the best option.



Figure 3.3: Homemade slime tests.

Despite that, a CT scan was performed to check its density in Hounsfield Units, as Figure 3.4 presents, resulting a considerably bigger density than water, around 300 HU, thus the idea of using slime was discarded.

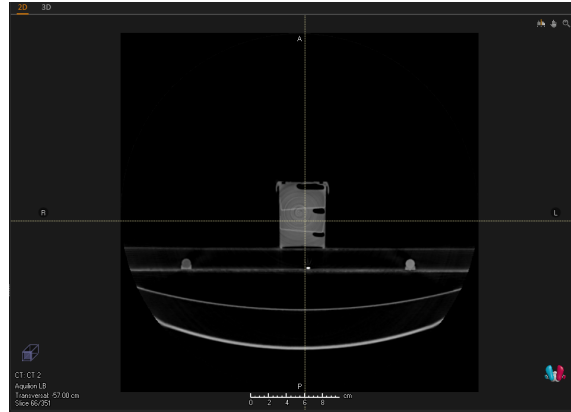


Figure 3.4: Slime CT scan.

After that, the use of agar or gelatin was considered. Agar is a natural gelling agent derived from red algae which is used specially to make desserts of gelatin form. Recently, this material has been utilized in breast phantom due to its properties and consistency [55].

In this case, different tests were performed, varying the concentration of agar in each test with the aim of obtaining a deformable but consistent result. The samples were 2gr of agar/500ml of water, 2gr of agar/250ml of water and 2gr of agar/100ml of water. In addition, another test with 6gr of gelatin/300ml of water was carried out. The most promising result was 2gr of agar/100ml of water, yet two problems were found. First, the consistency was almost perfect, but if some pressure was applied it did not deform, it broke as it can be seen in Figure 3.5. Second, as agar is an organic compound, it was affected by environmental agents e.g., fungus, and, in addition, it lost water after time.



Figure 3.5: Agar broken due to the finger pressure.

Due to these problems, agar and gelatin were discarded, and the use of resistance bags to encapsulate water or similar liquids was evaluated. In this case, the first tests were performed with camelback bags (Figure 3.6) and cold/heat bags (normally used for injuries) (Figure 3.7).



Figure 3.6: Camelback bag [56].



Figure 3.7: Cold/heat bag [57].

These materials were evaluated again with the help of the radiophysics department in Hospital Puerta de Hierro by using the CT scanner. As a result, the camelback bag filled of water has the appropriate density, -10.8 HU (Figure 3.8), and the cold/heat bag has a little bigger density, 20.6 HU (Figure 3.9), but it could be useful to simulate the mediastinum.

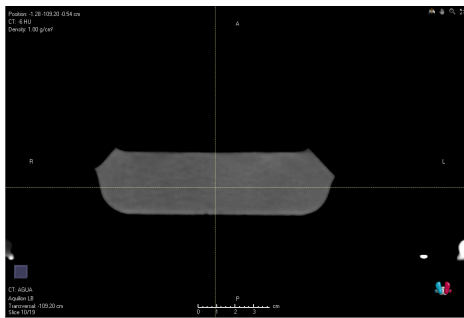


Figure 3.8: Camelback CT scan.

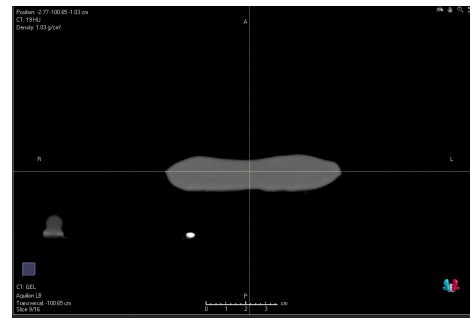


Figure 3.9: Cold/heat bag CT scan.

However, mainly in camelback bag, the problem was that it did not completely adapt to the mannequin as it had defined shapes.

Once it was proven that bags could be used to encapsulate water, a bag sealer for domestic use was purchased with the idea of manufacturing custom bags to fit the phantom. Apparently, this could be useful, but its effectiveness depended a lot on the type of plastic bag, and in most cases the joints between them end up opening. After that, the next proposal was the use of kerosene gel, a transparent gel substance used

usually in the creation of handmade candles. This material, as agar, is also employed in breast phantoms, and a problem similar to the mechanical resistance could happen, thus it was discarded.

Last, the construction of a latex mold was evaluated. The idea was to create a mold for the entire area corresponding to soft tissue, which would be filled with water. This mold was originated by a structure built with cardboard and covered by plastic. The resulted structure is shown in Figure 3.10:



Figure 3.10: Structure for latex mold.

The structure was covered by several layers of liquid latex for molds bit by bit, and once dried, it was removed from the cardboard. In this case, the latex mold could not comprise water, thus instead of filling it with water directly, it was filled by small bags of water, closed by a strong knot, and reinforced with silicone to assure any water leak. The final result together with the lungs is shown in Figure 3.20.

3.1.2. Lungs

Regarding the lungs, the search of materials was much easier than for soft tissues. Lungs are air-filled sacs; thus, their density can be approximate by the air density (-1000 HU).

For this reason, different foams were evaluated since they are materials with a significantly small density. The considered foams where [58]:

- D.20kg/m³- Soft (Moderate use backing)
- D.25Kg/m³- Half-hard (Moderate use seat)
- D.30kg/m³ Hard (Intensive use seat)
- D.40Kg/m³. Extra Hard

These materials fulfilled the density requirements. However, they presented a high mechanical resistance, thus they were difficult to deform.

Therefore, another foam with inferior density to 20kg/m^3 was evaluated. This foam is a polyurethane foam, similar to a current bath sponge. In order to evaluate its effectiveness, its density was measured in the CT scanner, getting a truly small result of -1005.5 HU as it can be seen in Figure 3.11, thus the material would be useful to simulate lungs.

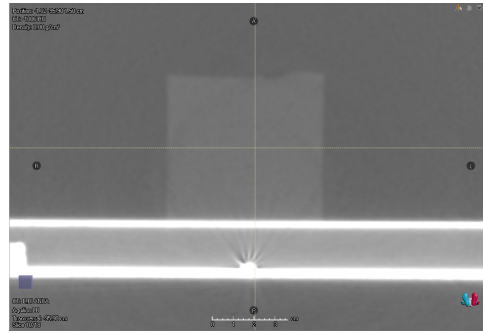


Figure 3.11: Polyurethane foam in CT scan.

As a result, the foam was cut in the shape of lungs differentiating the right and the left lung, as shown in Figure 3.12:



Figure 3.12: Lungs in polyurethane foam

3.1.3. Bones and muscles

On the other hand, it was important to consider the bones and muscles. Healthy bones have usually a bigger density than water, of around 1.25g/cm^3 . In case of muscles, the density is also bigger than water but smaller than bones, approximately

$1.06\text{g}/\text{cm}^3$ [59].

In this study, the essential elements considered were an outer shell and the diaphragm. A CPR mannequin commercially available (Maniquí RCP- AED Prestan) was chosen to simulate the outer shell (Figure 3.13). Moreover, a 3D printed piece of PLA was proposed as diaphragm. This piece was included in the mechanism for movement to simulate the breathing, thus it is shown in the following subsection.



Figure 3.13: CPR mannequin as outer shell [60].

The materials were measured in the Hospital, as shown in Figure 3.14 and it was checked that their densities were bigger than water, thus they were useful as bones and muscles.

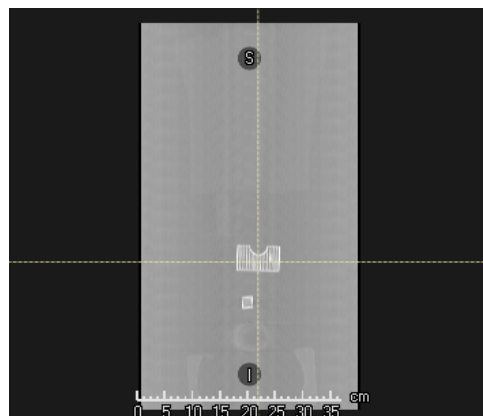


Figure 3.14: PLA in CT scan .

In addition, other bones such as the vertebrae or ribs printed in PLA were evaluated. However, they were not considered necessary, thus they were not included

in this prototype.

On the other hand, as mentioned at the beginning of this section, apart from the diaphragm to push the lungs in the AP direction, a structure to move lungs in the SI direction had to be considered. This structure was defined as two sheets on both sides of the mannequin that will flex with the movement of the mechanical platform. To find these sheets, a careful search was carried out in which the goal was to find a thin plastic that would bend and flex but strong enough to push on the lungs. As a result, it was proposed the use of a PVC plastic, shown in Figure 3.15, commonly utilized as a desk protector to avoid scratching the floor with desk chairs.



Figure 3.15: PVC plastic for desk chairs.

Then, the sheet was cut in two films of around 6cm x 50cm, shown in Figure 3.16:



Figure 3.16: Plastic sheets.

3.1.4. Markers

In addition, as in other phantoms mentioned in Section 1, the placement of marbles in certain positions were considered in order to study the trajectory that a tumor would follow during respiration by using a CT scanner. In addition, some of them should be placed inside the foams (“lungs”), and others should be located on the surface, to study the resulting internal-external correlation of the phantom movements.

3.2. Phantom configuration

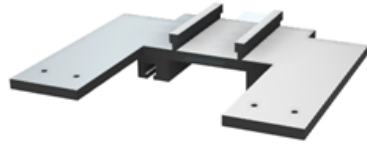
3.2.1. Mechanical structure

Once each material was defined and chosen, the next step was to design and develop the mechanical structure. The main function of the mechanical structure is to apply pressure produced by the two actuators in the “lungs” and “soft tissues”. As it was mentioned before, the goal of this MSc Thesis is to implement an AP movement and a SI movement that work independently. This means that one motor will control a movement and the other motor will produce the other movement, thus it was necessary to design a platform connected to the movement of each motor.

In this case, to minimize the necessary space for the structure, the platform for SI movement will be sliding on the platform that produce the AP movement.

The structure is formed by 3D pieces printed in PLA, pulleys, and belts. Therefore, the motor movements are transferred to the 3D pieces through the pulley system, and they will push the elements inside the mannequin.

The software Autodesk Fusion 360™ was used for the design of the 3D pieces, which are shown in Figure 3.17 (detailed in Appendix C):



(a) AP platform.



(b) SI platform.



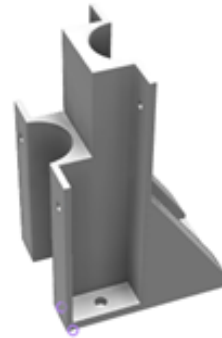
(c) Diaphragm.



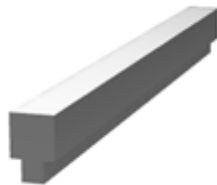
(d) Supporting structure for pulleys.



(e) Supporting structure for AP motor.



(f) Supporting structure for motors.



(g) Rail

Figure 3.17: 3D pieces designs.

AP platform, shown Figure 3.17a, will be moved forwards and backwards by one of the motors. This piece has two little cylinders in the middle in which the belt will be attached. Therefore, the circular movement of the motor will be transformed in

horizontal movement. On the other hand, the two plastic sheets will be joined by screws at the end of the piece, and they will flex while the piece moves. At the top of the piece there are two rails which will train the SI platform; and at the bottom there are hollows for the rails that will guide this platform

The functionality of SI platform, which is presented Figure 3.17b, is similar to the functionality of AP platform. In this case, it will be attached to the pulley of the second motor by a belt, and it will move also forwards and backwards. Two sticks will be pasted into the two cylindrical hollows, and they will be attached to the diaphragm piece, transferring it the movement.

The diaphragm piece (Figure 3.17c) will be moved due to the movement of the SI platform. This piece will be in charge of squashing the foams that simulate the lungs. Its shape, smaller in the sides, has been defined in order to allows the AP movement of the two plastic sheets.

The supporting structure for pulleys, shown in Figure 3.17d, will be located between the platforms and the mannequin. This structure will contain two pulleys attached by screws and the belts for SI and AP movements will pass through these pulleys. The supporting structure for the AP motor, exposed in Figure 3.17e, is joined to the supporting structure for motors, presented in Figure 3.17f. These pieces will maintain the motors in the desired position and will be able to resist the force exerted by the belts in the motors.

The rails (Figure 3.17g), as aforementioned, will guide the AP platform. They are two pieces attached to the ground by screws.

3.2.2. Assembly of the phantom

Once the pieces were printed and the other materials were acquired, the assembly of the phantom were carried out. Therefore, the mannequin and the rails were bolted to a wooden board. Then, the 3D printed pieces were attached, and the pulleys and belts were joined and inserted in the structure. The Figure 3.18 shows the configuration planned:

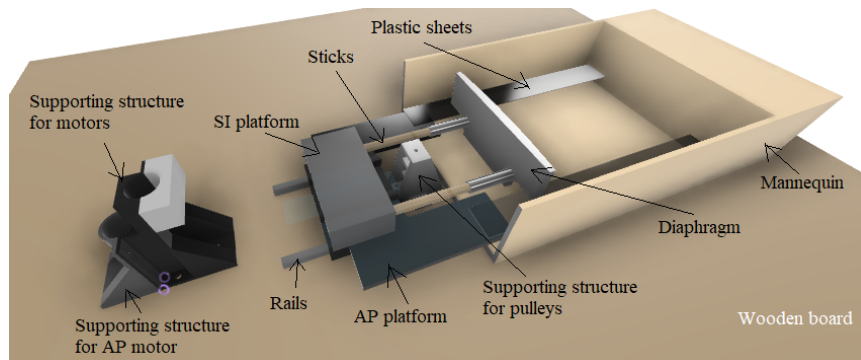


Figure 3.18: Configuration scheme.

To ensure that the two plastic sheets were bent, screws were placed at the end of the phantom and the sheets were leaned on it. In addition, small pieces of polystyrene were placed underneath the plastics to further promote the slightly bent position in rest position. The configuration resulted is shown Figure 3.19:



Figure 3.19: Resulted phantom configuration.

After that, the foam as lungs were inserted in the latex mold, and the bags of water were placed surrounding them. Then, this structure was inserted in the phantom as it can be seen in Figure 3.20.



Figure 3.20: Final configuration.

3.3. Movement implementation

3.3.1. Electronic components

Once the structure was built, the next objective was to simulate the breathing motion. For this purpose, the two DC motors were used, one to simulate the AP motion and one for the SI motion. In both cases, the motors were actuators with integrated magnetic encoder and gearbox in their shafts as shown in Figure 3.21:



Figure 3.21: DC motor with encoder and gearbox [61].

DC motors convert electrical energy into mechanical energy. They contain two parts, the stator and the rotor. The stator is where the magnet poles are located, and the rotor is the moving part of the motor, to which the current arrives through the brushes (Figure 3.22). When electric current flows through the coils of the motor, the electromagnetic field interacts with the magnetic field of the permanent magnet. If the poles of the permanent magnet and the rotating electromagnet coincide, a rejection and a magnetic torque is produced, which causes the rotor to break the inertia and start to rotate. To change the direction of rotation of the rotor, it is necessary to change the direction of the current provided to the rotor, inverting the polarity of the battery [62].

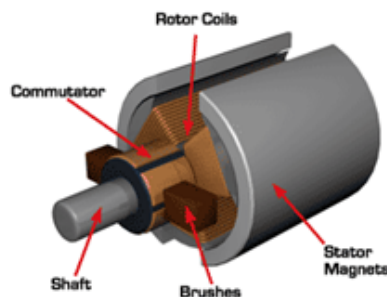


Figure 3.22: DC motor components [62].

Regarding the encoders, a two-channel Hall effect sensor is used by the gearmotors with encoders. It notices the rotation of the magnetic disk on a rear protrusion of the motor shaft and provides a resolution of 48 counts per revolution of the motor shaft by counting both edges of both channels. Therefore, by multiplying the gearbox reduction ratio of the motor by 48 it is possible to compute the counts per revolution of the gearbox output [61].

The encoder has six color-coded wires, as shown in Table 3.2:

Color	Function
Red	Motor power terminal (+)
Black	Motor power terminal (-)
Green	Encoder GND
Blue	Encoder Vcc
Yellow	Encoder A output
White	Encoder B output

Tabla 3.2: Encoder wires code.

The Hall sensor of the encoders requires an input voltage Vcc, between 3.5 and 20 V. The A and B outputs are 90° out of phase square waves from 0 V to Vcc. Therefore, the speed of the motor is indicated by the frequency of the transitions, and the order of them reveals the direction. Figure 3.23 shows an oscilloscope capture of the A and B encoder outputs, in yellow and blue respectively, using a motor voltage of 6 V and a Hall sensor Vcc of 5V [61].

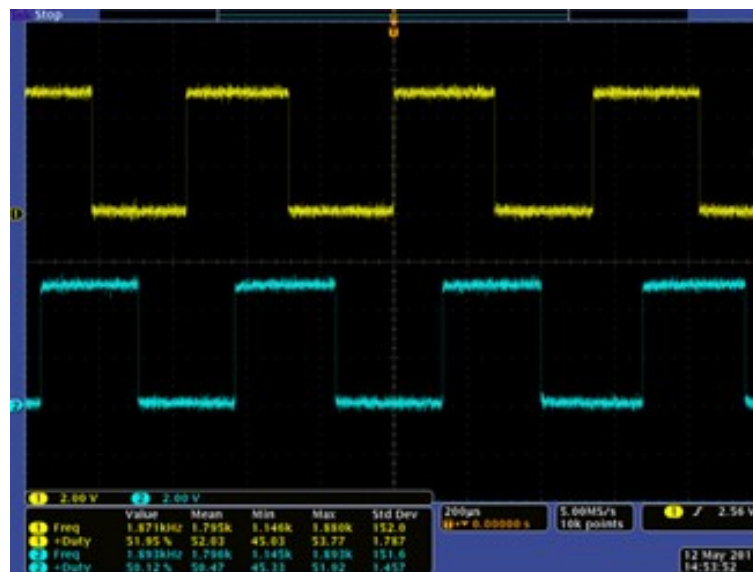


Figure 3.23: Oscilloscope capture [61].

By considering the rising and falling edges of A and B outputs, it is possible to get 48 counts per revolution of the motor shaft.

Regarding the gearbox, in this case the motors used were those available in the laboratory. They had 9:1 gear ratio and 34:1 gear ratio, used for SI motion and AP motion, respectively.

Then, to configure the two actuators, a microcontroller Arduino Due have been used. The Arduino Due (Figure 3.24) is a microcontroller board based on the Atmel SAM3X8E ARM Cortex-M3 CPU. It works at 84Mhz (3.3V) providing a much higher computing power than other microcontrollers. It is the first Arduino board based on a 32-bit ARM core microcontroller allowing to perform operations on 4-byte data in a single clock cycle. It has 54 digital input/output pins (of which 12 can be used as PWM outputs), 12 analog inputs, 4 UARTs (hardware serial ports), an USB OTG capable connection, and 2 DAC (digital to analog), among other. In addition, the board is compatible with all Arduino shields that work at 3.3V [63].



Figure 3.24: Arduino Due board [63].

DC motors cannot be controlled by an Arduino board by itself since the board provides less current than the motor needs. That is the reason why a motor drive expansion board is needed. In this case, the X-NUCLEO-IHM04A1 (shown in Figure 3.25) connected to the Arduino Due board has been used. The X-NUCLEO-IHM04A1 is a dual brush DC motor drive expansion board based on the L6206 (DMOS dual full bridge driver). It is able to drive dual bipolar DC or quad unipolar DC motors.

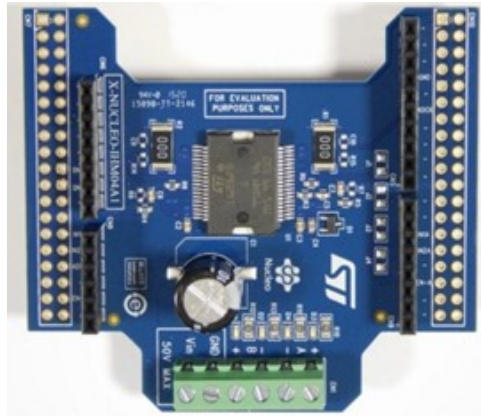


Figure 3.25: X-NUCLEO-IHM04A1 expansion board.

Therefore, these electronic components are connected as Figure 3.26 shows:

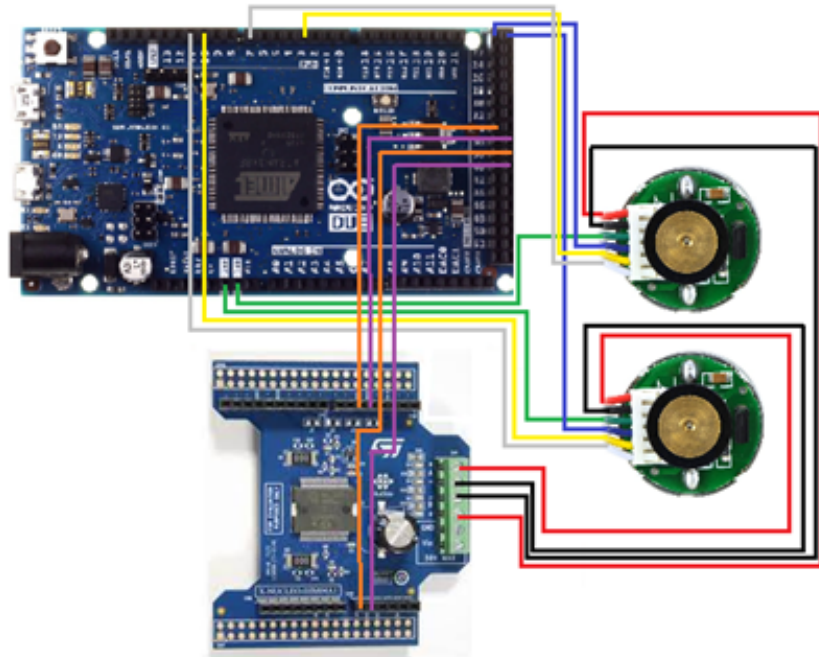


Figure 3.26: Connection scheme.

The connections represented in the scheme are explained in Table 3.3:

SI motor		AP motor	
Motor power terminal (+)	A+	Motor power terminal (+)	B+
Motor power terminal (-)	A-	Motor power terminal (-)	B-
Encoder GND	GND	Encoder GND	GND
Encoder Vcc	5V	Encoder Vcc	5V
Encoder A output	Pin 3	Encoder A output	Pin 10
Encoder B output	Pin 7	Encoder B output	Pin 11
IN1A	Pin 34	IN1B	Pin 39
IN2A	Pin 37	IN2B	Pin 41

Tabla 3.3: Pin connections.

3.3.2. Respiration curve description

After that, the motors are programmed. The approach in this case has been to design a PID controller [64] in such a way that a function describes the desired position of the motors at each moment. The controller, comparing this position with the actual position recorded by the encoder, will determine the voltage required to reach it.

Thus, before implementing the PID controller, it is necessary to describe the curve that will determine the position of the motors at any given moment. In this case, in order to consider different cases of different patients, four different respiratory rates have been described. To determine what would be the different frequencies, Table 2.1 was observed. Therefore, a very high respiratory frequency (close to the respiratory frequency of a child); a high frequency within the normal limits for an adult; a normal frequency for an adult; and a slow frequency were described. Thus, the periods defined for the respiratory cycles were 2.25 seconds, 3.5 seconds, 4.5 seconds and 5 seconds, respectively.

On the other hand, the shape of the curve described in Figure 2.7 was considered to determine the motor trajectories, since it reflects the changes in volume between inspiration and expiration and is related to the deformations produced in the thorax.

Therefore, it has been necessary to define the distance that the platforms will move in each breath. Regarding the SI movement, as mentioned in Section 2, the diaphragm moves between 1 and 2 cm at rest but it can move up to 10 cm in deeper breaths. In this case, considering a movement of 10cm very extreme and unrealistic during a clinical evaluation in which the phantom would be used, it has implemented a movement of about 5cm in normal cases, which could be slightly bigger than at rest but makes possible to consider a resistance to the deformation produced by the foam. In the 2.25 seconds respiratory frequency rate, the maximum displacement has been established as around 3.3cm since it would be more realistic. In the same way, regarding the AP movement, the deformation of the body is around 2 cm, thus a movement has been programmed to advance the AP platform up to 2 cm in normal cases and 1 cm in the fastest case.

Therefore, to define the curves for different frequencies and displacements, Figure 2.7 was considered and the desired amplitude (in Figure 3.27, 5 cm) was established as follows:

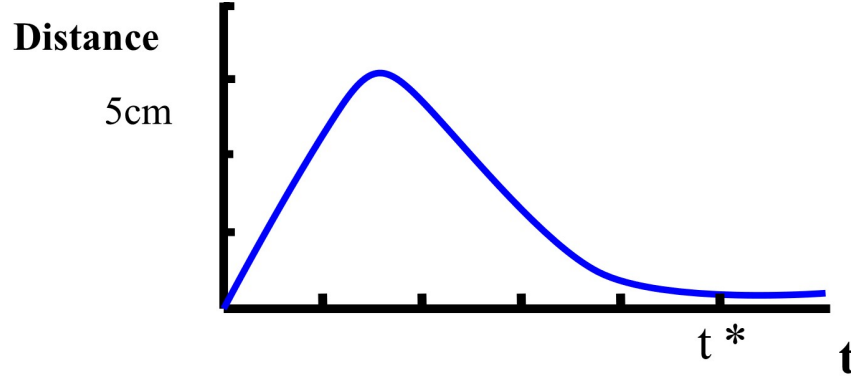


Figure 3.27: Distance respiration function.

Depending on each respiratory frequency rate, t^* will be a different value.

Therefore, in order to obtain the equation that represent the curve, different points were selected. In case of the frequency rate of 4.5 seconds in SI movement, the chosen points are shown in Table 3.4:

Time (s)	0.16	0.32	0.43	0.96	1.29	2.09	2.41	3.05	3.21	3.70	4.50	1.44	1.85
Distance (cm)	0.35	0.9	1.5	3.5	4.5	3.5	3	1.5	1	0.5	0.05	4.9	4.5

Tabla 3.4: Selected points to describe SI movement of 4.5 seconds period.

In addition, in the program the values of the motor displacements were used instead of the displacement values of the platforms. For this purpose, it is sufficient to use the linear and angular displacement equivalence:

$$s = \theta r \quad (3.1)$$

where s is the linear displacement, θ the angular position, and r the pulley's radius. In this case, r will be 0.5 cm since the pulley's diameter is 1 cm, thus:

$$\theta = \frac{s}{0.5} \quad (3.2)$$

Moreover, as the motors have a gearbox, it is necessary to consider the gearbox reduction ratio in the calculations. In other words:

$$\theta_M = \frac{s}{0.5} R \quad (3.3)$$

where θ_M is the motor position and R the gearbox reduction ratio (9.68 or 34 depending on the case).

Then, the values of distance were represented as motor positions, resulting the data exposed in Table 3.5 in case of frequency rate equal to 4.5 seconds:

Time (s)	0.16	0.32	0.43	0.96	1.29	2.09	2.41	3.05	3.21	3.70	4.50	1.44	1.85
Distance (rad)	23.8	61.2	102	238	306	238	204	102	68	34	3.4	333.2	306

Tabla 3.5: Selected points as displacement for SI movement and 4.5 seconds period.

Then, it was possible to represent the values as a dispersion diagram to establish a tendency line selecting a third-degree polynomial. In this case, the resulted plot was the one shown in Figure 3.28:

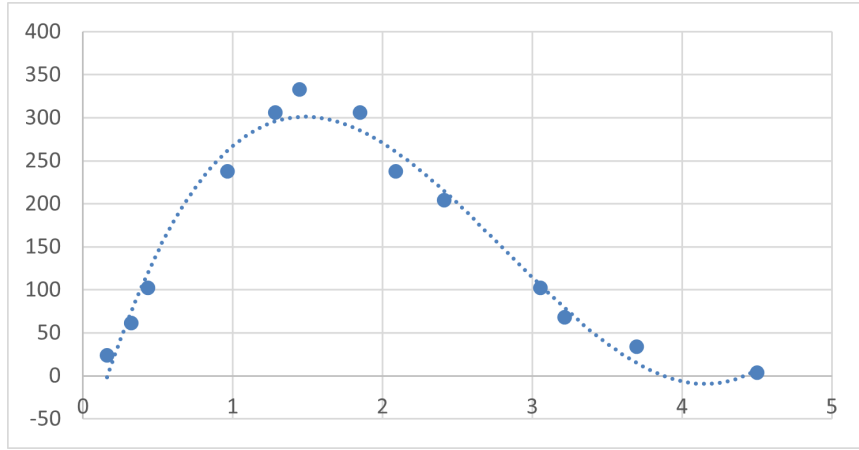


Figure 3.28: 4.5 seconds frequency rate plot.

The equation that will describe the motor position is:

$$\theta_{M(SI)_{4.5}}(t) = 32.496t^3 - 274.83t^2 + 600.57t - 91.048 \quad (3.4)$$

This procedure was repeated for both motors and the four aforementioned respiratory frequency rates. Thus, the values to obtain the curves in each case of the SI motor are shown in Table 3.6:

Motor values for SI movements							
2.25 sec		3.5 sec		4.5 sec		5 sec	
Time	Distance	Time	Distance	Time	Distance	Time	Distance
0.08	15.87	0.12	23.8	0.16	23.8	0.19	23.8
0.16	40.8	0.24	61.2	0.32	61.2	0.37	61.2
0.21	68	0.33	102	0.43	102	0.5	102
0.48	158.67	0.74	238	0.96	238	1.11	238
0.64	204	0.99	306	1.29	306	1.48	306
1.04	158.67	1.61	238	2.09	238	2.41	238
1.21	136	1.85	204	2.41	204	2.78	204
1.52	68	2.34	102	3.05	102	3.52	102
1.61	45.33	2.47	68	3.21	68	3.71	68
1.84	22.67	2.84	34	3.70	34	4.27	34
2.25	2.27	3.46	3.4	4.50	3.4	5.19	3.4
0.72	222.13	1.11	333.2	1.44	333.2	1.67	333.2
0.92	204	1.42	306	1.85	306	2.13	306

Tabla 3.6: Motor values for SI movement.

Resulting the four different curves, shown in Figure 3.29, 3.30, 3.31 and 3.32:

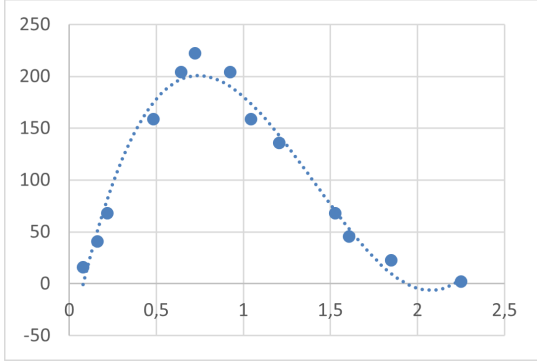


Figure 3.29: 2.25 seconds frequency rate SI motor plot.

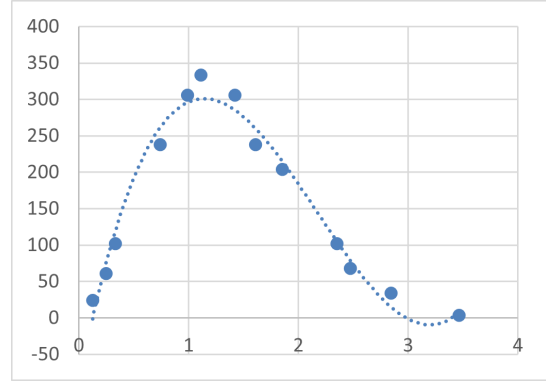


Figure 3.30: 3.5 seconds frequency rate SI motor plot.

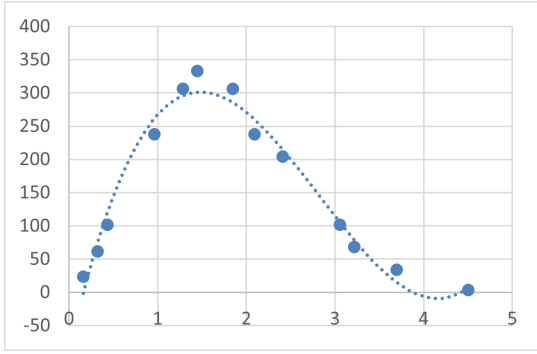


Figure 3.31: 4.5 seconds frequency rate SI motor plot.

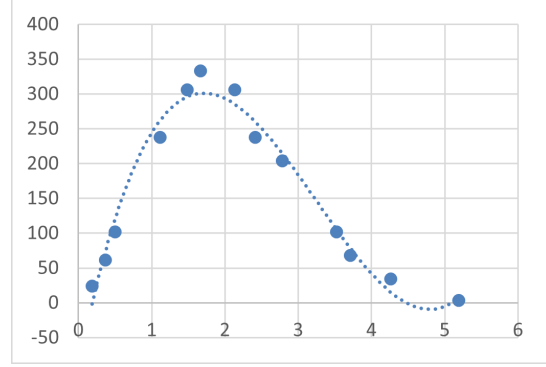


Figure 3.32: 5 seconds frequency rate SI motor plot.

And resulting the following equations:

$$\theta_{M(SI)_{2.25}}(t) = 173.31t^3 - 732.88t^2 + 800.76t - 60.699 \quad (3.5)$$

$$\theta_{M(SI)_{3.5}}(t) = 71.394t^3 - 464.46t^2 + 780.74t - 91.048 \quad (3.6)$$

$$\theta_{M(SI)_{4.5}}(t) = 32.496t^3 - 274.83t^2 + 600.57t - 91.048 \quad (3.7)$$

$$\theta_{M(SI)_5}(t) = 21.154t^3 - 206.43t^2 + 520.49t - 91.048 \quad (3.8)$$

In a similar way, the same process has been carried out for the AP motor. The values for each case are shown Table 3.7:

Motor values for AP movements							
2.25 sec		3.5 sec		4.5 sec		5 sec	
Time	Distance	Time	Distance	Time	Distance	Time	Distance
0.08	1.35	0.12	2.71	0.16	2.71	0.19	2.71
0.16	3.48	0.24	6.97	0.32	6.97	0.37	6.97
0.21	5.81	0.33	11.62	0.43	11.62	0.5	11.62
0.48	13.55	0.74	27.10	0.96	27.10	1.11	27.10
0.64	17.42	0.99	34.85	1.29	34.85	1.48	34.85
1.04	13.55	1.61	27.10	2.09	27.10	2.41	27.10
1.21	11.61	1.85	23.23	2.41	23.23	2.78	23.23
1.52	5.81	2.34	11.62	3.05	11.62	3.52	11.62
1.61	3.87	2.47	7.74	3.21	7.74	3.71	7.74
1.84	1.94	2.84	3.87	3.70	3.87	4.27	3.87
2.25	0.19	3.46	0.39	4.50	0.39	5.19	0.39
0.72	18.97	1.11	37.95	1.44	37.95	1.67	37.95
0.92	17.42	1.42	34.85	1.85	34.85	2.13	34.85

Tabla 3.7: Motor values for AP movement.

Resulting similar curves as in the SI movements, presented in Figure 3.33, 3.34, 3.35 and 3.36:

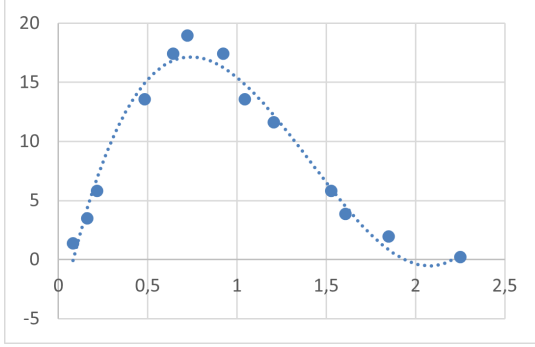


Figure 3.33: 2.25 seconds frequency rate AP motor plot.

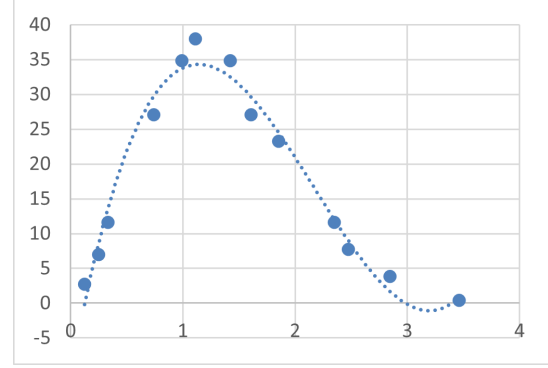


Figure 3.34: 3.5 seconds frequency rate AP motor plot.

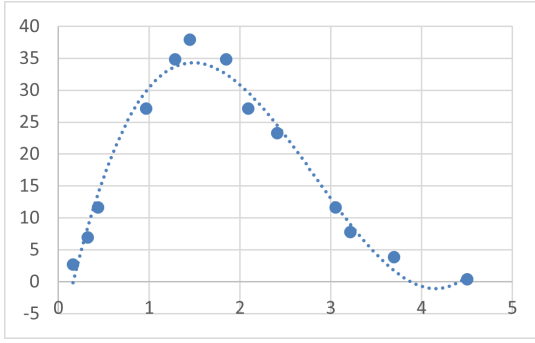


Figure 3.35: 4.5 seconds frequency rate AP motor plot.

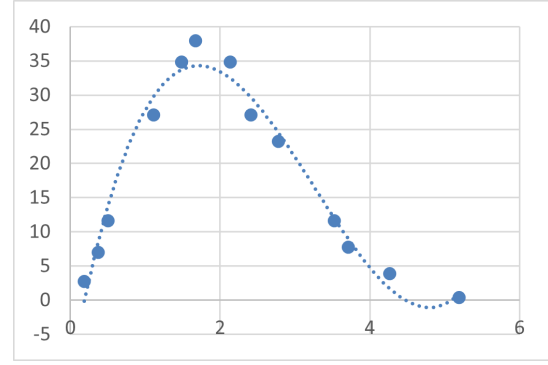


Figure 3.36: 5 seconds frequency rate AP motor plot.

And, as it is shown, the following equations:

$$\theta_{M(AP)_{2.25}}(t) = 14.803t^3 - 62.596t^2 + 68.394t - 5.1844 \quad (3.9)$$

$$\theta_{M(AP)_{3.5}}(t) = 8.1305t^3 - 52.894t^2 + 88.912t - 10.369 \quad (3.10)$$

$$\theta_{M(AP)_{4.5}}(t) = 3.7007t^3 - 31.298t^2 + 68.394t - 10.369 \quad (3.11)$$

$$\theta_{M(AP)_{5}}(t) = 2.409t^3 - 23.508t^2 + 59.275t - 10.369 \quad (3.12)$$

3.3.3. Arduino Implementation

As aforementioned, the coding of this project has been mainly based on the implementation of PID controllers. A PID is a controller that allows a closed loop system to be managed in order to achieve a desired output state. It is composed of three elements that provide Proportional, Integral and Derivative action (PID) [64] as it is shown in Figure 3.37.

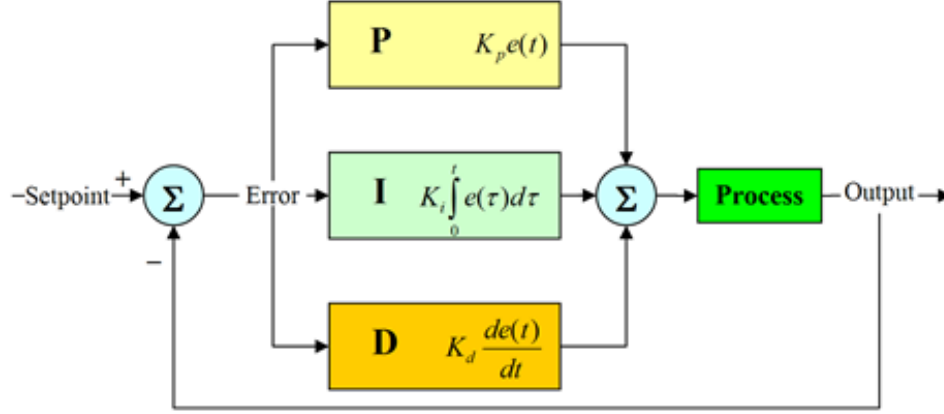


Figure 3.37: PID controller scheme [65].

The equation that described the functionality of a PID controller is the following:

$$c(t) = K_p e(t) + K_i \int e(t) dt + \frac{K_d \partial e(t)}{\partial t} \quad (3.13)$$

where $c(t)$ is the control signal, $e(t)$ is the error signal, K_p the proportional constant, K_i the integral constant, and K_d the derivative constant.

In that way, a signal *setpoint* is the reference signal and indicates the desired output of the system. Moreover, a signal *output* is registered, which corresponds to the real output of the system.

Then, as shown in Figure 3.37, the input to the PID controller is the error signal $e(t)$. This signal indicates to the controller the difference between the desired state or setpoint signal and the actual state output. Therefore, if the error signal is large, it means that the system state is far from the desired reference state. On the other hand, if the error is small, it means that the system has reached the desired state.

In order to obtain an error as small as possible, it is necessary to configure the values of K_p , K_i and K_d , which correspond, respectively, to the proportional, integral and derivative action of the PID controller. The characteristics of each are explained below.

Proportional action

This parameter is proportional to the error signal. Internally the proportional action multiplies the error signal by the constant K_p . This control action attempts to minimize the system error. Therefore, increasing the proportional action can increase the response speed of the system, decrease system error in steady state, and increase system instability [64].

By increasing the proportional, a point of equilibrium with sufficient system response speed and error reduction without making the system unstable can be found.

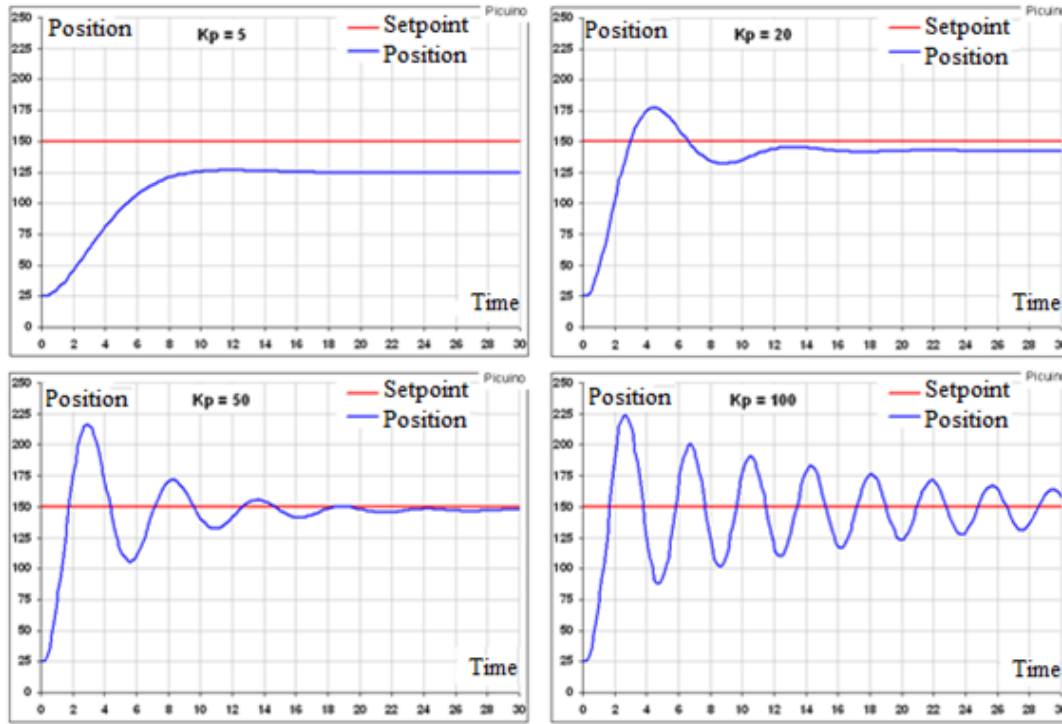


Figure 3.38: Proportional action results [64].

In Figure 3.38 different results with different values of K_p are shown. A small proportional action $K_p=5$ makes the system slow, taking several seconds to reach the stable position with an error of 25mm. With a proportional action $K_p=20$ the system is faster, taking less seconds to establish the permanent position. In addition, the error is reduced. On the other hand, considering higher values, the permanent error is further reduced. However, the response speed does not increase since the system becomes so unstable that it takes a long time to reach its final state. Then, according to the results, the best option in this example would be a proportional action $K_p=20$ [64].

Integral action

This control action calculates the integral of the error signal $e(t)$. In that way, the integral can be defined as the accumulation of the error signal. As time passes, small errors are added to make the integral action larger and larger. This reduces the steady-state system error. The disadvantage of using the integral action is that it adds some inertia to the system making it more unstable [64].

Increasing the integral action K_i , the system error in steady state decrease, the instability of the system increase, and the system speed increase slightly.

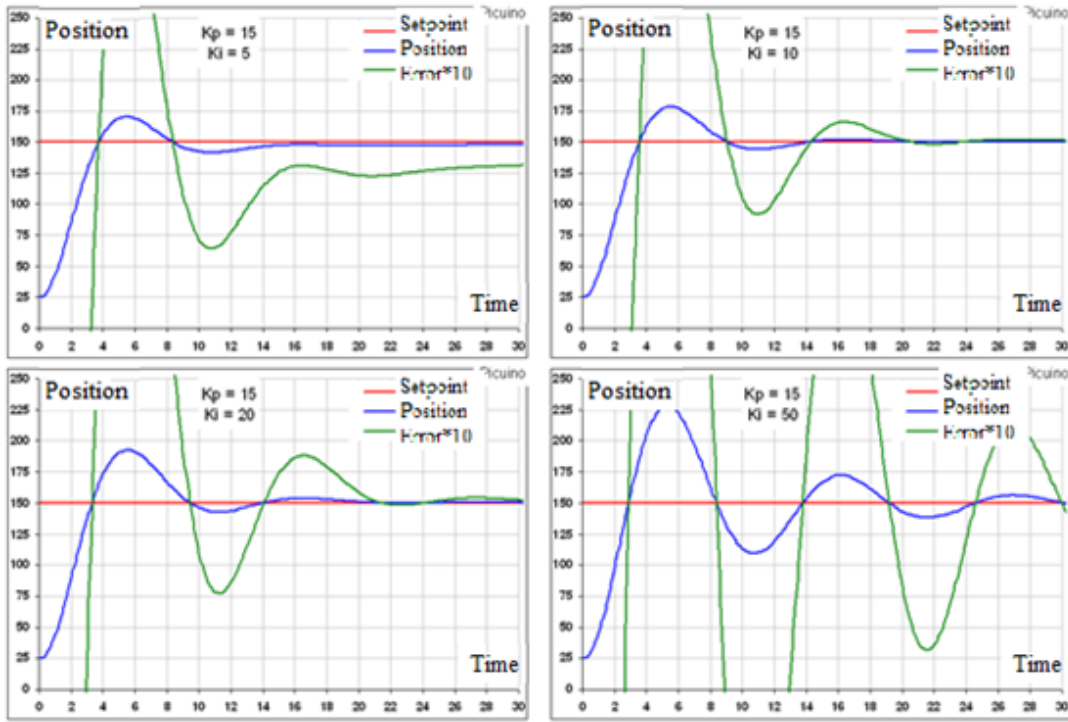


Figure 3.39: Integral action results [64].

In Figure 3.39, a bigger error signal (green) was added to better appreciate how the error decreases as the integral action increases. In addition, it is possible to observe how the system instability increases while K_i increases. For this reason, an integral control is often combined with derivative control to avoid system oscillations [64].

Derivative action

This control action is proportional to the derivative of the error signal $e(t)$. It is related to the “speed” of the error and is the factor that considers the inertia of the system. When the system moves at a high speed towards the reference point, an overshoot and oscillations occur around the reference due to the inertia. To avoid this problem, the controller recognizes the speed at which the system is approaching the setpoint in order to slow it down in advance as it approaches the desired reference and prevent it from overshooting [64].

Increasing the derivative control constant K_d allows to increase the stability of the controlled system, decrease the speed of the system slightly, and the steady-state error remains unchanged. Then, this control action will be used to stabilize a response that oscillates too much.

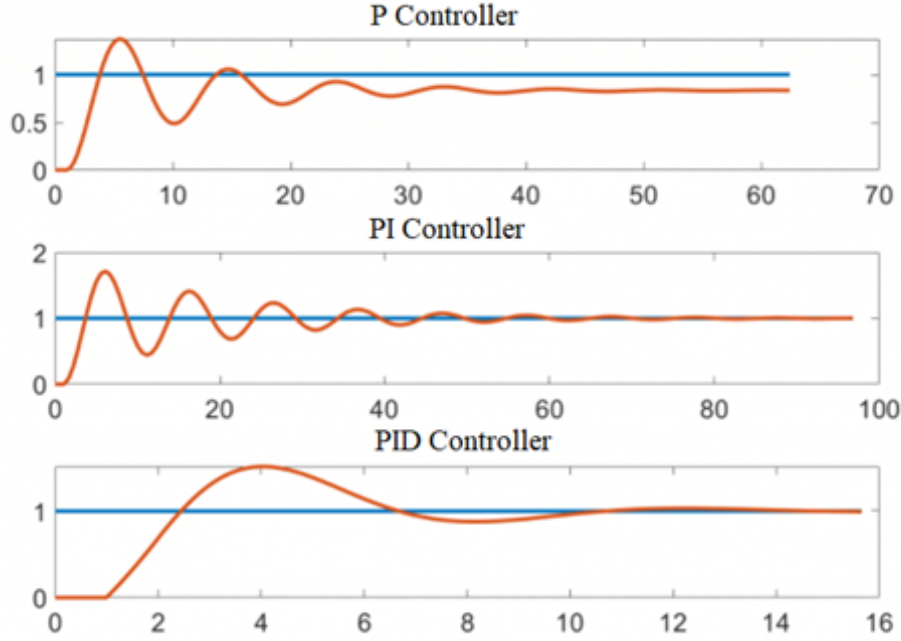


Figure 3.40: Derivative action results [66].

Therefore, Figure 3.40 shows the contribution of each constant in a PID controller. In first diagram (P Controller), the system reaches after some time a value close to the desired value but with errors. When the integral value is added (PI Controller), this error is eliminated, but more oscillations appear. After that, the derivative factor is added (PID Controller), decreasing these oscillations significantly [66].

Then, in programming it is important to understand how to tune the controller. In this case, the trial-and-error method has been used. The proportional action is the first one to be implemented. It is increased little by little to decrease the error and to increase the response speed. If the system reaches the desired speed response and error, the controller is tuned. In contrast, if instabilities appear before desired response is reached, the derivative action must be increased. Therefore, the K_d value will be modified little by little until it achieves stability. Then, in the case that the error was greater than desired, the constant K_i is increased. If the system becomes unstable before to achieve the desired response, the derivative action is modified again.

To implement each PID controller, it has been necessary to define each setpoint, which will be the position at which the motor is expected to be in each time. These setpoints are determined by the equations that were shown in the previous subsection, although it is necessary to make some modifications.

First, considering the graphs of each respiratory frequency rate, it is possible to observe that, after exhalations, the position takes some slight negative values. In this case, it would be unrealistic to consider negative positions, thus the independent coefficients were modified a little to raise the functions to positive values. The resulted

equations were:

$$\theta_{M(SI)_{2.25}}(t) = 173.31t^3 - 732.88t^2 + 800.76t - 52.699 \quad (3.14)$$

$$\theta_{M(SI)_{3.5}}(t) = 71.394t^3 - 464.46t^2 + 780.74t - 82.048 \quad (3.15)$$

$$\theta_{M(SI)_{4.5}}(t) = 32.496t^3 - 274.83t^2 + 600.57t - 82.048 \quad (3.16)$$

$$\theta_{M(SI)_5}(t) = 21.154t^3 - 206.43t^2 + 520.49t - 82.048 \quad (3.17)$$

$$\theta_{M(AP)_{2.25}}(t) = 14.803t^3 - 62.596t^2 + 68.394t - 4.4844 \quad (3.18)$$

$$\theta_{M(AP)_{3.5}}(t) = 8.1305t^3 - 52.894t^2 + 88.912t - 8.7844 \quad (3.19)$$

$$\theta_{M(AP)_{4.5}}(t) = 3.7007t^3 - 31.298t^2 + 68.394t - 8.7844 \quad (3.20)$$

$$\theta_{M(AP)_5}(t) = 2.409t^3 - 23.508t^2 + 59.275t - 8.7844 \quad (3.21)$$

Consequently, the graph describing SI movement would be modified as shown in Figure 3.41:

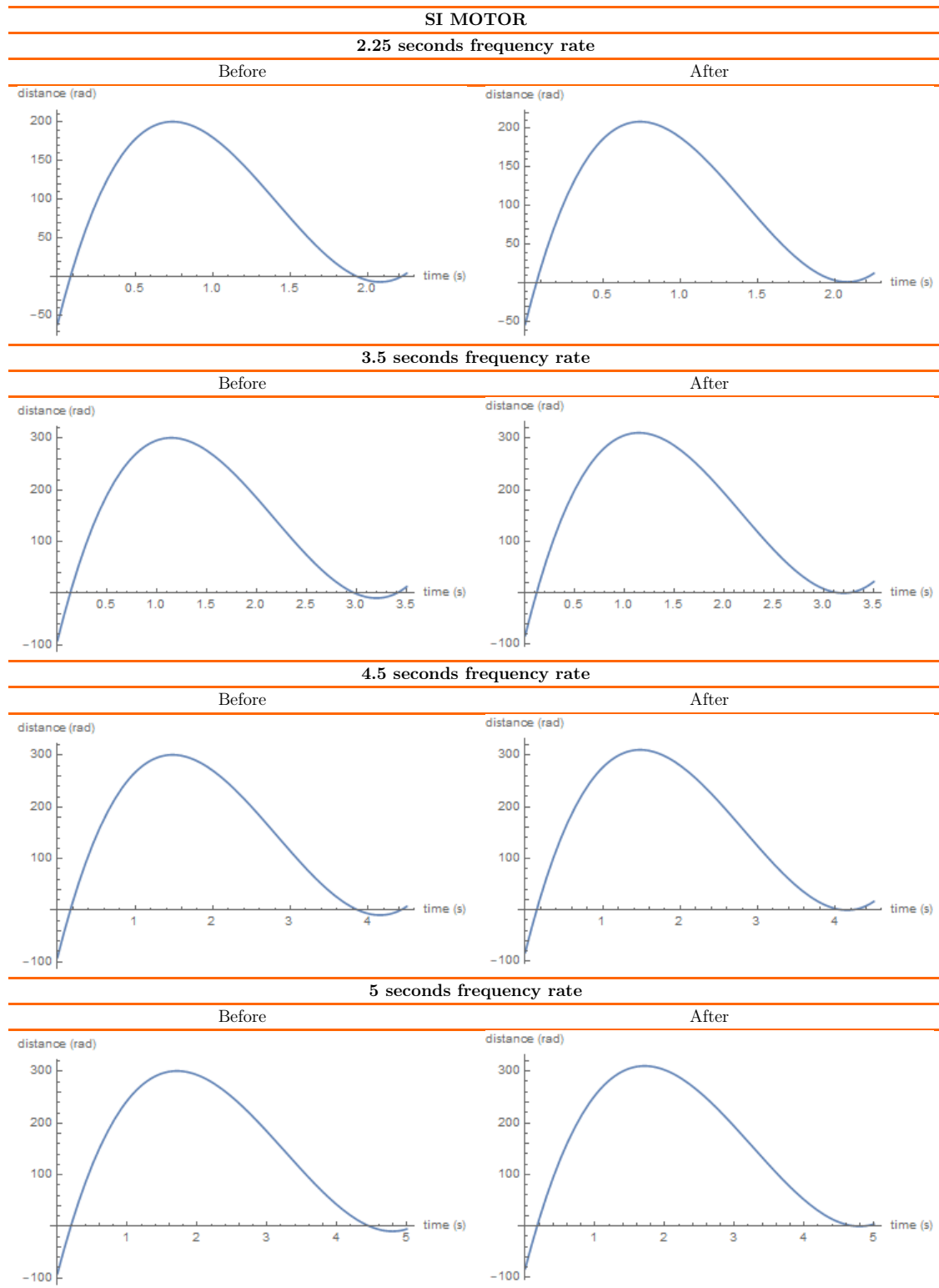


Figure 3.41: SI diagrams after first modification.

And the ones describing AP movement are shown in Figure 3.42:

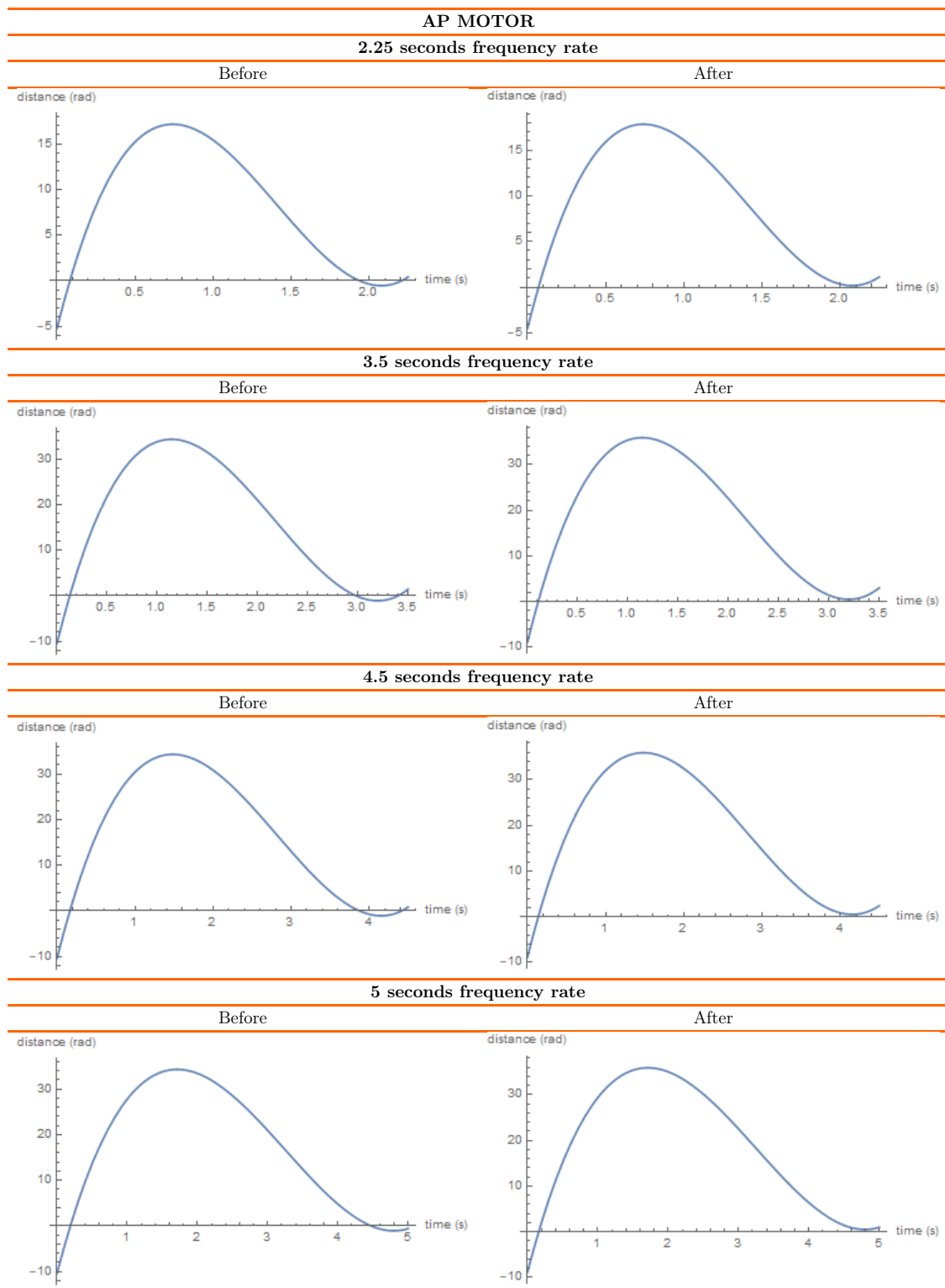


Figure 3.42: AP diagrams after first modification.

After that, observing again the plots, in all cases the positive values start after some time. Before that, the graphs take values that are notably negative. The idea

is to repeat the cycles periodically, thus the negative values at the beginning of each cycle would produce a large jump since these cycles finish taking a value close to 0. These jumps, apart from make the system inefficient, it is unrealistic. For this reason, a small value has been added to the time variable in each equation, causing a continuation as close as possible from one cycle to the next.

To establish this value, each equation has been solved for a time equal to its period, so that the value of the motor position at the last moment of the cycle is obtained. The motor position resulted in each case have been the following:

$$\theta_{M(SI)_{2.25}}(2.25) = 12.9152 \text{ rad} \quad (3.22)$$

$$\theta_{M(SI)_{3.5}}(3.5) = 21.9248 \text{ rad} \quad (3.23)$$

$$\theta_{M(SI)_{4.5}}(4.5) = 16.4075 \text{ rad} \quad (3.24)$$

$$\theta_{M(SI)_5}(5) = 3.902 \text{ rad} \quad (3.25)$$

$$\theta_{M(AP)_{2.25}}(2.25) = 1.12527 \text{ rad} \quad (3.26)$$

$$\theta_{M(AP)_{3.5}}(3.5) = 3.05129 \text{ rad} \quad (3.27)$$

$$\theta_{M(AP)_{4.5}}(4.5) = 2.43039 \text{ rad} \quad (3.28)$$

$$\theta_{M(AP)_5}(5) = 1.0156 \text{ rad} \quad (3.29)$$

After that, the equation is set to those positions and resolved, resulting the times at which motors achieve them. The value closest to 0 will be the time at which those positions are achieved for the first time, thus it will be established at the beginning of each cycle. In each case:

$$\theta_{M(SI)_{2.25}}(t) = 12.9152 \text{ rad} \Rightarrow t_0 = 0.089 \text{ s} \quad (3.30)$$

$$\theta_{M(SI)_{3.5}}(t) = 21.9248 \text{ rad} \Rightarrow t_0 = 0.145 \text{ s} \quad (3.31)$$

$$\theta_{M(SI)_{4.5}}(t) = 16.4075 \text{ rad} \Rightarrow t_0 = 0.178 \text{ s} \quad (3.32)$$

$$\theta_{M(SI)_5}(t) = 3.902 \text{ rad} \Rightarrow t_0 = 0.177 \text{ s} \quad (3.33)$$

$$\theta_{M(AP)_{2.25}}(t) = 1.12527 \text{ rad} \Rightarrow t_0 = 0.089 \text{ s} \quad (3.34)$$

$$\theta_{M(AP)_{3.5}}(t) = 3.05129 \text{ rad} \Rightarrow t_0 = 0.145 \text{ s} \quad (3.35)$$

$$\theta_{M(AP)_{4.5}}(t) = 2.43039 \text{ rad} \Rightarrow t_0 = 0.178 \text{ s} \quad (3.36)$$

$$\theta_{M(AP)_5}(t) = 1.0156 \text{ rad} \Rightarrow t_0 = 0.177 \text{ s} \quad (3.37)$$

Therefore, the resulting equations are:

$$\begin{aligned} \theta_{M(SI)_{2.25}}(t) = 173.31(t + 0.089)^3 - 732.88(t + 0.089)^2 + \\ 800.76(t + 0.089) - 52.699 \end{aligned} \quad (3.38)$$

$$\begin{aligned} \theta_{M(SI)_{3.5}}(t) = 71.394(t + 0.145)^3 - 464.46(t + 0.145)^2 + \\ 780.74(t + 0.145) - 82.048 \end{aligned} \quad (3.39)$$

$$\theta_{M(SI)_{4.5}}(t) = 32.496(t + 0.178)^3 - 274.83(t + 0.178)^2 + 600.57(t + 0.178) - 82.048 \quad (3.40)$$

$$\theta_{M(SI)_5}(t) = 21.154(t + 0.177)^3 - 206.43(t + 0.177)^2 + 520.49(t + 0.177) - 82.048 \quad (3.41)$$

$$\theta_{M(AP)_{2.25}}(t) = 14.803(t + 0.089)^3 - 62.596(t + 0.089)^2 + 68.394(t + 0.089) - 4.4844 \quad (3.42)$$

$$\theta_{M(AP)_{3.5}}(t) = 8.1305(t + 0.145)^3 - 52.894(t + 0.145)^2 + 88.912(t + 0.145) - 8.7844 \quad (3.43)$$

$$\theta_{M(AP)_{4.5}}(t) = 3.7007(t + 0.178)^3 - 31.298(t + 0.178)^2 + 68.394(t + 0.178) - 8.7844 \quad (3.44)$$

$$\theta_{M(AP)_5}(t) = 2.409(t + 0.177)^3 - 23.508(t + 0.177)^2 + 59.275(t + 0.177) - 8.7844 \quad (3.45)$$

Which correspond to diagrams shown in Figure 3.43 and 3.44:

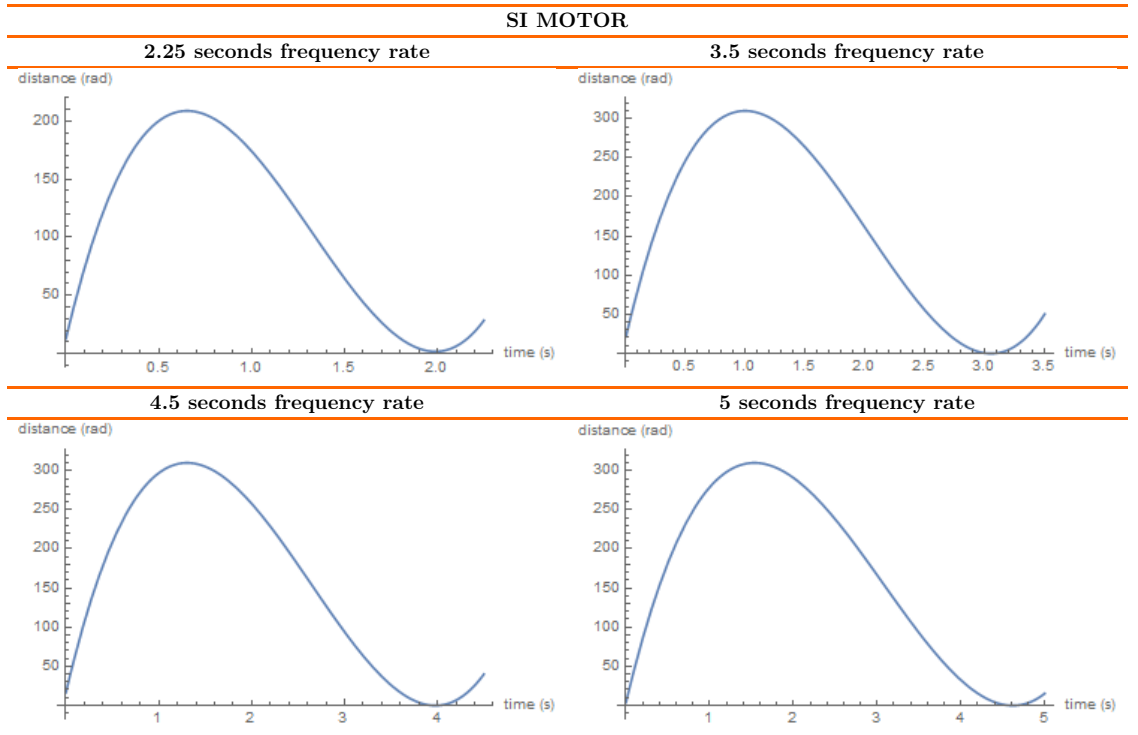


Figure 3.43: SI diagrams after second modification.

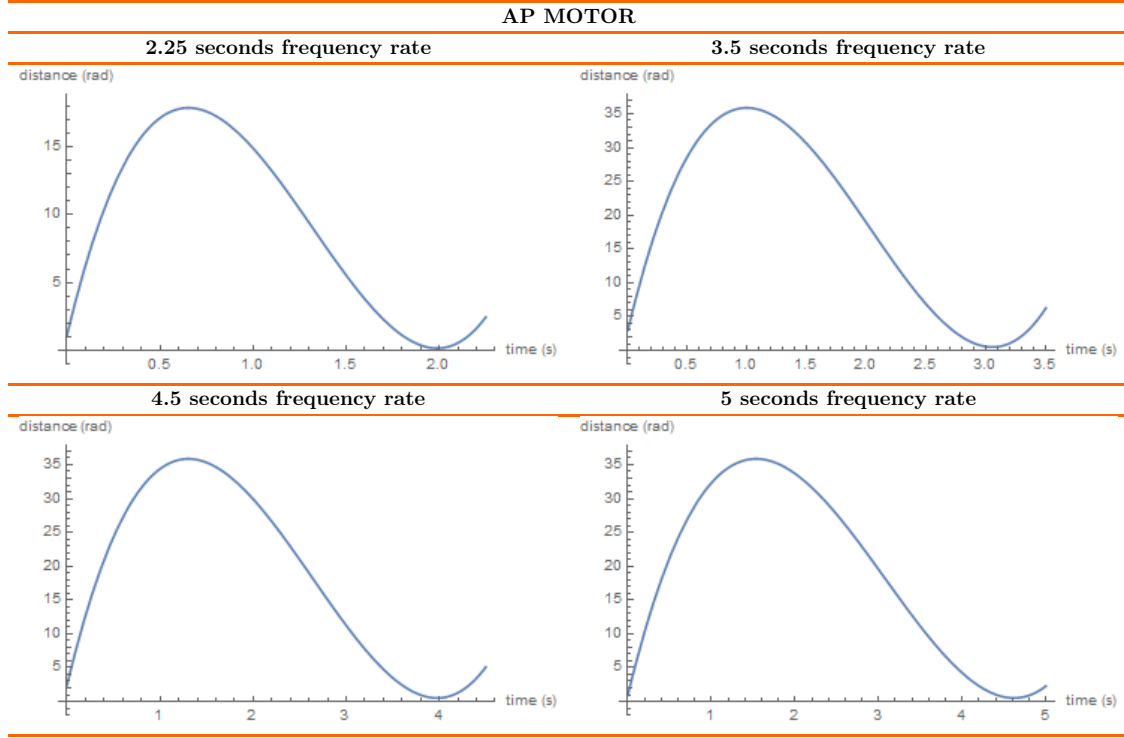


Figure 3.44: AP diagrams after second modification.

Therefore, in this work, a continuous reading of time is necessary. This is done by the `millis()` function defined in Arduino, which continuously records the time in milliseconds. The time is stored in a variable and is used to calculate in each loop the position of the desired motors at each moment as is described in each equation. In order to periodically repeat the cycles, a counter variable was defined. It is incremented by one each time a respiratory cycle ends, and makes the function start again being multiplied by the period of each cycle and subtracting it from the time the program has been in operation. Therefore, the resulting equations are the following:

$$\theta_{M(SI)_{2.25}}(t) = 173.31(t + 0.089 - 2.25cont)^3 - 732.88(t + 0.089 - 2.25cont)^2 + 800.76(t + 0.089 - 2.25cont) - 52.69 \quad (3.46)$$

$$\theta_{M(SI)_{3.5}}(t) = 71.394(t + 0.145 - 3.5cont)^3 - 464.46(t + 0.145 - 3.5cont)^2 + 780.74(t + 0.145 - 3.5cont) - 82.048 \quad (3.47)$$

$$\theta_{M(SI)_{4.5}}(t) = 32.496(t + 0.178 - 4.5cont)^3 - 274.83(t + 0.178 - 4.5cont)^2 + 600.57(t + 0.178 - 4.5cont) - 82.048 \quad (3.48)$$

$$\theta_{M(SI)_5}(t) = 21.154(t + 0.177 - 5cont)^3 - 206.43(t + 0.177 - 5cont)^2 + 520.49(t + 0.177 - 5cont) - 82.048 \quad (3.49)$$

$$\theta_{M(AP)_{2.25}}(t) = 14.803(t + 0.089 - 2.25cont)^3 - 62.596(t + 0.089 - 2.25cont)^2 + 68.394(t + 0.089 - 2.25cont) - 4.484(3.50)$$

$$\theta_{M(AP)_{3.5}}(t) = 8.1305(t + 0.145 - 3.5cont)^3 - 52.894(t + 0.145 - 3.5cont)^2 + 88.912(t + 0.145 - 3.5cont) - 8.7844(3.51)$$

$$\theta_{M(AP)_{4.5}}(t) = 3.7007(t + 0.178 - 4.5cont)^3 - 31.298(t + 0.178 - 4.5cont)^2 + 68.394(t + 0.178 - 4.5cont) - 8.7844(3.52)$$

$$\theta_{M(AP)_5}(t) = 2.409(t + 0.177 - 5cont)^3 - 23.508(t + 0.177 - 5cont)^2 + 59.275(t + 0.177 - 5cont) - 8.7844 \quad (3.53)$$

Which correspond to diagrams shown in Figure 3.45 and 3.46:

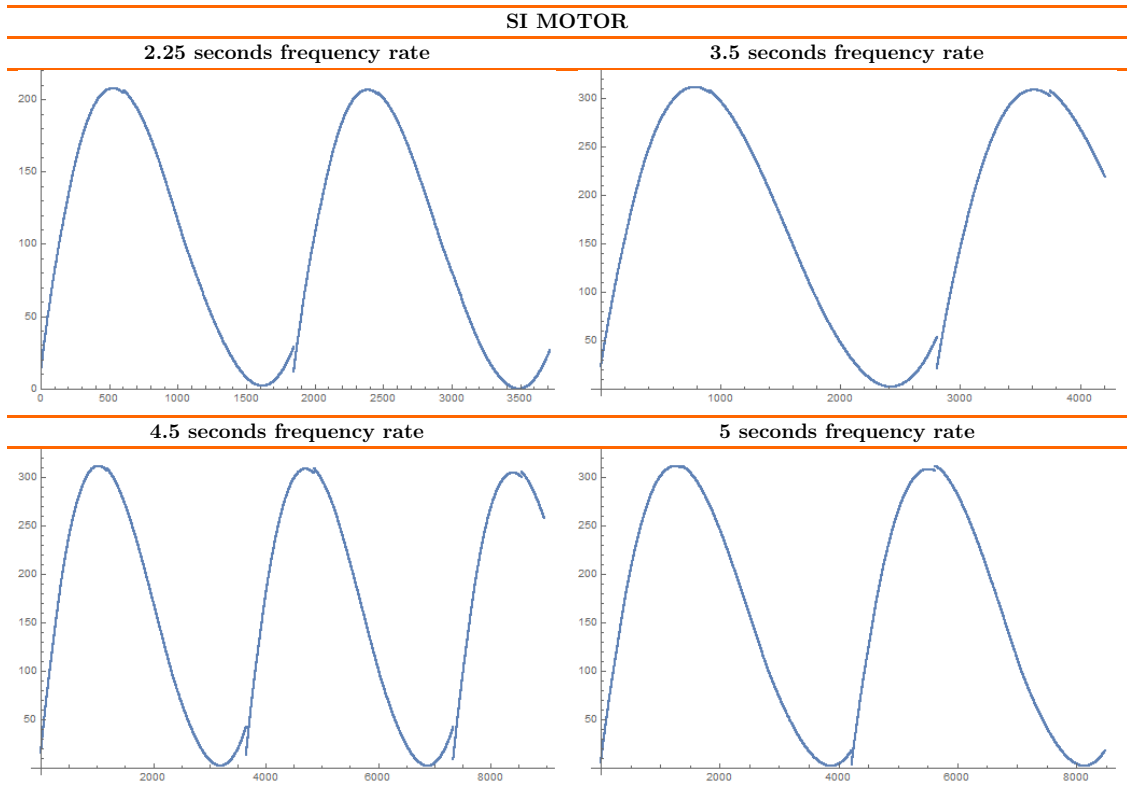


Figure 3.45: SI diagrams after last modification.

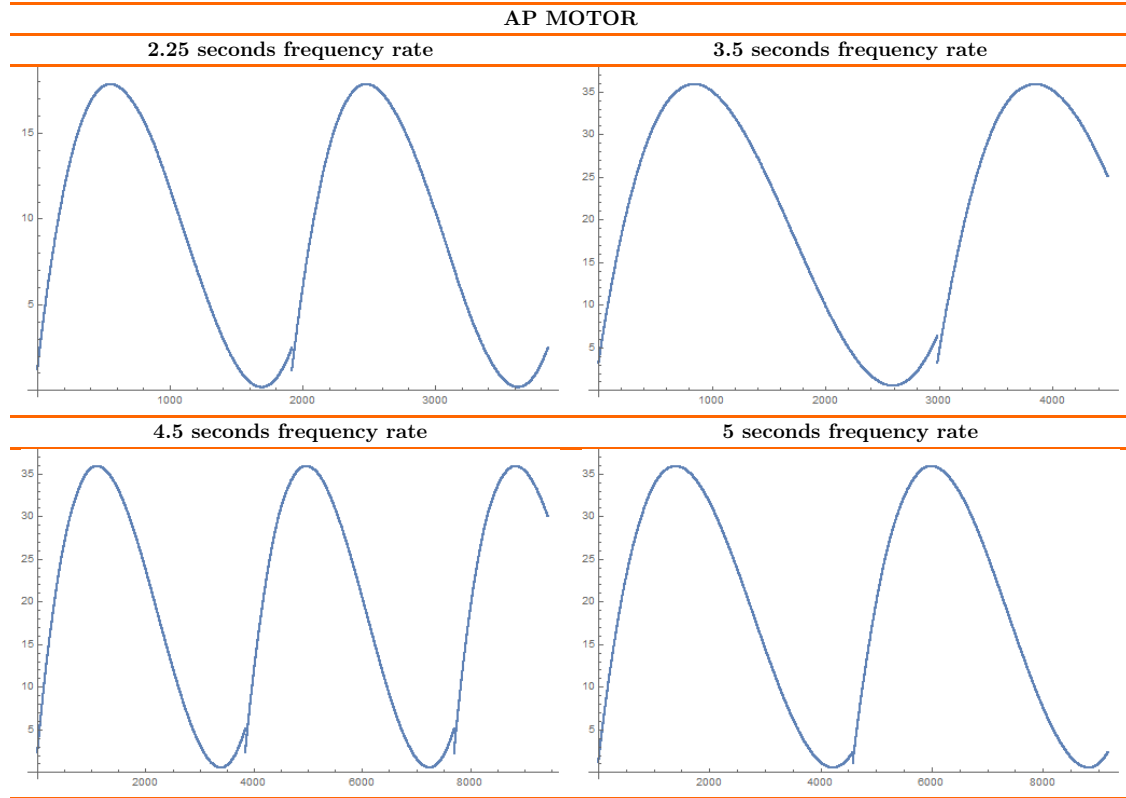


Figure 3.46: AP diagrams after last modification.

On the other hand, to make it more realistic, a random value was added using the `random()` function defined in Arduino. This value is defined at the beginning of the program and is modified in each cycle. Its range is $\pm 1/20$ of the independent coefficient of each equation, being added to the final result obtained. In addition, it is modified three times during each cycle, adding irregularities at the beginning of inspiration, when inspiration is ending, and when expiration slows down.

Once this has been done, each setpoint has correctly been defined, thus the PID controllers can be implemented. In this case, a function of the PID controller has been defined by comparing the setpoint with the actual value of the motor position measured by the encoder. Therefore, the error is obtained and multiplied by the controller's proportional constant. Then, the current motor position is compared with the position of the previous step and multiplied by the derivative constant of the controller in order to better adjust the PID. Both values added with the dependent factor of the integral constant define the output of the function.

The output obtained after executing this function is a PWM output. The PWM output will define the voltage required to feed the motor to reach the desired position defined by the setpoint. This output has values between 0 and 255 (or between -255 and 255 if both directions are considered), and the voltages in this case are going to move in a range between 0 and 5 (or between -5 to 5). Therefore, to transform the

PWM values into voltage it will be enough to use the following conversion:

$$Voltage = PWM \frac{5}{255} \quad (3.54)$$

In this project, the PID parameters have been defined on a case-by-case basis. Thus, for each respiratory rate and each motor the values of K_p , K_d and K_i of the motors have been different. These values have been calculated according to the explanation on the previous pages, defining first the K_p value, then the K_d , and finally adjusting it with K_i . The most important to consider in this work has been to achieve a fast establish time and smalls oscillations.

The tuning started with SI motor and the frequency rate equal to 3.5 seconds since it was easier to calibrate than the fastest frequency. Therefore, the tests which were carried out are shown in Figure 3.47:

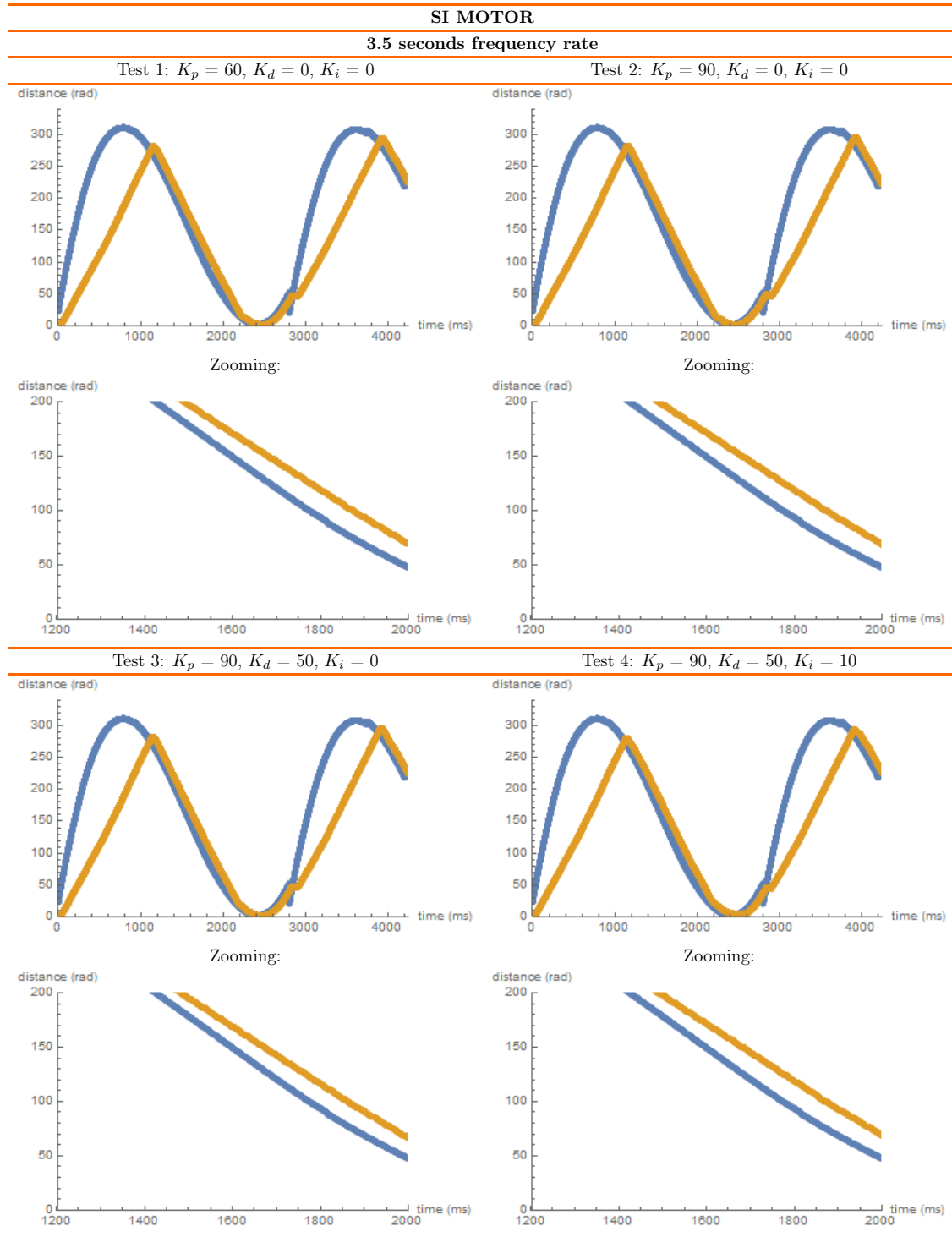


Figure 3.47: SI motor, 3.5 seconds frequency rate tuning.

As it can be seen in Figure 3.47, in the first test only one value was given to the proportional constant, in this case $K_p = 60$. It was observed that the system adjusted considerably well to the desired position but with a little delay. Then, in the second test it can be seen that the value of the proportional constant was increased. This was

almost completely adjusted, but some oscillations could be seen in the motor, so in the third test the value of the derivative constant was added, achieving an appropriate result. On the other hand, in the fourth test the value of the integral constant was modified to observe the action it produced. This produced more oscillations in the system, which could be avoid by increasing the derivative constant, but that would produce a slower respond. That is why in these cases the integral action will not be considered. Thus, the values chosen for the controller in this case are $K_p = 90$, $K_d = 50$ and $K_i = 0$.

After that, the controller for respiratory frequency rate equal to 4.5 seconds was tested as Figure 3.48 shows:

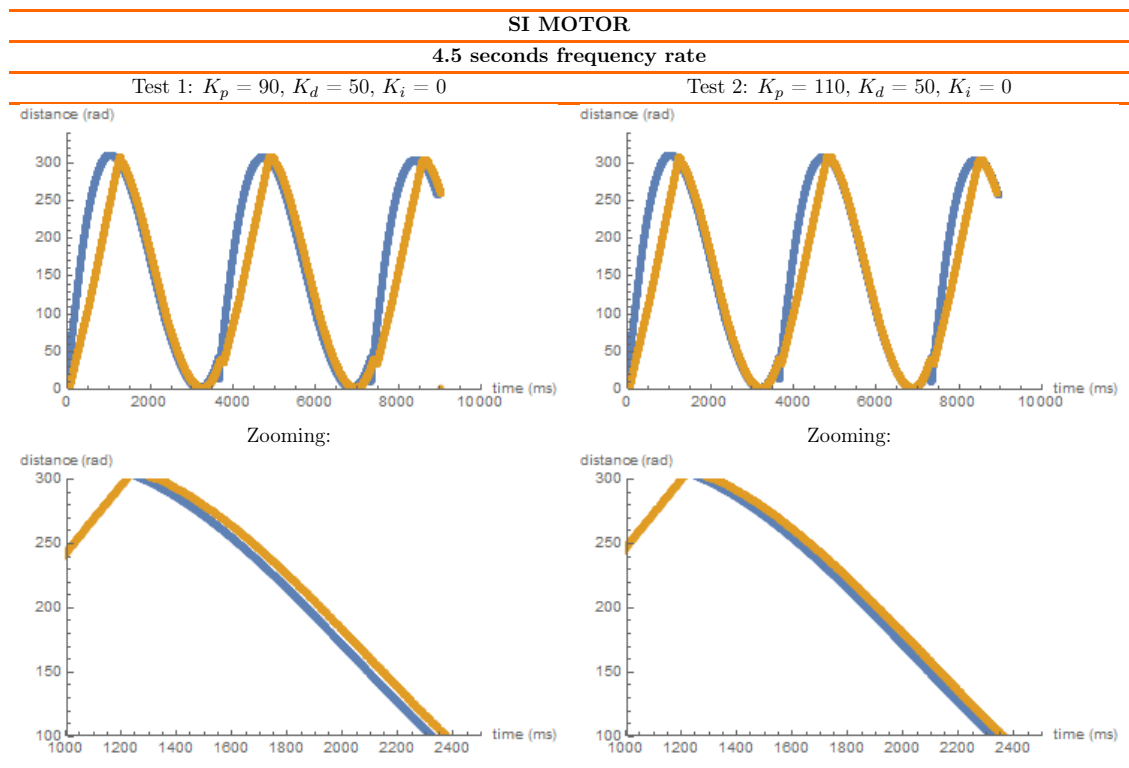


Figure 3.48: SI motor, 4.5 seconds frequency rate tuning.

First, the system was evaluated by using the constant values that worked in the previous controller. As it can be observed in test 1, the result was considerably promising. However, another test was carried out by increasing the K_p value, achieving a truly precise system. Therefore, the values to calibrate the PID are $K_p = 110$, $K_d = 50$, $K_i = 0$.

Then, the case of frequency rate equal to 5 seconds was evaluated (Figure 3.49).

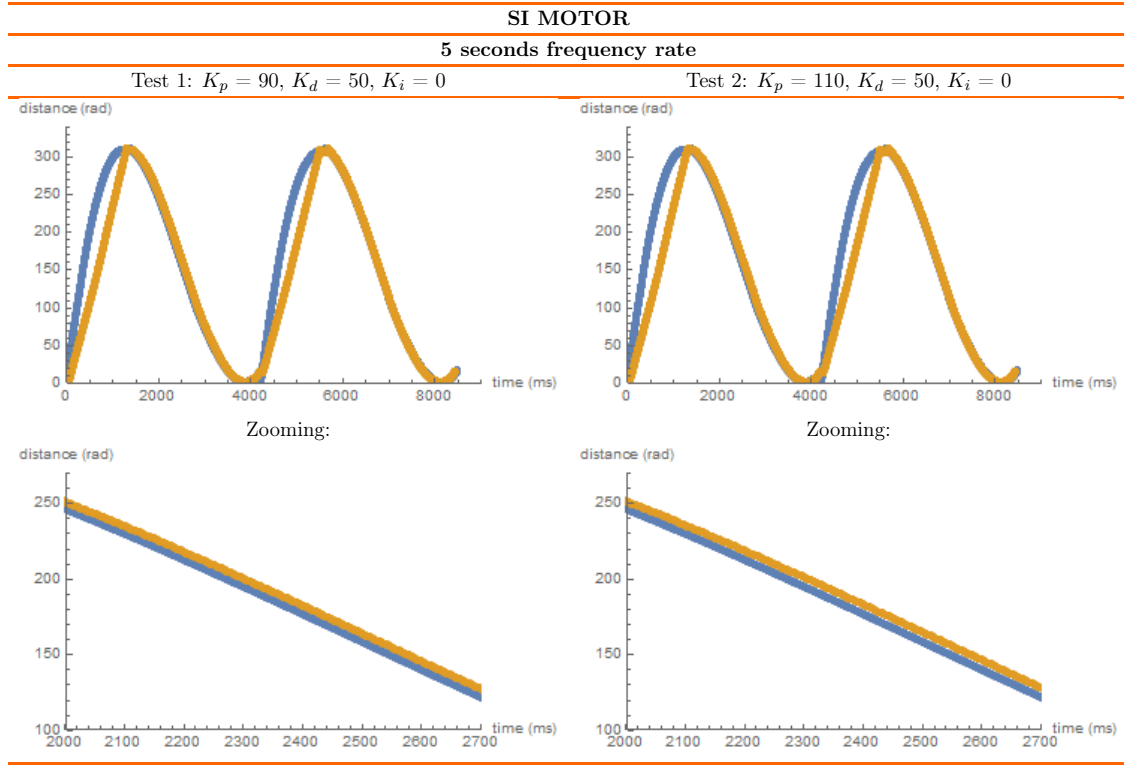


Figure 3.49: SI motor, 5 seconds frequency rate tuning.

In this case, the tests started by using the values of the previous controller. This was close to the desired output, but some oscillations appeared. To avoid them, as explained above, one solution would be to increase the value of K_d , but that increased the response time as seen in the second test. Therefore, it was decided that the best result was $K_p = 110, K_d = 50, K_i = 0$.

Once this was done, the controller was programmed for the 2.25 second frequency. In this case, being a very fast movement, it was impossible to completely adjust the controller, the optimum tuning could only be achieved in one section of the respiratory cycle. Therefore, the same values were used as in the previous case ($K_p = 110, K_d = 50, K_i = 0$), which ensured that the motor reached the reference position during exhalation, as Figure 3.50 shows:

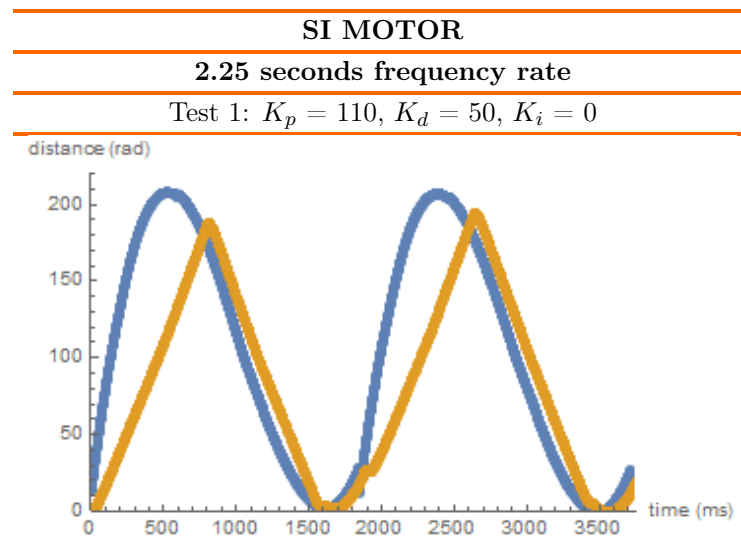


Figure 3.50: SI motor, 2.25 seconds frequency rate tuning.

For the motor in charge of the AP movement, similar tests were carried out. In this case, the movements are smaller, so the motor needs to be more precise in terms of response times. To achieve that accuracy, the value of K_p must be the one that minimizes the response time, which causes oscillations. These oscillations are reduced with the derivative action but, as explained above, if a very high derivative value is applied, the response time increases again. Therefore, some of the tests carried out at each frequency to adjust are shown in Figure 3.51:

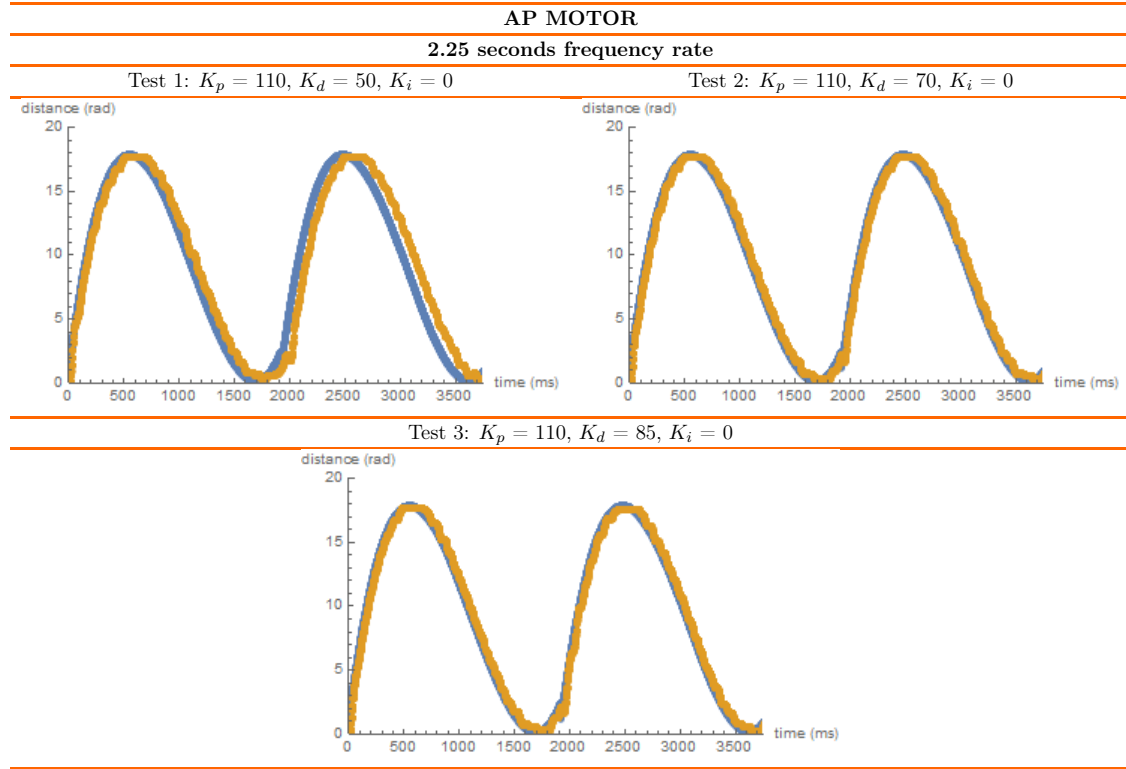


Figure 3.51: AP motor, 2.25 seconds frequency rate tuning.

In this case, oscillations appear in the controller. They cannot be avoided if a rapid response is desired. Therefore, the values chosen for this controller were $K_p = 110$, $K_d = 85$, $K_i = 0$ since it reduced some oscillations and maintained an accurate response time.

On the other hand, in frequency rate equal to 3.5 seconds, the controller was truly precise using the same values, as it can be seen in Figure 3.52:

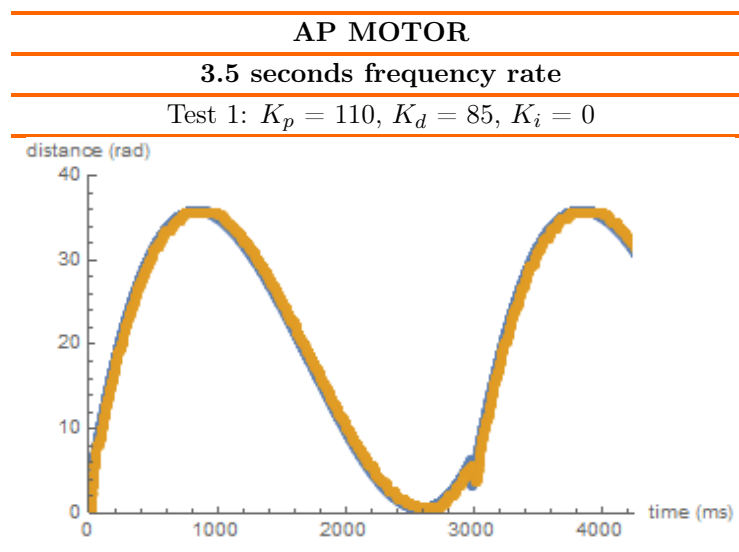


Figure 3.52: AP motor, 3.5 seconds frequency rate tuning.

These values were tested in a respiratory frequency rate equal to 4.5 seconds, but in this case some oscillations appeared. To avoid them, the derivative constant was increased as is shown in Figure 3.53:

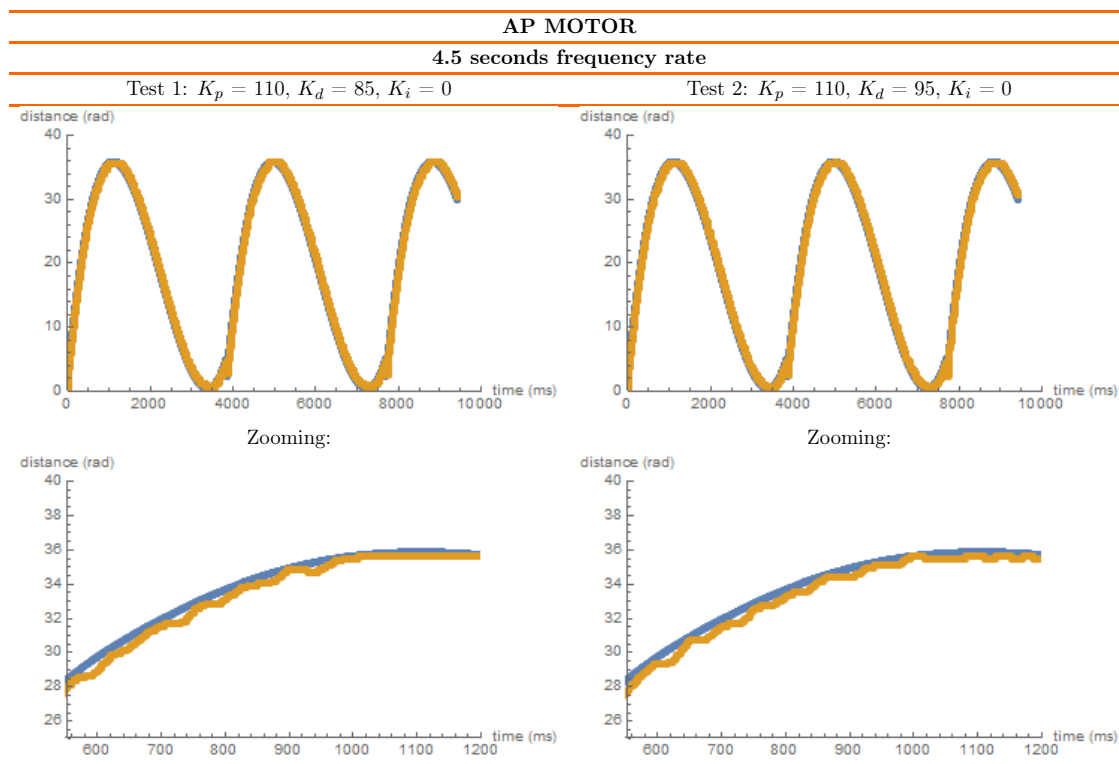


Figure 3.53: AP motor, 4.5 seconds frequency rate tuning.

Therefore, the values chosen for this controller were $K_p = 110$, $K_d = 95$, $K_i = 0$.

In a similar way, the constant in previous frequency rate was tested in 5 seconds frequency rate. This was considerably precise; thus, the values were maintained (Figure 3.54):

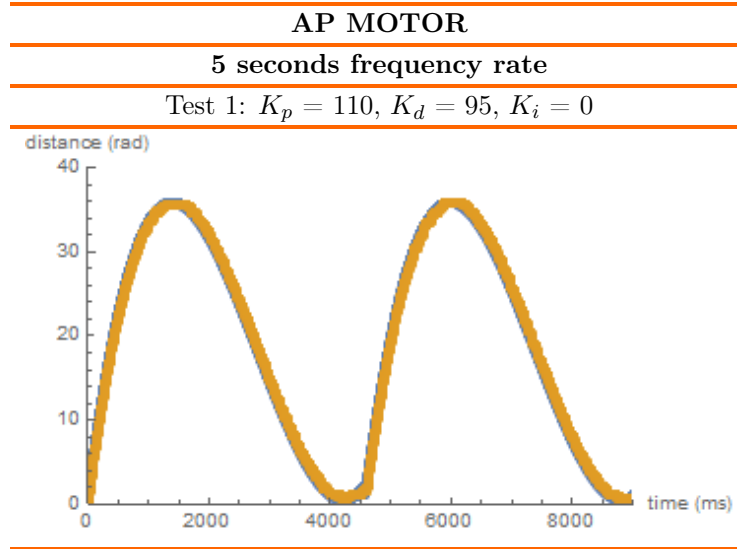


Figure 3.54: AP motor, 5 seconds frequency rate tuning.

Therefore, the values selected in each case are shown in Table 3.8:

SI MOTOR	
2.25 seconds frequency rate	3.5 seconds frequency rate
$K_p = 110$, $K_d = 50$, $K_i = 0$.	$K_p = 90$, $K_d = 50$, $K_i = 0$
4.5 seconds frequency rate	5 seconds frequency rate
$K_p = 110$, $K_d = 50$, $K_i = 0$.	$K_p = 110$, $K_d = 50$, $K_i = 0$
AP MOTOR	
2.25 seconds frequency rate	3.5 seconds frequency rate
$K_p = 110$, $K_d = 85$, $K_i = 0$.	$K_p = 110$, $K_d = 85$, $K_i = 0$
4.5 seconds frequency rate	5 seconds frequency rate
$K_p = 110$, $K_d = 95$, $K_i = 0$.	$K_p = 110$, $K_d = 95$, $K_i = 0$

Tabla 3.8: Summary of controller values.

Once all the controllers were tuned, the motors were incorporated into the phantom. The results obtained are reported in the next section.

Chapter 4

Results

4.1. Results and Modifications

After setting the controller values, the motors were introduced into the structure. Then, to insert the glass marbles as markers and to promote its deformation, the foams (“lungs”) were cut as shown in Figure 4.1:



Figure 4.1: Cut lungs.

After that, the SI movement produced by the motor with the 34:1 gearbox was analyzed. The results of each frequency rate in this case are shown in Figure 4.2, where blue line represents the setpoint and orange line is the motor position.

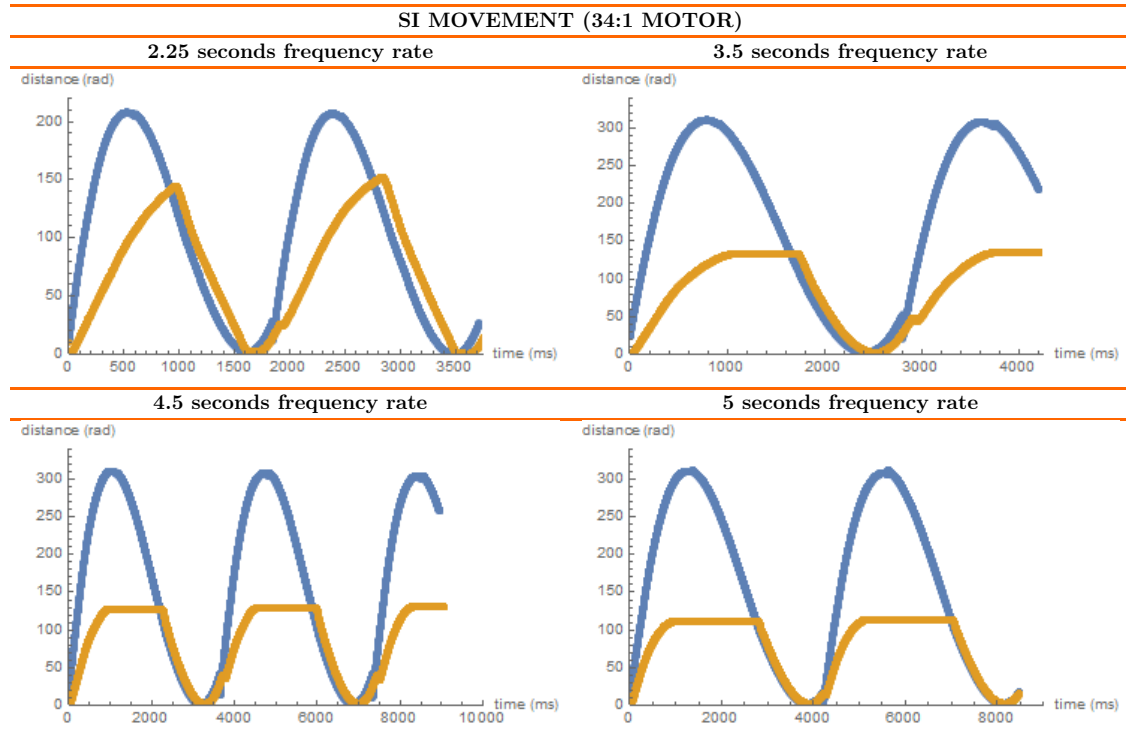


Figure 4.2: 34:1 motor in SI movement results.

Figure 4.2 shows that when the motor is introduced into the platform, the movement slows down slightly, causing a small delay between the desired position and the obtained position. In addition, the motor stops at a certain point and does not reach the position of greatest amplitude described by the setpoint. This stop occurs when the platform touches the lungs and crushes them. As the deformation of the foam increases, more force is needed. In that way, at one point, the motor does not have power enough to push the lungs further.

After that, the response of the 9.68:1 geared motor introduced on the platform for the AP motion (the one that bends the plastic sheets) is observed in Figure 4.3:

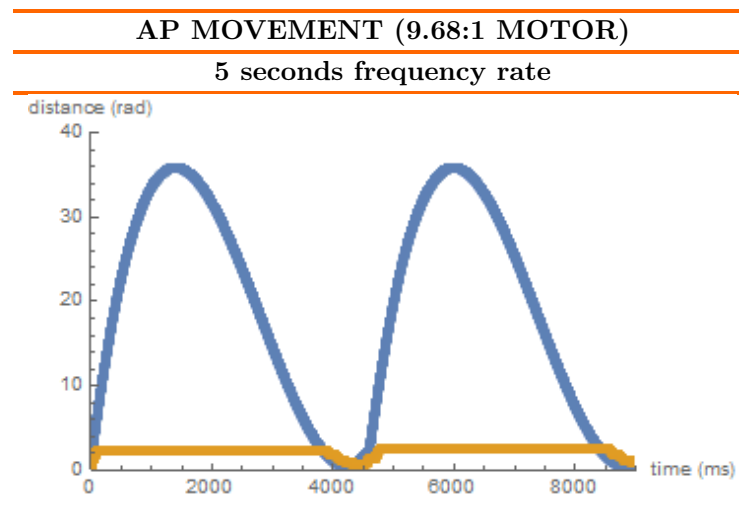


Figure 4.3: 9.68:1 motor in AP movement results.

In this case, the motor was tested at a frequency of 5 seconds, obtaining a rather poor result. As Figure 4.3 shows, the platform barely moves. This is because the 9.68:1 geared motor does not have the necessary torque to move the AP platform and bend the plastics. Trying to obtain a better solution, other plastic rods were built using polypropylene sheets. These sheets were cut to the desired dimensions. Then, three sheets were glued together with silicone to make the structure more rigid. The resulted structure is shown in Figure 4.4.



Figure 4.4: Polypropylene sheets.

Then, they were incorporated into the movement structure and the motor of 9.68:1 gearbox was tested again. The result was the same than with previous plastic sheets since the main problem was that the motor did not even have power to move the AP platform.

After that, the motors were changed, i.e., the 34:1 geared motor was inserted into the structure for the AP movement and the 9.68:1 geared motor was tested on the

SI platform. The previous position of the motors had been established since the SI movement could need more power as it had to deform more the foam. Thus, the new configuration was mainly implemented to test the effectiveness of the 34:1 geared motor in the AP motion. Great results were not expected for the 9.68:1 geared motor.

Therefore, as the motors had to reach new positions, the whole procedure explained in the previous Section to find the setpoint equations had to be repeated. Instead, an easier way could be carried out by normalizing the equations and multiplying them by the new desired distance. For example, using the 3.5 seconds frequency rate equation implemented for the SI movement in 34:1 gear motor, which maximum amplitude was 5cm:

$$\theta_{M(SI)_{3.5}}(t) = 71.394(t + 0.145 - 3.5cont)^3 - 464.46(t + 0.145 - 3.5cont)^2 + 780.74(t + 0.145 - 3.5cont) - 82.048 \quad (4.1)$$

To obtain the equation of a maximum amplitude of 2cm (desired amplitude in AP movement for 3.5 seconds frequency rate) it would be enough to multiply the equation by 2 and divide it by 5:

$$\theta_{M(AP)_{3.5}}(t) = [71.394(t + 0.145 - 3.5cont)^3 - 464.46(t + 0.145 - 3.5cont)^2 + 780.74(t + 0.145 - 3.5cont) - 82.048] \frac{2}{5} \quad (4.2)$$

This transformation was carried out for all the equations described in the Section 3, considering the old and new amplitudes, which are summarized in Table 4.1:

2.25 seconds frequency rate	
SI movement	AP movement
3.3cm	1cm
3.5 seconds frequency rate	
SI movement	AP movement
5cm	2cm
4.5 seconds frequency rate	
SI movement	AP movement
5cm	2cm
5 seconds frequency rate	
SI movement	AP movement
5cm	2cm

Tabla 4.1: Desired position (in centimeters) in each movement and frequency rate.

Therefore, the new equations for the SI and AP motions would be:

$$\theta_{M(AP)_{2.25}}(t) = [173.31(t + 0.089 - 2.25cont)^3 - 732.88(t + 0.089 - 2.25cont)^2 + 800.76(t + 0.089 - 2.25cont) - 52.699] \frac{1}{3.3} (4.3)$$

$$\theta_{M(AP)_{3.5}}(t) = [71.394(t + 0.145 - 3.5cont)^3 - 464.46(t + 0.145 - 3.5cont)^2 + 780.74(t + 0.145 - 3.5cont) - 82.048] \frac{2}{5} (4.4)$$

$$\theta_{M(AP)_{4.5}}(t) = [32.496(t + 0.178 - 4.5cont)^3 - 274.83(t + 0.178 - 4.5cont)^2 + 600.57(t + 0.178 - 4.5cont) - 82.048] \frac{2}{5} (4.5)$$

$$\theta_{M(AP)_5}(t) = [21.154(t + 0.177 - 5cont)^3 - 206.43(t + 0.177 - 5cont)^2 + 520.49(t + 0.177 - 5cont) - 82.048] \frac{2}{5} (4.6)$$

$$\theta_{M(SI)_{2.25}}(t) = [14.803(t + 0.089 - 2.25cont)^3 - 62.596(t + 0.089 - 2.25cont)^2 + 68.394(t + 0.089 - 2.25cont) - 4.4844] \frac{3.3}{1} (4.7)$$

$$\theta_{M(SI)_{3.5}}(t) = [8.1305(t + 0.145 - 3.5cont)^3 - 52.894(t + 0.145 - 3.5cont)^2 + 88.912(t + 0.145 - 3.5cont) - 8.7844] \frac{5}{2} (4.8)$$

$$\theta_{M(SI)_{4.5}}(t) = [3.7007(t + 0.178 - 4.5cont)^3 - 31.298(t + 0.178 - 4.5cont)^2 + 68.394(t + 0.178 - 4.5cont) - 8.7844] \frac{5}{2} (4.9)$$

$$\theta_{M(SI)_5}(t) = [2.409(t + 0.177 - 5cont)^3 - 23.508(t + 0.177 - 5cont)^2 + 59.275(t + 0.177 - 5cont) - 8.7844] \frac{5}{2} (4.10)$$

Which, considering only the first cycle, correspond to the diagrams of Figure 4.5:

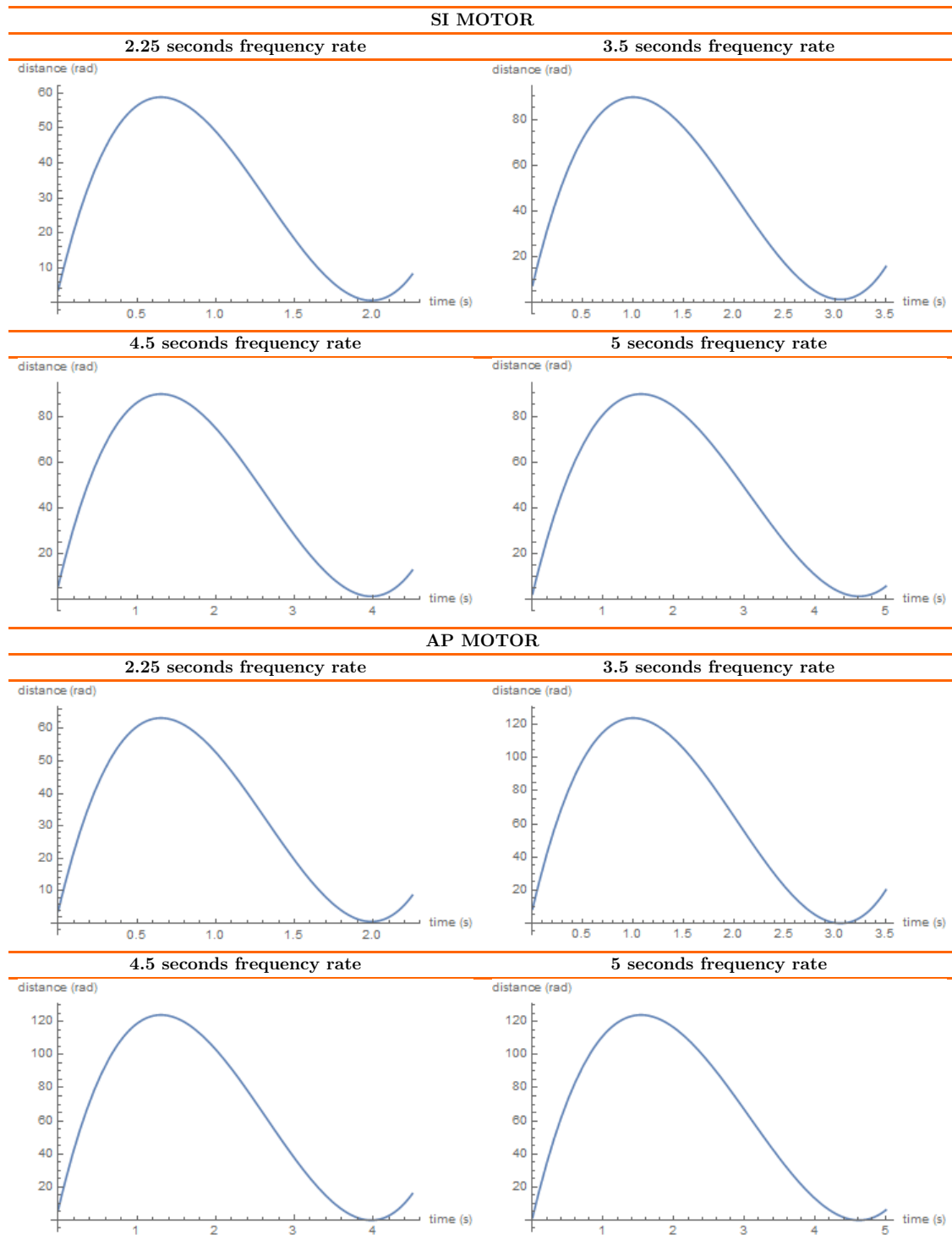


Figure 4.5: New equation diagrams.

Then, each motor was placed in its new positions and the result was observed. Using the 34:1 gear motor as the actuator for bending the plastic sheets that simulate AP movement, the results at each frequency rate are shown in Figure 4.6:

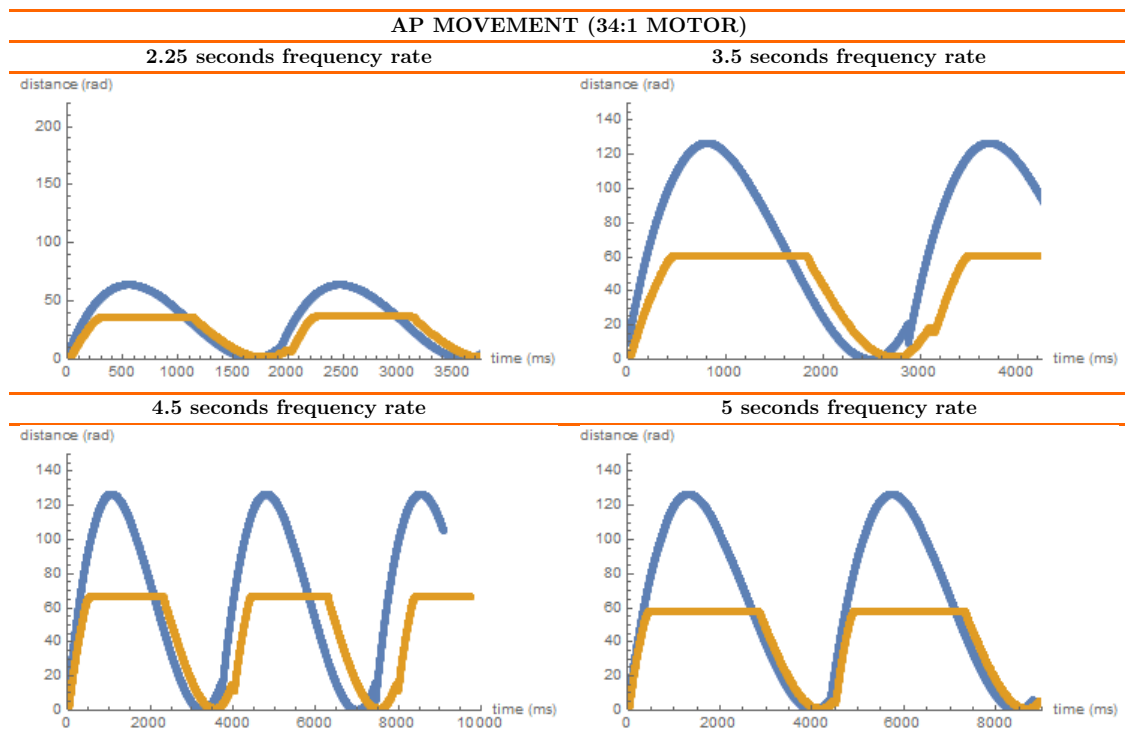


Figure 4.6: 34:1 motor in AP movement results.

Figure 4.6 shows how motor manages to bend the plastic sheets and hold them flexed. In addition, the graphs indicate that the motor does not reach the position of greatest amplitude. However, the movement that is produced achieves to raise the lungs a few centimeters. The problem in this case is, as the bar is rigid, the motor must exert enough force to keep it bending and sometimes it does not work, making the motor going back and producing jumps during the movement. These jumps are unrealistic and can damage the motor, so to avoid them, the rigid sheets were replaced by the ones made of polypropylene shown in Figure 4.4. Therefore, the results are shown in Figure 4.7:

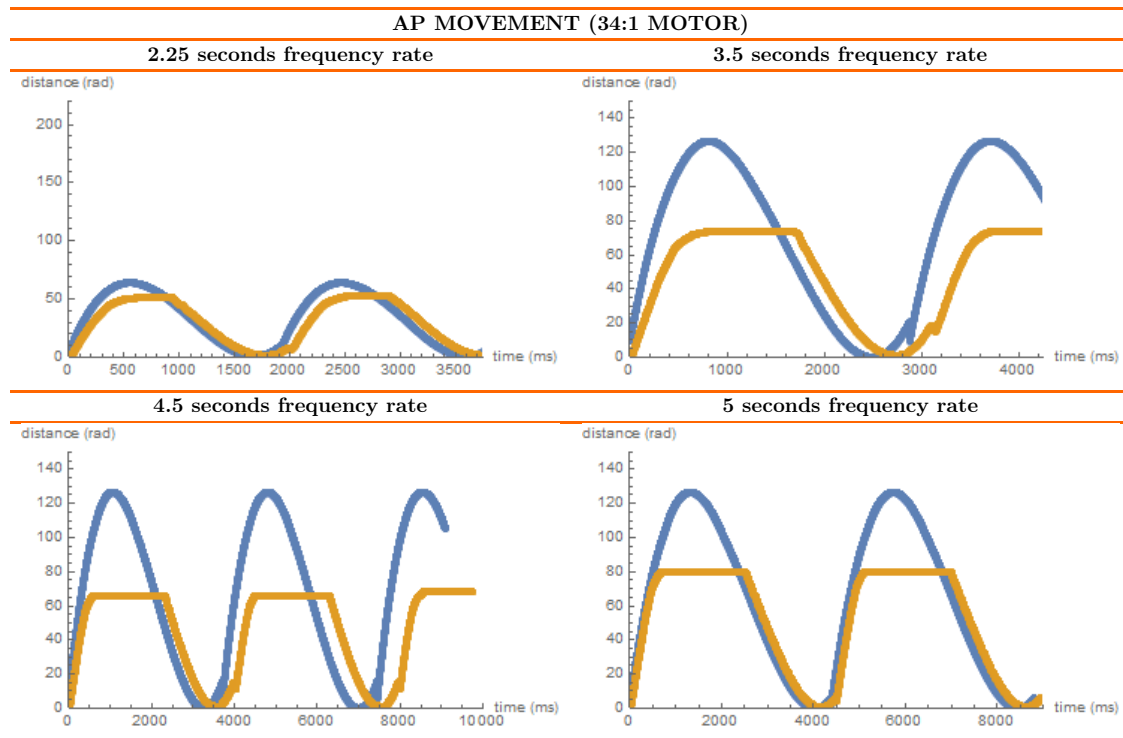


Figure 4.7: 34:1 motor in AP movement results with polypropylene sheets.

As Figure 4.7 shows, with this modification the motor was able to reach positions closer to the maximum amplitude than in the previous case. In addition, it was able to maintain these positions. As it did not have so much force against it, there was no backward movement and no jumps. On the other hand, these sheets, despite being less rigid than those of the previous case, produced movement of the lungs, so it would be an appropriate alternative. Figure 4.8 shows how the plastic sheets bend due to the motor displacement:



Figure 4.8: Bent plastic sheets.

On the other hand, the use of the motor with gearbox ratio of 9.68:1 in the SI movement is shown in Figure 4.9:

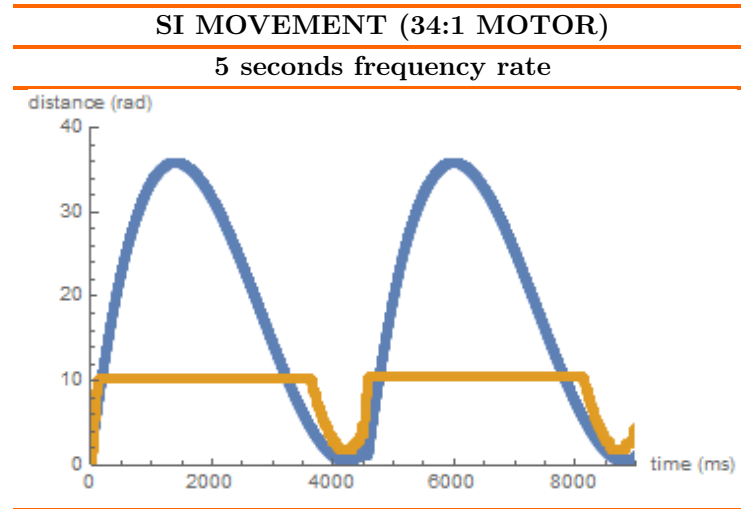


Figure 4.9: 9.68:1 motor in SI movement results.

The motor was tested for frequency rate of 5 seconds. As Figure 4.9 shows, the motor was not able to reach the desired positions. In fact, the movement shown corresponds to the movement of the platform until it reaches the foams. Once this position is achieved, the motor stops, without deforming the lungs even a little bit.

4.2. Result conclusions

These results show that the motor with 34:1 gearbox ratio is much more effective than the one with 9.68:1 gearbox ratio. When this project was started, the mechanical resistance of lungs and plastic sheets was not considered high enough to prevent the movement of the motors. Instead, the important role of such resistances in this work has been demonstrated.

In the case of the flexible plastic bars, the final result has been considerably satisfactory, since some deformation is observed. However, considering an alternative to be able to bend the more rigid plastic bars would be interesting. This could help to resist and move more weight inside the mannequin if necessary.

In the case of the deformation of lungs, it was expected to achieve a slightly larger deformation. Excluding the frequency rate option of 2.25 seconds, the desired displacement was 5cm. As mentioned above, this movement was slightly excessive compared to the displacement of the diaphragm of a person at complete rest. However, this value was established to achieve a satisfactory deformation of the foams and to better observe the trajectories defined by the markers. Taking that into account, the result would be appropriate if the person considered is completely at rest. In larger displacement the power of the motor would not be enough.

After the results obtained, the use of motors with larger gearboxes was evaluated, since they have more power and could achieve larger deformations. On the other

hand, motors with larger gearboxes would imply that they are slower and, in this MSc Thesis the speed is essential. In terms of time, as figure representing the movements of the 34:1 geared motor shows (Figure 4.2 and 4.7), the motor displacement does not completely match the setpoint. It describes the curve, but with a delay, which is also accumulated in each cycle. This is because the motor of this gearbox cannot reach the required speed to reach the desired positions in time.

Therefore, considering replace the motors with others with different gearboxes, the final decision was to use two 34:1 gearbox motor. That is why, higher gearboxes would not reach the optimum speed, and lower ones would hardly deform the lungs or bend the plastic sheets. Therefore, other motor models should be used. The final equations implemented in the Arduino have been:

$$\theta_{M(SI)_{2.25}}(t) = 173.31(t + 0.089 - 2.25cont)^3 - 732.88(t + 0.089 - 2.25cont)^2 + 800.76(t + 0.089 - 2.25cont) - 52.69 \quad (4.11)$$

$$\theta_{M(SI)_{3.5}}(t) = 71.394(t + 0.145 - 3.5cont)^3 - 464.46(t + 0.145 - 3.5cont)^2 + 780.74(t + 0.145 - 3.5cont) - 82.048 \quad (4.12)$$

$$\theta_{M(SI)_{4.5}}(t) = 32.496(t + 0.178 - 4.5cont)^3 - 274.83(t + 0.178 - 4.5cont)^2 + 600.57(t + 0.178 - 4.5cont) - 82.048 \quad (4.13)$$

$$\theta_{M(SI)_5}(t) = 21.154(t + 0.177 - 5cont)^3 - 206.43(t + 0.177 - 5cont)^2 + 520.49(t + 0.177 - 5cont) - 82.048 \quad (4.14)$$

$$\theta_{M(AP)_{2.25}}(t) = 52.42(t + 0.089 - 2.25cont)^3 - 222.08(t + 0.089 - 2.25cont)^2 + 242.65(t + 0.089 - 2.25cont) - 15.97 \quad (4.15)$$

$$\theta_{M(AP)_{3.5}}(t) = 28.56(t + 0.145 - 3.5cont)^3 - 185.78(t + 0.145 - 3.5cont)^2 + 312.30(t + 0.145 - 3.5cont) - 32.82 \quad (4.16)$$

$$\theta_{M(AP)_{4.5}}(t) = 13.00(t + 0.178 - 4.5cont)^3 - 109.93(t + 0.178 - 4.5cont)^2 + 240.23(t + 0.178 - 4.5cont) - 32.82 \quad (4.17)$$

$$\theta_{M(AP)_5}(t) = 8.46(t + 0.177 - 5cont)^3 - 82.57(t + 0.177 - 5cont)^2 + 208.20(t + 0.177 - 5cont) - 32.82 \quad (4.18)$$

Chapter 5

Conclusions

5.1. Conclusions

In this MSc Thesis the design and improvement of a thoracic mannequin which could simulate the respiratory movement for dosymetric analysis in radiotherapy have been defined. To do that, several steps were followed, all of them equally important. The first step was the study of the respiratory system, cancer and clinical methods involved in it, such as radiotherapy. Once these factors were understood and with sufficient knowledge of the movements involved in respiration, it was necessary to find at least three materials with different densities to simulate soft tissues, lungs, bones, and muscles. After that, a structure to produce the desired AP and SI movements was designed and built. Then, two motors were programmed for different frequency rates of respiration by defining PID controllers for each movement and each period. Lastly, the motors were inserted in the mechanical structure and the results were analyzed.

All these points fulfill a main characteristic of numerous scientific studies: they are reproducible. First, considering the materials that have been defined to simulate each density, they can be easily and cheaply found.

On the other hand, the mechanical structure, was mainly built by pieces printed on 3D printers, a tool whose use is becoming more popular and increasingly easy to find. In addition, the designed pieces are not difficult to replicate and print. They were carefully measured so that they all fit together, and their effectiveness has been demonstrated.

Then, an open-source Arduino board has been used for the implementation of the movement, easy to use and program, and compatible with different models of motors and drivers. In addition, by programming it as a controller, the position in which the motion platform is located is checked in real time, making the system more accurate.

Regarding the motors, after several tests, it has been determined that the best option is to use 34:1 geared 12V motors of the motor models at hand. These motors were chosen among the available ones found in the laboratory, being the ones that would best fit the desired power/speed specifications, although not achieving the desired optimum response. Among the proposals for future lines, related below, a

study of other similar Arduino-compatible motors that would completely reach the speed and power requirements described for the phantom could be carried out.

5.2. Future Lines

Remarkable results have been achieved during this MSc Thesis. However, some improvements could be studied to achieve the developing of a completely perfect phantom.

First, as mentioned in previous section, a study of accurate motors for this system could be carried out. In this way, the use of more powerful and faster motors could be considered. Taking into account the new motors, it would be enough to modify the equations described for the movement, considering that they are implemented for motors with 34:1 gearbox. On the other hand, if the size of these motors were similar to that the ones chosen in this work, it would not even be necessary to modify the mechanical structure.

Then, four frequency rates have been defined in the project considering that any patient's breathing would be within these ranges. However, it could be studied how to personalize the movement depending on each patient. This would mean that measuring parameters in them, the phantom could efficiently and realistically simulate the patient's breathing. In this regard, VisionRT® system or Varian RPM® system are responsible for recording patient movements. Therefore, it would be necessary to study how to translate the recorded data and relate it to the phantom in order to describe the desired movement.

On the other hand, any simulated motion should be analyzed with computed tomography scans to check the position of the markers in each case and to be able to determine the accuracy of the implementation. These tests should be carried out every time a modification is made to the phantom. In addition, considering the movements recorded in relation to the displacements of the motors, trajectories of the radiotherapy beam could be described. In this way, the treatment could be automated if a very close relationship were found between the movement of the thorax and the displacement of a tumor inside it.

Last, once this was carried out and its efficiency demonstrated, it would be interesting to develop other mannequin models. In this way, models could be designed closer to a woman's body, another one where people with a higher weight were considered, or even another one with a smaller body and closer to a child/teenager.

References

- [1] Statista. Tipos de cancer mas mortales en el mundo en 2020. <https://es.statista.com/estadisticas/636256/mortalidad-por-cancer-muertes-a-nivel-mundial-por-tipo/#:~:text=En%20el%20a%C3%B1o%202020%2C%201,pulm%C3%B3n%20en%20todo%20el%20mundo,2021.> [Accessed online] 16-06-2021.
- [2] GECP. Lung Cancer Research. Los tumores de pulmon, primera causa de muerte por cancer en españa en 2020. <https://www.gecp.org/los-tumores-de-pulmon-primera-causa-de-muerte-por-cancer-en-espana-en-2020/#:~:text=Los%20datos%20parciales%20de%20mortalidad,de%20todas%20las%20muertes%20por,2020.> [Accessed online] 16-06-2021.
- [3] Servicios Sociales e Igualdad Ministerio de Sanidad. El consumo de tabaco en españa y el mundo, en datos y gráficos. <https://www.epdata.es/datos/consumo-tabaco-espana-datos-graficos/377#:~:text=El%2022%25%20de%20la%20poblaci%C3%B3n,partir%20de%20los%2075%20a%C3%B1os,2021.> [Accessed online] 16-06-2021.
- [4] Asociacion Española Contra el Cancer. Tratamientos del cancer de pulmon y secuelas. <https://www.aecc.es/es/todo-sobre-cancer/tipos-cancer/cancer-pulmon/secuelas-tratamientos-cancer-pulmon#:~:text=Los%20tratamientos%20m%C3%A1s%20frecuentemente%20empleados,s%C3%ADntomas%20que%20presenta%20cada%20enfermo,2018.> [Accessed online] 16-06-2021.
- [5] Lee Y. Shin H. Ji S. Park S. Kim J. Jang H. & Kang Y Kim, J. Development of deformable moving lung phantom to simulate respiratory motion in radiotherapy. *Medical dosimetry : official journal of the American Association of Medical Dosimetrists*, 2(41):113–117, 2016.
- [6] & Zhang X Zhou, J. A lung phantom model to study pulmonary edema using lung ultrasound surface wave elastography. *Ultrasound in medicine & biology*, 11(44):2400–2405, 2018.
- [7] Madhuranthakam A. J. Lenkinski R. & Bankier A. A Molinari, F. Ultrashort echo time mri of pulmonary water content: assessment in a sponge phantom at 1.5 and 3.0 tesla. *Diagnostic and interventional radiology*, 1(20):34–41, 2014.
- [8] Samsuzzaman M. Kibria S. & Islam M Islam, M.T. Experimental breast phantoms for estimation of breast tumor using microwave imaging systems. *IEEE Access*, 1(6):78587–78597, 2018.
- [9] Ji Z. Ding W. Ye F. Fu, Y. and C. Lou. Thermoacoustic imaging over large field of view for three-dimensional breast tumor localization: A phantom study. *Medical Physics*, 11(41):110701, 2014.

- [10] Wroblewski J. Lederlin M. Dinkel J. Eichinger M. Koenigkam-Santos M. Biederer J. Kauczor H. U. Puderbach M. U. & Jobst B. J. Wielpütz, M. O. Computer-aided detection of artificial pulmonary nodules using an ex vivo lung phantom: influence of exposure parameters and iterative reconstruction. *European Journal of Radiology*, 5(84):1005–1011, 2015.
- [11] Richard N Symonds-Taylor J. Bedford J. L. & Webb-S Nioutsikou, E. Quantifying the effect of respiratory motion on lung tumour dosimetry with the aid of a breathing phantom with deforming lungs. *Physics in medicine and biology*, 14(51):3359–3374, 2006.
- [12] Lam K. Litzenberg-D. & Balter J Kashani, R. Technical note: a deformable phantom for dynamic modeling in radiation therapy. *Medical Physics*, 1(34):199–201, 2007.
- [13] Biederer J. Lohberger-F. Fabel M. & Hartmann G. H. Remmert, G. Four-dimensional magnetic resonance imaging for the determination of tumour movement and its evaluation using a dynamic porcine lung phantom. *Physics in medicine and biology*, 18(52):401–415, 2007.
- [14] Heath E. Stroian-G. Collins D. L. & Seuntjens J. Serban, M. A deformable phantom for 4d radiotherapy verification: design and image registration evaluation. *Medical Physics*, 3(35):1094–1102, 2008.
- [15] Serban M. Seuntjens-J. & Cygler J. E. Cherpak, A. 4d dose-position verification in radiation therapy using the radpos system in a deformable lung phantom. *Medical Physics*, 1(38):179–187, 2011.
- [16] Suh T. S.-& Lee D. S. Chang, J. Development of a deformable lung phantom for the evaluation of deformable registration. *Journal of applied clinical medical physics*, 1(11):3081, 2010.
- [17] Foltz W. D. Velec M. Moseley J. L. Al-Mayah A. & Brock K. K. Niu, C. J. A novel technique to enable experimental validation of deformable dose accumulation. *Medical Physics*, 2(39):765–776, 2012.
- [18] Richter D. Schuy C. Schubert E. Haberer T. Durante M.-& Bert C. Steidl, P. A breathing thorax phantom with independently programmable 6d tumour motion for dosimetric measurements in radiation therapy. *Physics in medicine and biology*, 8(57):2235–2250, 2012.
- [19] Seco J. Lu X. Q. Ebe K. Mayo C.-Ionascu D. Winey B. Giakoumakis N. Aristophanous M. Berbeco R. Rottman J. Bogdanov M. Schofield D. & Lingos T. Court, L. E. Use of a realistic breathing lung phantom to evaluate dose delivery errors. *Medical Physics*, 11(37):5850–5857, 2010.
- [20] & Sawant A. Cheung, Y. An externally and internally deformable, programmable lung motion phantom. *Medical Physics*, 5(42):2585–2593, 2015.

-
- [21] Sabouri P. Repetto C. & Sawant A. Ranjbar, M. A novel deformable lung phantom with programably variable external and internal correlation. *Medical Physics*, 5(46):1995–2005, 2019.
 - [22] Cleveland Clinic. Respiratory system: Functions, facts, organs & anatomy. <https://my.clevelandclinic.org/health/articles/21205-respiratory-system#:~:text=The%20respiratory%20system%20is%20the,waste%20gases%20like%20carbon%20dioxide,2020>. [Accessed online] 16-06-2021.
 - [23] Pediatric Pulmonary Division. Normal lung function. <https://pulmonary.pediatrics.med.ufl.edu/centers-programs/asthma-program/normal-lung-function/>, 2021. [Accessed online] 16-06-2021.
 - [24] British Lung Foundation. How your lungs work. <https://www.blf.org.uk/support-for-you/how-your-lungs-work/about-the-lungs#:~:text=The%20lungs%20absorb%20oxygen%20from,gas%20when%20you%20breathe%20out,2021>. [Accessed online] 16-06-2021.
 - [25] Huang C. & Matthews G. Chambers, D. *Static Lung Volumes*, volume 12. Cambridge University Press, Cambridge, 1993.
 - [26] Andrienne Santos. Diaphragm overview. <https://www.healthline.com/human-body-maps/head-arteries-nerves#2>, 2018. [Accessed online] 16-06-2021.
 - [27] Bordoni B. Safarini OA. Anatomy, thorax, ribs. <https://www.ncbi.nlm.nih.gov/books/NBK538328/>, 2021. [Accessed online] 16-06-2021.
 - [28] Physiopedia. Muscles of respiration. https://www.physio-pedia.com/Muscles_of_Respiration, 2021. [Accessed online] 16-06-2021.
 - [29] Simon Kidd. How to activate your diaphragm to improve breathing and performance. <http://breakingmuscle.com/cycling/how-to-activate-your-diaphragm-to-improve-breathing-and-performance>, 2015. [Accessed online] 16-06-2021.
 - [30] Sharma S. Haddad M. Physiology, lung. <https://www.ncbi.nlm.nih.gov/books/NBK545177/>, 2020. [Accessed online] 16-06-2021.
 - [31] Moustarah F. Desai JP. Pulmonary compliance. <https://www.ncbi.nlm.nih.gov/books/NBK538324/>, 2020. [Accessed online] 16-06-2021.
 - [32] Physiopedia. Lung compliance. https://www.physio-pedia.com/Lung_Compliance, 2021. [Accessed online] 16-06-2021.
 - [33] Quizlet. Respiratory mechanics. <https://quizlet.com/116609670/respiratory-mechanics-i-flash-cards/>, 2020. [Accessed online] 16-06-2021.

- [34] & Vesin J. Mirmohamadsadeghi, L. Respiratory rate estimation from the ecg using an instantaneous frequency tracking algorithm. *Biomed*, 1(14):66–72, 2014.
- [35] Amirnazarullah M.N. Jafri M.M. & Abdullah S. Hadis, N.S. Iot based patient monitoring system using sensors to detect, analyse and monitor two primary vital signs. *Biomed*, (1535), 2020.
- [36] Respelearning. Normal breathing. <https://www.respelearning.scot/topic-1-anatomy-and-physiology/normal-breathing>, 2018. [Accessed online] 16-06-2021.
- [37] Nirvana Fitness. Normal respiratory frequency & volume. <https://nirvana.fitness/normal-respiratory-frequency---volume-20-04-2015.html>, 2015. [Accessed online] 16-06-2021.
- [38] Wheatley I. Respiratory rate 4: breathing rhythm and chest movement. *Nursing Times*, 9(144):49–50, 2018.
- [39] Jun Horie Hideo Kaneko. Breathing movements of the chest and abdominal wall in healthy subjects. *Respiratory care*, 9(57):1442–1451, 2012.
- [40] & Kristinsdóttir E. K. Ragnarsdóttir, M. Breathing movements and breathing patterns among healthy men and women 20-69 years of age. *Respiration; international review of thoracic diseases*, 1(73):48–54, 2006.
- [41] Mauro A. L. D’Angelo M. G. Turconi A. C. Bresolin-N. Pedotti A. & Aliverti A. Romei, M. Effects of gender and posture on thoraco-abdominal kinematics during quiet breathing in healthy adults. *Respiratory physiology & neurobiology*, 3(172):184–191, 2010.
- [42] Lu W. W. Luk K. D. & Karlberg E. M Leong, J. C. Kinematics of the chest cage and spine during breathing in healthy individuals and in patients with adolescent idiopathic scoliosis. *Spine*, 13(24):1310–1315, 1999.
- [43] American Cancer Society. What is cancer? <https://www.cancer.org/cancer/cancer-basics/what-is-cancer.html>, 2020. [Accessed online] 16-06-2021.
- [44] Cleveland Clinic. Cancer overview. [https://my.clevelandclinic.org/health/diseases/12194-cancer-overview#:~:text=Cancer%20is%20a%20disease%20that,%20or%20malignant%20\(cancerous](https://my.clevelandclinic.org/health/diseases/12194-cancer-overview#:~:text=Cancer%20is%20a%20disease%20that,%20or%20malignant%20(cancerous), 2016. [Accessed online] 16-06-2021.
- [45] CancerConnect. Overview of lung cancer. <https://news.cancerconnect.com/lung-cancer/overview-of-lung-cancer#:~:text=Lung%20cancer%20is%20characterized%20by,they%20appear%20under%20a%20microscope>, 2021. [Accessed online] 16-06-2021.
- [46] Lung Cancer Risk Assessment Tool. Does lung cancer screening make sense for me? https://www.aats.org/aatsimis/AATSWeb/Resources/Lung_Cancer_Screening/AATSWeb/Association/About/Resources/Lung_Cancer_Risk_

- Assessment_Tool.aspx?hkey=29f118a8-d7a6-4bcd-a9b3-7e85484881b8, 2018. [Accessed online] 16-06-2021.
- [47] American Lung Association. Lung cancer staging. <https://www.lung.org/lung-health-diseases/lung-disease-lookup/lung-cancer/learn-about-lung-cancer/lung-cancer-staging#:~:text=Small%20cell%20lung%20cancer%20is%20described%20using%20two%20stages%3A%20limited,opposite%20lung%20or%20distant%20organs>, 2021. [Accessed online] 16-06-2021.
- [48] Center for Disease Control & Prevention. How is lung cancer diagnosed and treated? https://www.cdc.gov/cancer/lung/basic_info/diagnosis_treatment.html, 2020. [Accessed online] 16-06-2021.
- [49] Gianfaldoni R. Wollina U. Lotti J. Tchernev G. & Lotti T. Gianfaldoni, S. An overview on radiotherapy: From its history to its current applications in dermatology. *Macedonian journal of medical sciences*, 4(5):521–525, 2017.
- [50] National Cancer Institute. External beam radiation therapy for cancer. <https://www.cancer.gov/about-cancer/treatment/types/radiation-therapy/external-beam>, 2018. [Accessed online] 16-06-2021.
- [51] American Association of Physicists in Medicine. The management of respiratory motion in radiation oncology. https://www.aapm.org/pubs/reports/RPT_91.pdf, 2006. [Accessed online] 16-06-2021.
- [52] Schubert J. DenOtter TD. Hounsfield unit. <https://www.ncbi.nlm.nih.gov/books/NBK547721/>, 2021. [Accessed online] 16-06-2021.
- [53] Nic Anthony. How to hounsfield: Blood or ascites. <http://blog.clinicalmonster.com/2020/06/02/how-to-hounsfield-in-emergency-medicine/>. [Accessed online] 21-06-2021.
- [54] Keeeper. Cómo hacer slime. las recetas más populares. https://www.keeeper.com/es/como_hacer_slime/. [Accessed online] 16-06-2021.
- [55] Morcelles K. & Bertemes-Filho Sirtoli, V. G. Electrical properties of phantoms for mimicking breast tissue. *IEEE Engineering in Medicine and Biology Society*, pages 157–160, 2017.
- [56] Decathlon. Bolsa de agua 2l. https://www.decathlon.es/es/p/bolsa-de-agua-2-1/_/R-p-184912?mc=8399482&LGWCODE=1&gclid=Cj0KCQjwktKFBhCkARIsAJeDT0jjiEiXsq-sXsyxR6cHdy9slAmNcA4e4TsSfFvyQitdcs38i-WsT8caAiwcB&gclidsrc=aw.ds. [Accessed online] 16-06-2021.
- [57] Decathlon. Compresas calor frio m. https://www.decathlon.es/es/p/compresa-calor-frio-m-bolsa-frio-reutilizable-talla-m/_/R-p-304181?mc=8518815. [Accessed online] 16-06-2021.
- [58] Espuma a medida. Espuma cuadrangular. <https://www.espumaamedida.com/espuma-cuadrangular.html>. [Accessed online] 16-06-2021.

- [59] Sportlife. ¿que pesa mas el musculo o la grasa? https://www.sportlife.es/blogs/nutricionydeporte/que-pesa-mas-la-grasa-o-el-musculo_200290_102.html. [Accessed online] 16-06-2021.
- [60] Iberomed. Maniqui rcp-aed adulto. prestna. basico. https://iberomed.es/emergencias/formacion-y-simuladores/maniqui-rcp-aed-adulto-prestan.html?gclid=EAIaIQobChMI48CMv5mj5AIVkUPTCh3BvgUJEAkYDyABEgINgPD_BwE%3Fgclid%3DEAIaIQobChMI48CMv5mj5AIVkUPTCh3BvgUJEAkYDyABEgINgPD_BwE. [Accessed online] 16-06-2021.
- [61] Pololu. 75:1 metal gearmotor 25dx66l mm lp 12v with 48 cpr encoder (no end cap). <https://www.pololu.com/product/3266>. [Accessed online] 16-06-2021.
- [62] Aprendiendo Arduino. Motor dc). <https://aprendiendoarduino.wordpress.com/tag/motor-dc/>, 2018. [Accessed online] 16-06-2021.
- [63] Arduino Store. Arduino due. <https://store.arduino.cc/arduino-due>. [Accessed online] 16-06-2021.
- [64] Picuino. Controlador pid. <https://www.picuino.com/es/arduprog/control-pid.html>. [Accessed online] 16-06-2021.
- [65] Iñigo Gutiez. Programacionessiemens. <https://programacionsiemens.com/pid-en-step7/>, 2013. [Accessed online] 16-06-2021.
- [66] Sergio Andres Castaño. Sintonia de control pid. <https://controlautomaticoeducacion.com/control-realimentado/ziegler-nichols-sintonia-de-control-pid/>. [Accessed online] 16-06-2021.

Appendix A

Ethical, economic, social and environmental aspects

A.1. Introduction

This MSc Thesis has been carried out through a collaboration between the radiophysics department of the Hospital Universitario Puerta de Hierro and the robotics department of the Escuela Técnica Superior de Ingeniería de Telecomunicaciones. In this way, the medical knowledge of the hospital and the technological resources of robotics have been merged, making a multidisciplinary work of Biomedical Engineering.

As mentioned in Section 1, lung cancer is the type of cancer that produces the most deaths worldwide, doubling the number of deaths caused by the next most lethal type of cancer. Lung cancer patients who are treated with radiotherapy must receive a much higher dose than in other cancers because the breathing movement makes uncertain the location of the tumor. Thus, the need to focus the radiotherapy beam arises, and for this purpose, phantoms are proposed to help describe the path followed by the tumor.

Then, the main objective of this project was to build a thoracic mannequin capable of mimicking the respiratory movement of a person. In this way, this solution not only will help patients, but also the hospital staff as it allows for more effective treatment, helping them to save resources.

A.2. Description of relevant impacts

Firstly, the social impact has been analyzed. As aforementioned, lung cancer is the most lethal cancer and therefore this solution could have a great impact on the people affected improving their quality of life. On the other hand, another relevant factor would be the environmental impact. In this sense, the phantom has been built mainly with high durability plastics to minimize environmental impact. In addition, the

materials used in the mannequin are easy to find and not very expensive, thus it could be said the solution is a low-cost phantom.

A.3. Detailed analysis of some of the main impacts

The most remarkable aspect of this project is its social and clinical impact. This solution makes possible to efficiently analyze the movement of a lung tumor in a patient by considering the patient's breathing. Its purpose is to improve radiotherapy treatment, helping to focus the irradiated dose. This would allow the healthy cells surrounding the tumor to remain unaffected by the radiotherapy, helping to minimize such damage to the patient. In this way, the side effects that could occur in the affected person would be reduced, achieving an improvement in their quality of life, and also giving more possibilities for the removing of the tumor.

On the other hand, regarding the environmental aspect, different factors were analyzed. Firstly, most of the materials used in the phantom are plastic. It could be considered that the environmental impact is high due to the use of these materials. However, a deep analysis was carried out to ensure the high durability of the chosen plastics, thus, the environmental impact would not be that high. Similarly, about planned obsolescence, only that of the motors used should be considered.

In another aspect, considering the functionality of the phantom, a very economical solution has been developed. All the materials used can be easily obtained, some are sold for domestic use or for handicrafts. This also ensures the reproducibility of the solution, giving it more value. In addition, considering that it improves the patient's treatment, it would help to reduce hospital and patients' expenses.

Finally, being a solution that simulates a patient but does not interact with the patient, there is no risk involved in terms of personal injury. Moreover, it does not record human data so it could also not imply a threat in terms of data privacy and similar rights.

A.4. Conclusions

After this analysis, the social, clinical, economic, and environmental impacts become evident. Socially and clinically, it means a breakthrough in the radiotherapy treatment of lung cancer. As it has been said, it improves the patient's quality of life, improves the treatment performed in the hospital, and helps to reduce costs for such treatments as they are more effective. On the other hand, it is reflected that to reduce the environmental impact, each material used was well analyzed in order to guarantee its durability.

In addition, the results do not pose any danger to patients or physicians, nor do they question any ethical principles that might be found in other types of solutions.

On the other hand, it would be interesting, as mentioned in the conclusions of the project, to create variants of the phantom that adapt to different bodies, such as women, children or people with a higher weight. This would ensure an optimal social impact by guaranteeing accurate treatment for everyone.

Finally, when considering improvements in the phantom, it would be necessary to take into account all the impacts analyzed during this appendix, so that they continue to be respected along the same lines and do not pose any problems.

Appendix B

Economic budget

The economic budget implied in the development of this MSc Thesis will be shown in the following tables. First, as it has been an important aspect in this project, the material costs will be defined. After that, the Human Resources and other costs will be indicated.

Material costs:

Discarded material for soft tissue	Cost (€)
Slime	1
Materials for homemade slime	10
Agar	12.5
Gelatine	2
Camelback bag	9.99
Cold/heat bag	5.99
Bag sealer	10
Discarded material for lungs	
High density foams	70.92
Other discarded material	
DC motor 9.68:1 LP 12V	28.82
DISCARDED MATERIAL COSTS	151.22

Tabla B.1: Discarded material costs.

Useful materials	Cost (€)
Liquid latex for molds (1L)	10.42
Plastic bags	3.75
Low density foam	13.45
CPR-AED mannequin Prestan	154.9
PLA filaments for 3D printer	8.78
Wooden sticks	3
Pullies	22.97
Bents	7.28
Plastic screws	8.32
Arduino Due	38.25
DC motors 34:1 LP 12V	60.9
Motor driver	13.54
Wooden board	20.5
Silicone bars	1
Polypropylene sheets	1
PVC sheets	15
USEFUL MATERIAL COSTS	383.06

Tabla B.2: Useful materials costs.

Discarded material costs (€)	151.22
Useful material costs (€)	383.06
TOTAL MATERIAL COSTS (€)	534.28

Tabla B.3: Total materials costs.

Technical costs:

Technical costs	Price (€)	Time of use (months)	Amortization (years)	Total (€)
Computer	800	4	6	44.44
Arduino software	Free			
Wolfram Mathematica software	Free (student license)			
TOTAL TECHNICAL COSTS				44.44

Tabla B.4: Total technical costs.

Human resources costs:

Human resources costs	Hours	Price/Hour (€)	Total (€)
Engineer tutor	20	60	1200
Medical tutor	12	60	720
Engineer junior	450	30	13500
TOTAL HUMAN RESOURCES COSTS			15420

Tabla B.5: Total human resources costs.

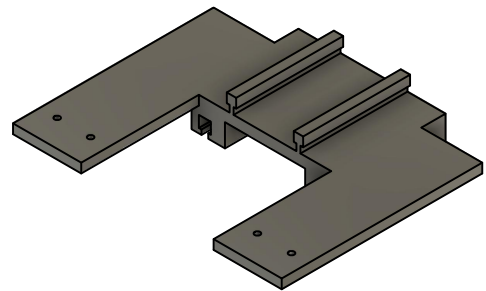
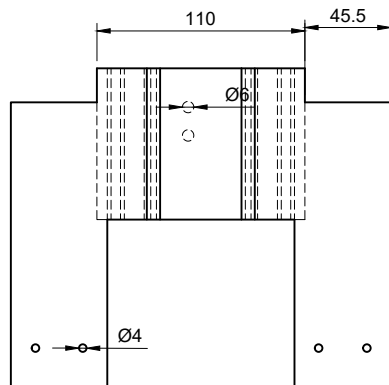
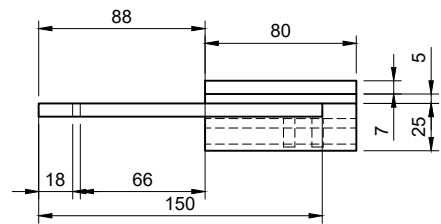
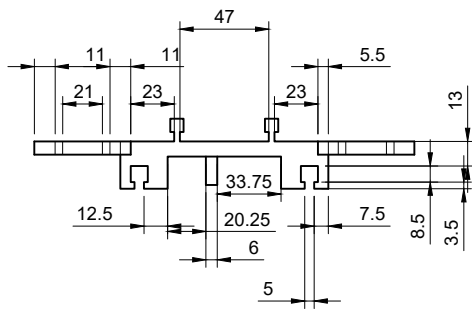
Total material costs (€)	534.28
Total technical costs (€)	44.44
Total human resources costs (€)	15420
TOTAL BUDGET (€)	15998.72

Tabla B.6: Total budget.

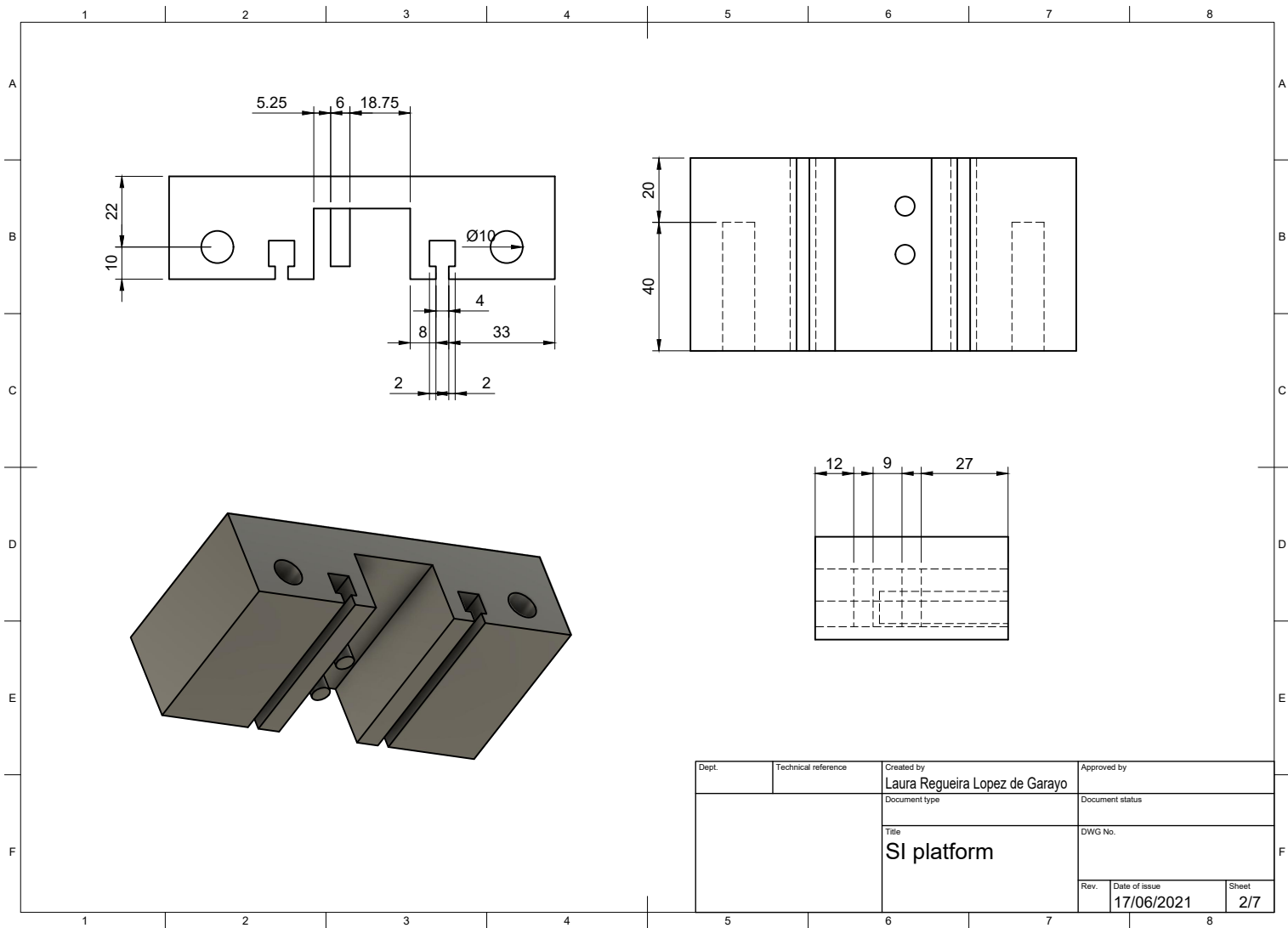
Appendix C

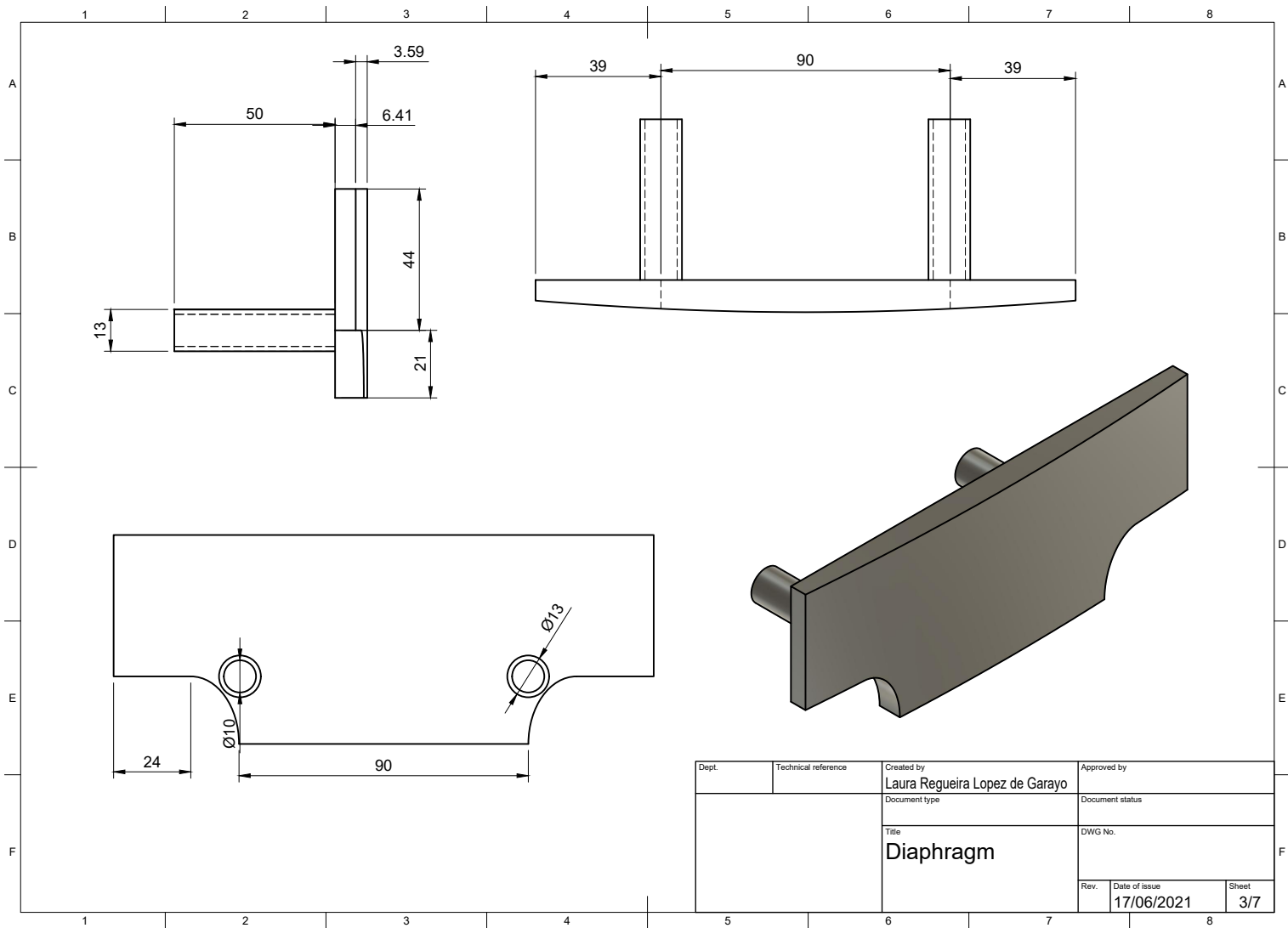
Drawings of the 3D pieces

This appendix shows the drawings of the 3D printed pieces for the mechanical structure of the phantom.

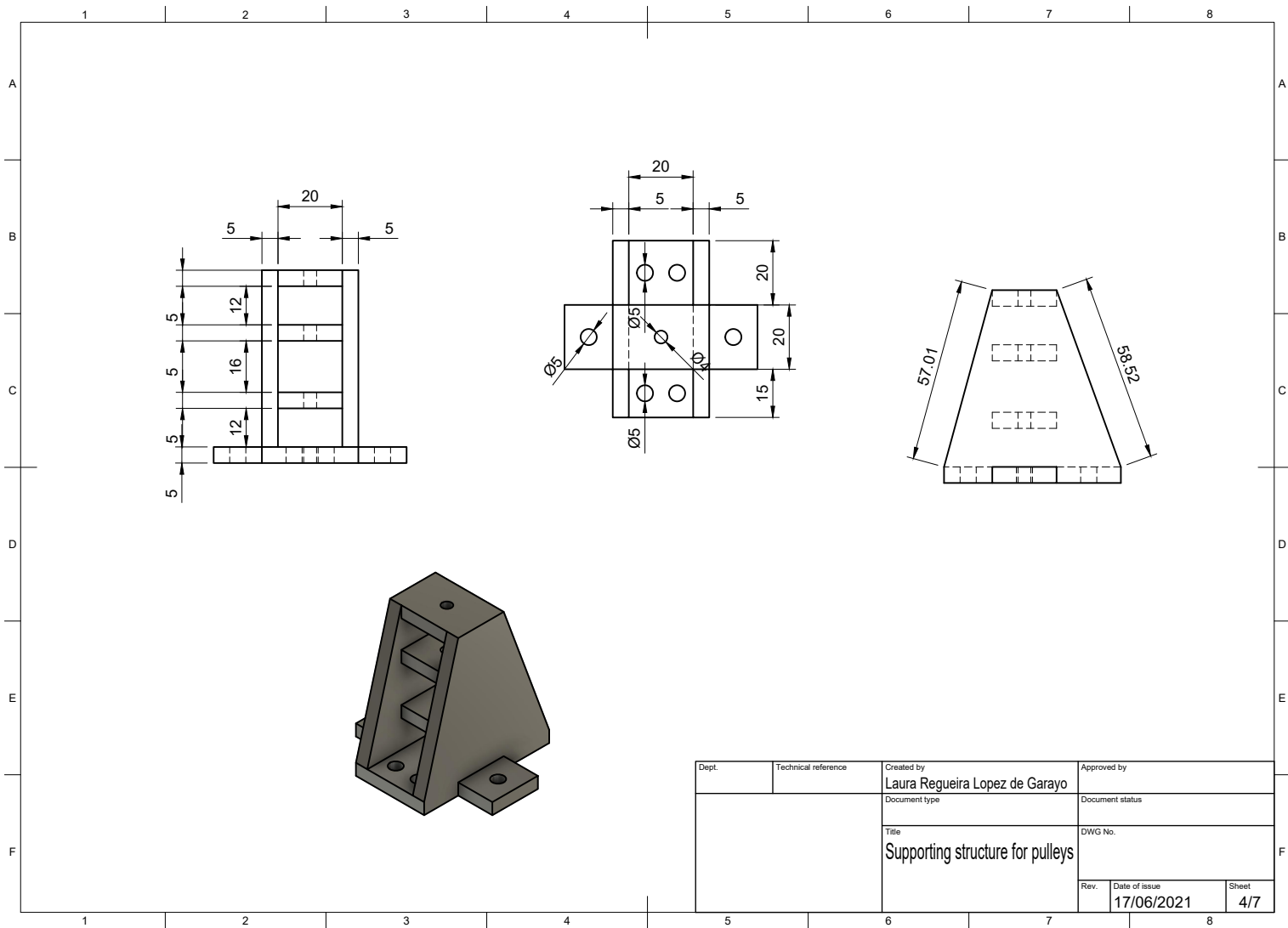


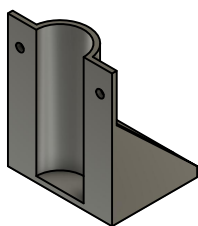
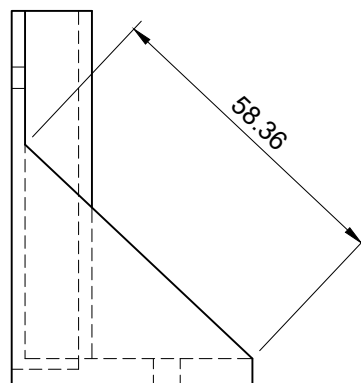
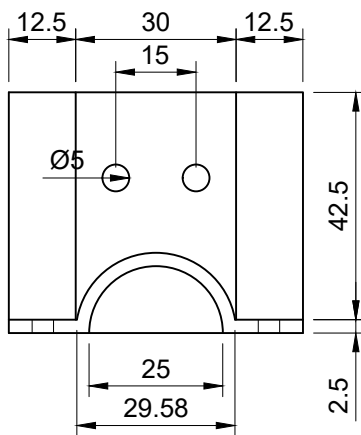
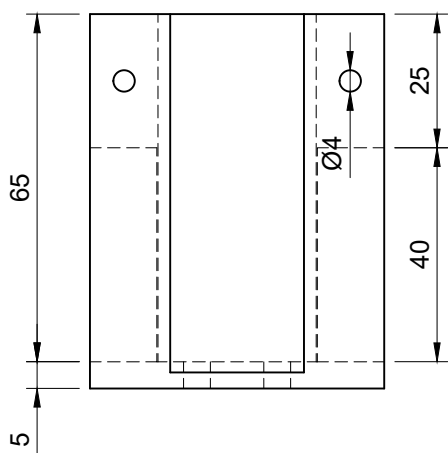
Dept.	Technical reference	Created by Laura Regueira Lopez de Garayo	Approved by
		Document type	Document status
		Title AP platform	DWG No.
		Rev.	Date of issue 17/06/2021
			Sheet 1/7



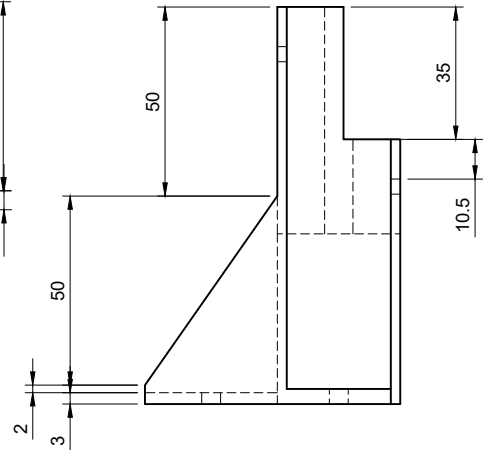
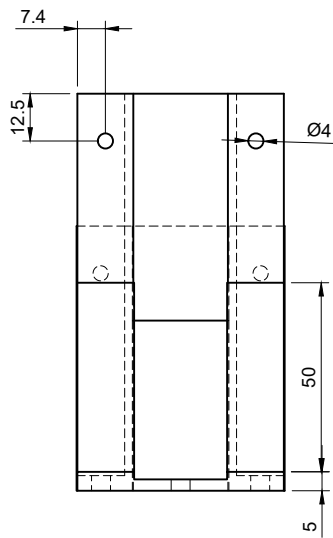
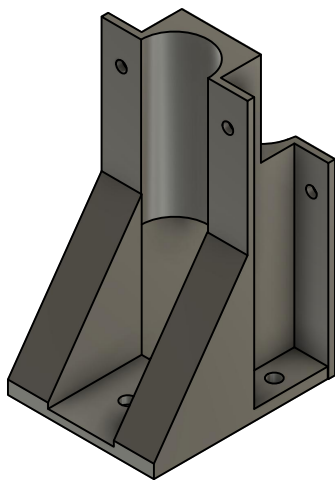
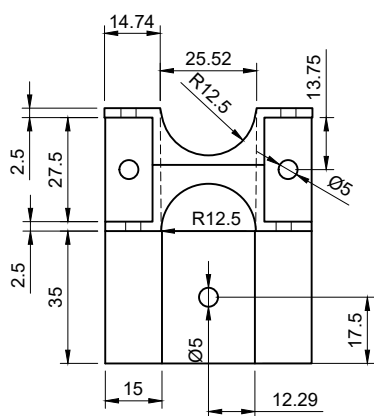


Dept.	Technical reference	Created by Laura Regueira Lopez de Garayo	Approved by
		Document type	Document status
		Title Diaphragm	DWG No.
		Rev.	Date of issue 17/06/2021
			Sheet 3/7





Dept.	Technical reference	Created by Laura Regueira Lopez de Garayo	Approved by		
		Document type	Document status		
		Title Supporting structure for AP motor	DWG No.		
			Rev.	Date of issue 17/06/2021	Sheet 5/7



Dept.	Technical reference	Created by Laura Regueira Lopez de Garayo	Approved by
		Document type	Document status
		Title Supporting structure for motors	DWG No.
		Rev.	Date of issue 17/06/2021
			Sheet 1/1

